Ethylene from natural gas by direct catalytic oxidation

Commission of the European Communities

energy

Ethylene from natural gas by direct catalytic oxidation

Report

EUR 13061 EN

Commission of the European Communities

energy

Ethylene from natural gas by direct catalytic oxidation

J.W.M.H. Geerts, J.M.N. van Kasteren, K. van der Wiele
Eindhoven University of Technology
Laboratory of Chemical Process Technology
PO Box 513
5600 MB Eindhoven
The Netherlands

Contract No EN3C-0038-NL (GDF)

Final report

Directorate-General
Science, Research and Development

1991

Published by the
COMMISSION OF THE EUROPEAN COMMUNITIES
Directorate-General
Telecommunications, Information Industries and Innovation
L-2920 Luxembourg

Cataloguing data can be found at the end of this publication

Luxembourg: Office for Official Publications of the European Communities, 1991

ISBN 92-826-2235-5 Catalogue number: CD-NA-13061-EN-C

Printed in Belgium

0. SUMMARY

This report describes the research in the field of oxidative coupling of methane to ethylene carried out at Eindhoven University of Technology (The Netherlands). The aim of this work comprised the development of a process for the production of ethylene directly from natural gas by partial oxidation.

The work was focused on four mayor aspects: Optimizing the physical parameters of the catalyst, defining the optimum reactor design and reaction conditions, collecting data for the modelling of the chemical reaction and process design and economic evaluations.

The preparation method for the catalyst studied (Li doped MgO) was optimized with respect to catalytic performance (C_{2+} yields of 19% have been reached). Special attention was paid to the catalyst morphology, lithium content and particle size. Essential for the Li/MgO catalytic activity and selectivity is the presence of lithium. The lithium appeared to be rather mobile, which resulted in lithium loss during operating conditions making catalyst deactivation to a mayor concern.

The most suitable reactor is a fluidised bed reactor, because of the high exothermicity of the reaction. New fluidised bed catalysts (e.g. Sm, Na, Ca, Al oxides) have been developed which have an excellent fluidisation behaviour and good catalytic performance.

The optimal reaction conditions for reaching the maximal C_{2+} yield (18%) for the longest time were: T= 800°C, P=1 atm, CH_4/O_2=5, W/F=0.6 g.s/ml.

The reaction mechanism can be described as a complicated mixture of heterogeneous (catalytic) and homogeneous (gas phase) reactions occurring simultaneously. Methane reacts with an adsorbed oxygen species at the catalyst surface, resulting in methyl radicals which are released into the gas phase. Coupling to ethane takes place in the gas phase. Ethane is dehydrogenated on the catalyst or in the gas phase to ethylene, which in turn gets easily oxidized into CO and CO_2. The latter is mainly formed at the catalyst surface.

A computer program has been developed which simulates the reaction network (>150 elementary radical reactions) of the homogeneous gas phase.

A process design and economic feasibility study for the production of ethylene from natural gas via oxidative coupling shows that this process is technically feasible and that it is economically attractive, when C_{2+} yields of 25% (C_{2+} selectivity>60%) are achieved.

Regarding the production of methanol from natural gas by direct partial oxidation a study has shown that presently known catalysts are still far from the selectivities and yields required for a commercial operation. A mayor breakthrough in catalyst development should be aimed at.

CONTENTS

0. SUMMARY III

1. AIMS OF THE RESEARCH 1

2. INTRODUCTION 1

3. THEORY 2
   3.1. THERMODYNAMIC CALCULATIONS 2
   3.2. CATALYST TYPES 3

4. DESCRIPTION OF THE WORK 4

5. EXPERIMENTAL 6
   5.1. REACTOR SET-UPS 6
   5.2. PREPARATION OF CATALYSTS. 11

6 RESULTS OF CATALYTIC TESTING EXPERIMENTS IN DIFFERENT REACTOR TYPES 12
   6.1. FIXED BED 12
   6.2. DEVELOPMENTS OF CATALYSTS FOR FLUIDISED BED REACTORS. ... 16
   6.3. MOLTEN SALTS IN A BUBBLE COLUMN REACTOR AS CATALYSTS FOR THE OXIDATIVE COUPLING OF METHANE. 19

7. REACTION MECHANISM AND KINETICS OF THE OXIDATIVE COUPLING OF METHANE OVER Li/MgO. 21
   7.1. COMPARISON BETWEEN CATALYTIC AND NON-CATALYTIC METHANE CONVERSION. 21
   7.2. INFLUENCE OF THE PROCESS CONDITIONS. 22
   7.3. HOMOGENEOUS GAS PHASE EXPERIMENTS IN A CSTR. 24
   7.4. LOW PRESSURE CATALYTIC REACTIONS 26
   7.5. PLASMA EXPERIMENTS 28
   7.6. TRANSIENT RESPONSE MEASUREMENTS. 30
   7.7. THE INVESTIGATION OF INDIVIDUAL REACTION STEPS 33
   7.8. DIFFERENTIAL KINETIC MEASUREMENTS IN A FIXED BED REACTOR 36
   7.9. KINETICS OF THE "PARTIAL" OXIDATION OF ETHANE AND ETHYLENE. 39
   7.10. ELEVATED PRESSURE EXPERIMENTS 41
   7.11. KINETIC MODELLING 42

8. PROCESS DESIGN AND ECONOMIC EVALUATION STUDIES 44
   8.1. ETHYLENE FROM NATURAL GAS BY DIRECT PARTIAL OXIDATION. .. 44
   8.2. METHANOL FROM NATURAL GAS. PROVEN AND NEW TECHNOLOGIES. 48

9. CONCLUSIONS 52

10. ACKNOWLEDGEMENT 53

11. LIST OF REFERENCES 54

TABLES AND FIGURES OF THE REPORT 59

1. AIMS OF THE RESEARCH

Our aim was to design an optimal catalyst (particle size, pore structure, surface properties) in view of the complicated kinetics and the exothermicity of the reaction. Data were collected for modelling the chemical reaction and for determining the optimal reaction conditions and reactor design. Another aim was to investigate the technical and economical feasibility of the oxidative coupling of methane process to set targets for the development of catalysts. In the framework of our cooperation with Limerick University, a similar study has been made for the production of methanol from natural gas by direct partial oxidation.

2. INTRODUCTION

Natural gas is an important resource for the European Community Member States. Its proven reserves exceed 100,000 milliard cubic meters (Ref. 1). Despite of its low costs it has not been used extensively for the production of chemicals. Especially when the carbon efficiency of a conversion process would be high it is an interesting raw material. So, for the chemical industry it would be extremely valuable to be able to convert natural gas into olefines such as ethylene and propylene.

Natural gas is composed of various products with methane being the major one. It can be converted into ethylene by direct partial oxidation. The desired reaction in this process is:

$$2\ CH_4 + O_2 \text{----}> C_2H_4 + 2\ H_2O$$

Two carbon atoms are coupled in this process, therefore it is also called the oxidative coupling of methane. A catalyst is very beneficial in this process; it is used (I) to increase the reaction rates, so a lower reaction temperature can be applied and (II) to decrease the formation of the by-products carbon oxides, which have a low commercial value and are costly in consuming "expensive" oxygen and methane.

Keller and Bhasin (Ref. 2) were the first to report on the catalytic direct conversion of methane to ethylene. They tested a large number of catalyst systems at atmospheric pressure and temperatures of 500° - 1000°C in a cyclic mode of operation: the catalyst was first oxidized with oxygen before pure methane was fed to the reactor. This was repeated in a continuous cycle. Among the best catalyst systems were PbO/Al_2O_3 and Mn_2O_3/Al_2O_3 with which they reached C_{2+} yields up to 5%. Since then many investigators have reported on catalytic systems for oxidative coupling of methane (Ref. 3,4,5,6). Li doped MgO was the most promising system with which a C_{2+} yield up to 19% was possible. Much of the work in this report is focused on this catalyst system.

When this study was started, the mechanism and kinetics of the oxidative coupling of methane were a fair blank spot in human knowledge. A better understanding and an increased level of knowledge are a great help for developing better performing catalysts, and modelling the chemical reaction and for determining the optimal reaction conditions and reactor design.

3. THEORY

3.1. THERMODYNAMIC CALCULATIONS

The equilibrium composition of the pyrolysis of pure methane and that of the pyrolysis in combination with methane oxidation has been calculated. The formation of elementary carbon was assumed not to occur, which simplified the calculations. Figure 3.1.1 shows the conversion and yields (= the product of conversion and selectivity) of methane pyrolysis. The selectivities and yields have been defined on carbon basis. It is very clear that ethylene is the main hydrocarbon product at high temperatures in the chemical equilibrium state. However, the methane conversion is limited. If methane pyrolysis is carried out at elevated pressure, see Figure 3.1.2, the conversion is even lower. When the pressure is decreased, the product composition shifts from alkanes to alkenes to alkynes, C_2's being the main products. C_3 hydrocarbons are only present in small amounts.

When oxygen is added, the methane conversion is much higher, due to the high Gibbs free reaction energy of oxygen with hydrocarbons. In the equilibrium state the oxygen conversion is always complete when hydrocarbons are in excess. A cumulative volume fraction diagram of equilibrium compositions (initial $CH_4/O_2 = 10$) is plotted in Figure 3.1.3. At moderate temperatures the methane is converted into hydrogen and carbon monoxide. At higher temperatures, however, the products include CO_2, water and hydrocarbons, with poor yields of the latter.

Gas phase experiments at varying residence time, Figure 3.1.4, show that kinetics govern the product distribution. The experiments were carried out in a quartz reactor of a micro flow reactor set-up, described elsewhere (Ref. 7). Short contact times give high selectivities with respect to the desired C_2H_4 and C_2H_6, but at poor conversions, whereas long residence times (left part of the figure) favour the formation of carbon oxides and high conversion. The oxidation of CO to CO_2 in the gas phase (Ref. 8) is rather slow, which explains the very long residence times required to get carbon dioxide. Note that the points on the vertical axis, representing the calculated chemical equilibrium state, are covered very nicely by extrapolations of the experimental values. In agreement with the assumption that the formation of elementary carbon was negligible and could be omitted in the calculations, no carbon deposits were detected whenever oxygen was applied in the reactor feed and extremely long gas residence times were avoided.

Conclusions

In the calculated chemical equilibrium state, ethylene is the main product of methane pyrolysis when the formation of elementary carbon is excluded. The ethylene yield however is limited, due to a limited methane conversion that even gets worse when the pressure is increased. Addition of oxygen leads to a much higher methane conversion, however at low C_{2+} selectivities. Extrapolation of the results of gas phase experiments to the condition of infinite residence time gives an excellent fit with values calculated for the equilibrium state.

3.2. CATALYST TYPES

For catalytic oxidative coupling of methane the literature reports many catalytic systems (Refs. 2-6). They can be summarized into two main groups: Catalysts with reducible oxides (e.g. Mn_2O_3/Al_2O_3) and catalysts with irreducible oxides. The last group can be divided into two groups (e.g. Li_2CO_3/MgO or Sm_2O_3). Mn_2O_3 oxidizes methane with lattice oxygen. The lattice oxygen is replaced by gas phase oxygen in a continuous redox cycle. Li_2CO_3/MgO however, cannot be reduced by methane but takes up oxygen at vacancies which are very reactive in methane activation. Sm_2O_3 does not take up oxygen but is believed to have adsorbed oxygen species (O_2^-, O_3^-) at the surface which are very reactive towards methane activation.
Our catalytic research has been concentrated on the Li_2CO_3/MgO catalyst system since it was the most promising catalyst at the start of our research. However, we also tested other catalysts (e.g. Mn_2O_3/Al_2O_3, Sm_2O_3, Na/CaO) especially for the use in a fluidised bed reactor in which case the catalyst morphology is a decisive factor for applicability.

4. DESCRIPTION OF THE WORK

Introduction

The work carried out at the Laboratory of Chemical Process Technology of Eindhoven University of Technology (The Netherlands) within the EC sub-programme "Optimization of the Production and Utilization of Hydrocarbons" from December 1986 until Dec. 1989 can be divided into three parts:

Experimental work.

Experiments were carried out in continuous flow set-ups specially designed and built for the methane coupling research. Most of the work was focused on the Li/MgO catalyst system, one of the most promising catalytic system for the oxidative coupling of methane. The experiments comprised extensive testing of the influence of process conditions, the catalyst preparation method in relation to its properties and the performance of several reactor types (fixed, fluidised bed, bubble column). The reaction mechanism and kinetics of the methane coupling over Li/MgO were determined by combination of varies kinds of experiments, each carried out in specially designed equipment, constructed for this project:

-By means of a specially designed set-up with a continuous stirred tank reactor (CSTR) the role of gas phase reactions were investigated.

-Low pressure experiments were carried out in a special reactor with an on line mass spectrometer to reveal the role of heterogeneous reactions.

-Transient isotope switching experiments performed in a specially designed flow reactor, provided with a second on line mass spectrometer, revealed the oxygen pathway during methane coupling under steady state operating conditions.

-Differential kinetic measurements of the methane coupling in a fixed bed reactor resulted in kinetic parameters for the methane, ethane and ethylene reaction over Li/MgO.

-Admixing experiments with methane/ethane/oxygen and methane/ethylene/oxygen mixtures revealed relative reaction rates between methane, ethane and ethylene.

-Radical reactions were studied in a plasma reactor designed in cooperation with the Physics Department at our University.

-High pressure experiments performed in a specially designed and built set-up showed that gas phase reactions predominate at increased pressures.

Modelling work.

The results from the experimental work were used for numerical description by computer modelling for kinetic models describing the oxidative coupling of methane. A gas phase model was developed which gives a good description of the measured gas phase coupling within experimental error. Based on this simulation the catalyst role was incorporated into this gas phase model as an attempt to model the whole methane coupling process in the presence of a catalyst.

Process development studies.

Two process process design and economic feasibility studies were carried out:
"Ethylene from natural gas by direct partial oxidation".
"Methanol from natural gas. Proven and new technologies".
This work resulted in aims for the research to be reached to make the processes economically attractive. Especially the methanol study links up with the work carried out by our EC contract partner in Limerick, Ireland, who investigates the conversion of methane to methanol and formaldehyde by direct partial oxidation.

5. EXPERIMENTAL.

5.1. REACTOR SET-UPS

Set-up for integral and differential measurements.

This paragraph describes the laboratory flow reactor systems with which integral and differential measurements were carried out with different reactor types.
The set-up consists of a feed, reactor and analysis section as shown in Figure 5.1.1. The feed and analysis section is almost the same for all the set-ups that were constructed. The normal operating procedure for catalytic experiments with the set-ups can be summarized:

After heating up of the catalyst to the desired reaction temperature, typically 800 °C, under a flow of helium, a reaction gas was introduced. A flow rate was established with mass flow controllers (Hitec) (typically 50-500 ml/min) consisting of methane (Hoekloos 99.6%), oxygen (Hoekloos 99.9%) and helium (Hoekloos >99.995%).

The product gases were analyzed by gas chromatography. The column packings were Porapak R (3m) for the separation of CH_4, CO_2, C_2H_4, C_2H_6, C_3H_6, C_3H_8 and H_2O and a 5-A molecular sieve (3m) for the separation of H_2, O_2, CH_4 and CO. The porapak was operated at 70°C and the molecular sieve at 110°C. Both columns were connected to a Thermal Conductivity Detector (TCD) in a Carlo Erba 4300 gaschromatograph with helium as the carrier gas. The analysis was carried automatically with the aid of two pneumatically controlled sampling valves. A complete product analysis took about 20 min. With this method a carbon balance of at least 98% was achieved.

Fixed bed reactor set-up.

Figure 5.1.2. shows the quartz micro fixed bed reactor operated at 1 atm used for kinetic experiments. In the kinetic experiments the methane or oxygen flow was altered at the cost of helium so that the total flow rate did not change. The differential experiments were carried out after the catalyst (0.25 gram) had stabilized (48 hours).

Fluidised bed reactor set-up.

In principal, this reactor set-up is similar to the one shown in Figure 5.1.1. Extra features are a flame ionization detector at the GC, which is especially useful to detect accurately the higher hydrocarbons. Furthermore, the reactor section was constructed in a special way to be able to measure under both down-flow and up-flow conditions (i.e. fixed bed and fluidised bed). The reactor, designed as a fluidised bed, is made from quartz and has an inner diameter of 0.02 m. It was placed in an electrically heated furnace of 0.30 m and the catalyst (2-30 g) lied on a quartz filter plate, which functioned under up-flow conditions as a gas distributor. The temperature was measured with a Cr/Al thermocouple placed in a thin quartz tube in the centre of the catalyst bed. In Figure 5.1.3 axial temperature profiles of the reactor are shown as measured under up- and down-flow conditions. It is evident that the direction of the flow has a striking effect. The

fluidised bed has an uniform temperature throughout the entire bed.

Bubble column reactor set-up.

A micro flow reactor system operated at atmospheric pressure, see Figure 5.1.1, was used as the bases of this set-up. The fixed bed reactor was replaced by a bubble column reactor. The latter was made of quartz and had an inner diameter of 0.016 m and a column length of 0.2 m. Methane, oxygen, helium and carbon dioxide were fed to the reactor through a central dip pipe (outer diameter 0.004 m) at feed rates of 19.5, 4.4, 13.0, and 0.43 cm^3/min STP respectively. The methane/oxygen ratio was 4.4 and the dilution with helium ensured that the reaction heat produced did not influence the reactor temperature. This temperature was kept uniform over the whole bubble column by inserting it in an air fluidised sand bed which was electrically heated.

Recycle reactor set-up.

A recycle reactor set-up has been built. The set-up can be divided into four main parts. The feed section, in which the feed gases are mixed and their flows are measured and controlled, the reactor section, in which the heart of the set-up, the recycle micro fixed bed reactor, is situated, the gas selection section, in which the gas that flows through the injection valves is selected, and the analysis section, which consists of the injection valves, wet gas meters, soap film meters and a GC with capillary columns. In the last section the composition of a gas is determined. Except for the reactor section, the set-up is more or less similar to the one shown in Figure 5.1.1.

In this set-up the product gases are recycled over the reactor by a gas pump. The recycle flow rate is calculated from the pressure drop over an orifice plate and the composition of the stream, which is equal to the product composition. By changing the recycle ratio from 0 to 30 the reactor behaviour can be changed from plug flow to ideally mixed. The reactor used in this set-up, see Figure 5.1.2, has a diminished diameter behind the catalyst bed, because especially in the CSTR mode of operation post-catalytic reactions have to be prevented.

The gas samples are automatically taken just before and after the reactor and are in turn automatically analyzed. A number of securities have been built in, such that the system can be operated during the night without human interference.

Low pressure reactor set-up

A way of discriminating between homogeneous and heterogeneous reactions is to carry out experiments at reduced pressures. At reaction pressures of 100 Pa and below, radical reactions in the gas phase are only taking place to a very low extent. In this way it is possible to determine the contribution of heterogeneous reactions to the overall kinetics.

For this purpose a low pressure reactor was designed and built, which can operate at a pressure range of 10 to 500 Pa.

The low pressure reactor set-up is shown in Figure 5.1.4. The set-up consists of a feed

section with which a gas mixture can be prepared and stored in a feed gas container. From this feed gas the gas mixture is transported to the reactor via valve K2 and variable leak-valve R1. From there most of the gas is pumped off via three-way valve K4. Only a small amount of the product gas is used for analysis leaking via K5 and R2 to a quadrupole mass spectrometer (Leybold-Heraeus Q-200). Beside flow experiments also batch experiments were performed by closing valve K4 and leaving only the small gas leak to the mass spectrometer. The flow in the reactor was lowered to zero and diffusion at the low pressures applied caused ideally mixing compared to reaction. The reactor can be considered as an ideally mixed batch reactor.

The reactor is the same reactor as used in the atmospheric pressure experiments (Figure 5.1.2).

The analysis is performed by the Q-200 which is controlled by a computer. The concentrations of the components in the gas mixture are determined via a multiple regression program. This program uses reference spectra of the pure components to determine which ones are present (qualitative) in the gas mixture and to what extend (quantitative). The program does so by linear regression analysis which determines an appropriate relationship between a variable (y_1,..y_n) and the quantities of one or more components (1,..,p). The regression has the following form:

$$\begin{vmatrix} y_1 \\ y_2 \\ \\ \\ y_n \end{vmatrix} = b_0 + b1 \begin{vmatrix} x_1 \\ x_2 \\ \\ \\ x_n \end{vmatrix}_{\text{Comp } 1} + b_2 \begin{vmatrix} x_1 \\ x_2 \\ \\ \\ x_n \end{vmatrix}_{\text{Comp } 2} + \ldots + b_p \begin{vmatrix} x_1 \\ x_2 \\ \\ \\ x_n \end{vmatrix}_{\text{Comp } p}$$

The regression function is a mathematical procedure which chooses from a library of reference spectra (components 1 until p) a group of spectra with each its own fragmentation spectrum (x_1,..x_n). The sum of this is multiplied by its own concentration coefficient (b_0,..,b_p) to give the best fit to the measured spectrum (y_1, .. ,y_n), i.e. the sum of the least squares of the residuals

$$\sum_{i=1}^{n} (y_i - y_i)^2$$

must be minimal. The factors (b_1,..,b_p) determine the concentration of the components together with a sensitivity factor.

Before the experiments can be carried out the quadrupole has to be calibrated. This means that the mass spectra of the expected components in the reaction mixture have to be recorded. This was done with neon as internal standard. In this way it is possible to determine a sensitivity factor for the different components. The "fingerprints" of the pure components are stored in a data file which is used to fit the spectra of the reaction mixture. Two calibration mixtures were prepared and analyzed by computer in order to check the regression procedure. This is shown in Table 5.1.1.

Plasma reactor set-up

Radical reactions play a very important role in the oxidative coupling of methane over Li/MgO catalysts. The role of the Li/MgO catalyst in radical reactions has been investigated by means of a striated column of a d.c. glow discharge in Ar. With this technique it is possible to activate methane with Ar metastable molecules, which have a discrete energy of 11.5 eV. This energy is too low to ionize methane or abstract all the hydrogen atoms in one step.

The methane activation experiments were carried out in a striated column of a d.c. discharge in Ar. Figure 5.1.5. shows the reactor set-up. The reactor set up consists of a feed gas section with which an argon/methane (70:1) or a CH_4/O_2 mixture can be fed to the reactor. A typical flow rate used was 18.75 ml/min.

The reactor consists of a quartz tube (L=60cm, d=2.5cm) to which a cathode, anode and variable gas inlet are connected. The glow discharge is created by applying a 3kV voltage between cathode and anode at a reactor pressure of 3.2 mbar. The electric current is limited to 8.3 mA by means of a series resistor. The influence of the negative glow (near the cathode) with its relatively high electric field and high mean energy of the electrons is eliminated by placing the cathode in a separated chamber. The anode is shielded with a quartz tube to eliminate reaction at the anode. The gas inlet can be varied over the reactor length to be able to study the influence of contact time. The wall of the reactor can be cooled down to liquid nitrogen temperature. In this way the reaction products are frozen at the reactor wall and a dissociation by metastable atoms will be prevented.

A plasma reaction was carried out by turning on the electric power for 1 minute during which the argon/methane was fed to the reactor via the variable gas inlet. The influence of catalyst surfaces on radical coupling reactions is studied by placing an amount of catalyst into the reactor filling the space between gas inlet and anode. Activation of the Li/MgO catalyst was performed by UV irradiation with a 500 W Hg lamp in the presence of gas phase oxygen. The activated catalyst was exposed to the methane/argon mixture and the reaction was carried out as described above.

The products formed are collected in a cold trap (77K) and analyzed after heating to room temperature and pressurizing with helium. The analysis is performed with a Carlo Erba 4200 gas chromatograph with a flame ionization detector connected to a phenylisocyanate column to separate CH_4, C_2H_6, C_2H_4, C_2H_2, C_3H_8, C_3H_6, C_{4+}.

Set-up for transient isotopic switching experiments

Isotopic switching experiments were performed to elucidate the working principle of the Li/MgO catalyst under relevant process conditions. Figure 5.1.6 shows the flow scheme of the set-up which was built and used.

With the feed section it is possible to create two gas mixtures consisting of e.g. $CH_4/^{16}O_2/He$ and $CH_4/^{18}O_2/He$ with a typical total flow rate of 100 ml/min each. The isotope was fed to the system from a lecture bottle. The two gas mixtures are fed to the reactor section with which it is possible via 4 way valve K1 to switch between the two feed gas mixtures. The quartz reactor used is the same as used in the kinetic experiments (Figure 5.1.2). Beside the catalyst (typical 0.25 g) the reactor was filled with quartz particles in order to eliminate the influence of dead volume and eliminate back-mixing effects. After the catalyst bed the reactor volume was kept as small as possible by reducing the reactor diameter. Analysis of the gas mixture was performed with a

quadrupole mass spectrometer (Balzers QMG 511) and a Carlo Erba 4200 gas chromatograph. The reactor outlet was connected directly via a fused silica capillary to the quadrupole which made fast ion monitoring possible controlled by a laboratory computer. At the same time a series of up to 16 samples of the product gas can be trapped in loops on a 34 port sampling valve for subsequent GC analysis. Isotopic switching experiments under steady state conditions require that the concentrations in each of the feed gas mixtures are identical and that there is no pressure difference between them. That's why mass flow controllers are indispensable. The pressure difference between the two gas flows was eliminated by adjusting a needle valve in the bypass.
Typical flow rates were 3.6 ml/min methane, 9.15 ml/min O_2/He (1:4) and 45.4 ml/min He. The temperature was 800°C and the catalyst amount 0.25 g Li/MgO. The catalyst was aged for 50 hours before experimentation in order to stabilize it and eliminate the influence of catalyst deactivation.

Fixed bed reactors for ethane and ethylene oxidation experiments.

The oxidation of ethylene is a very rapid reaction, compared to the oxidative coupling of methane. The reactors and furnaces in use for the methane oxidation gave not very satisfactory temperature profiles under the conditions applied for the oxidation of ethylene. So, a new type of reactor was designed and a sand bed fluidised by air was made and installed as the heating medium of the reactor, see Figure 5.1.7.

The new, designed reactor is inserted in the fluidised sand bed, which has an almost uniform temperature through the whole bed. At the outer side of the in- and outlet tubes of the reactor a cooling jacket, through which cold air flows, takes care of a very steep increase in temperature of the reaction gases and, as most probably is even more important, see Chapter 7.2 about post-catalytic reactions, a very steep decrease in temperature at the outlet too. The cooling air flows co-currently with the reaction gas in order to prevent condensation of water at the reactor outlet. As can be seen in Figure 5.1.8, the temperature gradient is maximum 500 °C/cm and the profile is very flat for over 20 cm. So, the axial temperature profile inside the reactor is a very good approximation of the ideal block profile.

Elevated pressure reactor set-up

A micro fixed bed reactor set-up has been constructed to carry out experiments under elevated pressure. Essentially, this set-up is similar to those operating at atmospheric pressure, but the increased pressure requires an extended set of extra built-in items, see Figure 5.1.9. First of all, the connection between the quartz reactor and the metal tubes is not suited for reactor pressures exceeding 2 bar. Therefore, a dome is placed around the reactor and furnace. This dome has a separated pressure controller that keeps the nitrogen pressure inside the dome 0.5 bar higher than the reactor pressure. Secondly, extended safety precautions and measurements were made to ensure safe operation during night times. A quartz reactor with an inner diameter of 0.007 m has been used.

5.2. PREPARATION OF CATALYSTS.

Three different catalysts preparation techniques were used:

-Method 1:

The metal oxides with dopants are solved in water to get a catalyst with a good dispersion of the dopants. The water is evaporated at 80°C under continuous stirring with a mechanical mixer. The remaining catalyst paste is dried at 140°C. To convert the carbonate, hydroxides or nitride groups into oxides the catalyst is calcined at high enough a temperature (usually 900°C). Finally the catalyst is ground and crushed to the desired particle size.

The Lithium doped magnesia was prepared by this method.

-Method 2: Impregnation:

This technique was used to prepare fluidised bed catalysts. The active component was solved in concentrated nitric acid. The resulting solution was used to impregnate carrier materials like alumina and silica. Drying and calcination and sometimes crushing completed the preparation.

-Method 3: Co-precipitation:

The metal oxide and the dopants are solved in nitric acid to be sure of complete solvation. The evaporation, drying and calcination step are similar to the wet impregnation method.

6 RESULTS OF CATALYTIC TESTING EXPERIMENTS IN DIFFERENT REACTOR TYPES

6.1. FIXED BED

Introduction

This paragraph deals with the Li/MgO catalyst which is suitable only in a fixed bed reactor. Its performance has been tested in a quartz micro fixed bed reactor, as well as the influence of its preparation method on the coupling activity.
Catalyst pretreatment experiments were carried out in order to investigate whether activation of the Li/MgO catalyst with oxygen was possible.
Finally catalyst deactivation was investigated and its working principle determined.

Influence of catalyst preparation

Li/MgO catalysts with a lithium content of 7 wt% Li/(Li+MgO) were prepared from different lithium and magnesium salts. The use of different lithium or magnesium salts can result in catalysts with different structure and with different catalytic properties.
Table 6.1.1 shows the various catalysts prepared and their pore volume as determined by the mercury penetration method.

From Table 6.1.1 it is clear that the lithium nitrate catalyst has the highest pore volume; much higher than all other catalysts prepared. As a result the surface area is much higher. Therefore the activity is also expected to be much higher.
All catalysts prepared were tested in a micro fixed bed reactor at 800 °C with a continuous feed of methane (50 ml/min), oxygen (10 ml/min) and helium (40 ml/min). The contact time (W/F) was 300 g.s/l and the methane/oxygen ratio was 5.

Figure 6.1.1 shows the methane and oxygen conversion as a function of the time on stream (h).
The LiF/MgO catalyst is missing because the reactor broke during the first hour of the experiment. The fluoride is very aggressive to the quartz glass and destroys its structure.
During reaction time the oxygen conversion shows a maximum. This is typical for the Li/MgO catalysts calcined at temperatures higher than the reaction temperature used.
The starting salt in the catalyst preparation has a strong influence on the course of the activity. As expected the lithium nitrate catalyst initially has the highest activity and selectivity. However, a much more pronounced performance was expected, with respect to the porosity data. Instead the lithium carbonate magnesium oxide catalyst reaches an even higher activity level and shows a much slower deactivation, once the first 8 hours have been passed.
When comparing the different catalysts one must keep in mind that all the catalysts, except for the LiF/MgO , consist of lithium carbonate and magnesium oxide phases after calcination.
That the lithium carbonate phase is essential for the oxidative coupling selectivity is proven by the LiF/MgO catalyst, because it showed no activity or selectivity during the short period of time it could be measured. Because product selectivity is coupled to

activity, comparison of the catalysts can best be done by comparing the C_{2+} yields. This is shown in Figure 6.1.2, where the C_{2+} yields are plotted against the time on stream. The $LiNO_3/MgO$ catalyst maintains a C_{2+} yield of 15% for 10 hours but then rapidly deactivates. The Li_2CO_3/MgO has a better stability in time because it deactivates more slowly. Summarizing it can be said that the catalyst preparation strongly influences the course of activity, especially during early reaction times, but that the difference in coupling performance is not very pronounced.

The influence of catalyst pretreatment

As mentioned in the introduction more active centres should be created by oxygen pretreatment of the catalyst. The pretreatment time is believed to influence the catalyst performance.
Oxygen pretreatment consists of flushing the catalyst (at reaction temperature (800 °C)) with artificial air (He 80%, O_2 20%) during a variable number of minutes followed by a flush with pure helium to remove all the excess oxygen. After pretreatment the reaction is carried out under standard conditions (T_r= 800 °C, W/F= 300 g.s./l. CH_4/O_2=5, CH_4/He=1.25)
Figure 6.1.3 shows the methane and oxygen conversion as a function of the reaction time for different pretreatment times. It shows that the initial activity increases with increasing pretreatment time as expected. However, when the time proceeds, this is no longer valid. A pretreatment time of 1 minute appears to raise the catalyst activity the fastest. The deactivation then is the fastest too. A long pretreatment time makes the catalyst more stable. This would lead to the conclusion that a long pretreatment time is ideal for the catalyst performance.
Comparison between C_{2+} yield as shown in Figure 6.1.4 gives a better picture of the influence of the catalyst pretreatment. Clearly an oxygen pretreatment is beneficial for the C_{2+} yield, because no pretreatment results in a lower C_{2+} yield. The time of oxygen pretreatment is not very crucial. Although a short pretreatment time results in a faster activation it also causes a faster deactivation.

The influence of catalyst bed dilution with quartz

By diluting the catalyst bed with quartz the occurrence of homogeneous gas phase reactions in the catalyst bed should be measurable, as dilution increases the gas volume with respect to the amount of catalytic material.
0.4 Gram of catalyst is diluted with different quantities of quartz on weight basis. These mixtures were tested under standard conditions (W/F= 250 g.s/l).
Figure 6.1.5 shows the methane and oxygen conversion as a function of the reaction time for different degrees of dilution. It appears that quartz dilution has a surprising strong influence on the activity of the catalyst. The higher the degree of dilution the faster the catalyst deactivates. At the highest degree of dilution the catalyst deactivates already from start-up of the reaction. This deactivation is most probably due to loss of lithium, which is accelerated by quartz dilution, because of formation of silicates. The maximal oxygen conversion moves to shorter reaction times the higher the degree of dilution is.

Catalyst deactivation experiments

Deactivation measurements with Li/MgO catalysts were carried out at 800°C, CH_4/O_2 = 5, atmospheric pressure and a 1:1 dilution with helium. Starting with a 7 wt% Li/Li+MgO catalyst a rapid loss of lithium is observed : 2 wt% in the first 15 hours (Figure 6.1.6). However, the catalytic activity is not decreasing in the first 10 hours; instead it even increases. This means that new active centres are formed and that only part of the lithium is active. This is confirmed by experiments with a 0.2 wt% Li/Li+MgO catalyst (Figure 6.1.7.). In spite of the low lithium content this catalyst is reasonable active and selective. The loss of lithium is mainly due to reaction of lithium with water vapour to form LiOH (volatile) and reaction with the quartz reactor wall to form catalytically rather inactive Li_2SiO_3.

Driscoll et al. (Ref. 9) stated that Li^+O^- centres stabilized in the MgO matrix were the active centres for the generation of methyl radicals from methane. Especially the role of MgO is essential in his theory because of the substitution of Mg^{2+} ions ($r_{Mg}2+ = 0.66$ Å) in the MgO lattice by Li^+ ions ($r_{Li}+ = 0.68$Å) from the Li_2CO_3 phase. Korf et al (Ref. 10). have shown that carbon dioxide, continuously added to the gas phase, reduces the activity of the Li/MgO catalyst, while a short treatment of a deactivated Li/MgO catalyst with carbon dioxide restores the initial activity for some time. These results support our experiments with the differently prepared Li/MgO catalysts that the presence of Li_2CO_3 is essential for an active and selective catalyst.

To prove that Li_2CO_3 can generate an active catalyst, Li_2CO_3 was impregnated on an inert carrier: ZrO_2. Figure 6.1.8 shows the activity of Li_2CO_3/ZrO_2 as function of time on stream. Clearly the oxygen conversion increases to a maximum followed by a decrease to almost no activity. Indeed the performance of this catalyst is identical to Li/MgO, except for a lower activity due to a lower surface area. The activity lasts as long as lithium carbonate is present. The interaction of ZrO_2 (r_Z4+ = 0.79 Å) with Li_2CO_3 ($r_{Li}+ = 0.68$Å) at 800°C is far less than that of Li_2CO_3 with MgO. Only at very high temperatures (>1000°C) detectable amounts of lithium zirconate (Li_2ZrO_3) are formed. This lithium zirconate is itself a catalyst for the oxidative coupling of methane with a reasonable activity and a high C_{2+} selectivity. However Li_2ZrO_3 is not the active phase in the Li_2CO_3/ZrO_2 catalyst, because also the activity of Li_2ZrO_3 can be increased temporarily by doping it with Li_2CO_3 (Figure 6.1.9). Also this catalyst looses its activity more rapidly than Li/MgO. Due to the interaction of Li_2CO_3 with MgO the loss of the lithium phase is retarded. In that respect the carrier plays an essential role: stabilization of the lithium phase. These results clearly show that Li_2CO_3 is essential for an active lithium catalyst. Combining of all this leads to a possible working principle of the Li/MgO catalyst shown in Figure 6.1.10.

Li_2CO_3 decomposes in the presence of oxygen to an active centre and CO_2. This active centre reacts with methane to form a methyl radical. Deactivation of the catalyst occurs due to reaction of Li_2CO_3 with water to LiOH which evaporates or with quartz to lithium silicates which are almost inert.

Conclusions

The catalyst structure has an influence on the activity and selectivity. The same preparation method gives, starting with different lithium and magnesium salts, in principle the same catalyst concerning the phases existing : lithium carbonate and

magnesium oxide.
Essential for the catalytic mechanism is the presence of the Li_2CO_3 phase without which the catalyst is only little active and not at all selective. It is known that Li_2CO_3 melts and decomposes at the reaction temperature of 800 °C to Li_2O and CO_2. This Li_2O assumably formes the desired active phase.
The $LiNO_3$/MgO catalyst has a high pore volume and a large surface area compared to the other prepared Li/MgO catalyst. This appears to be favourable for the coupling reactions: a stable C_{2+} yield of 15% for 10 hours. However, deactivation of this catalyst is also quite fast, because the lithium can also be lost more easily due to the higher surface area.
An oxygen pretreatment is favourable for the activity and selectivity of the catalyst. A short pretreatment time speeds up the activation period of the Li/MgO catalyst, but also speeds up the deactivation so that the total life time of the catalyst is diminished. The pretreatment time is not very crucial to the catalyst performance
Dilution of the catalyst bed with quartz particles increases the deactivation rate. This is due to loss of lithium via reaction of lithium with the quartz glass under formation of lithium silicates. This silicate holds the lithium tightly so that it can no longer be of use for the formation of reactive centres. The more quartz is present in the catalyst bed the more this reaction will take place.
The deactivation experiments show that lithium is the active component in Li/MgO and that it is lost quite rapidly during reaction. Only a small part of the total lithium content of the catalyst is responsible for the activity. Very small amounts of lithium are sufficient to create an active and selective Li/MgO catalyst. The interaction of Li_2CO_3 with MgO is essential for the stability of the catalyst. Lithium carbonate supported on an inert carrier like sintered ZrO_2 results also in an active and selective catalyst but less stable.

6.2. DEVELOPMENTS OF CATALYSTS FOR FLUIDISED BED REACTORS.

Introduction

A reactor design study, see Ref. 11, has shown that a fluidised bed reactor is to be preferred as the reactor type in a plant at a commercial scale. Some advantages are: an excellent temperature control, an easy heat recovery, a simple reactor construction, possibility of a cold injection of the feed which diminishes undesired gas phase oxidation, and usage of the free-board-zone as an ethane cracker. Figure 5.1.3 indeed shows a uniform temperature throughout the entire fluidised bed, whereas the fixed bed temperature profile as measured in the same laboratory reactor is far from being flat.

Catalysts which perform very satisfactory in a fixed bed reactor can sometimes be worthless inside a fluidised bed reactor, even when the correct particle size is chosen. Of crucial importance is the fluidisability of the catalyst in such a reactor. This puts some constraints to the catalysts which can be used. The particle size must lie between certain limits and must remain the same under reaction conditions. Crushing of particles due to their low mechanical strength, clustering of particles due to sintering effects and sticking of particles to the wall due to electrical forces are common examples of failures in fluidisation. All these phenomena have been overcome and have resulted in catalysts, which can be applied successfully in a fluidised bed reactor.

Performances of the non - carried catalysts.

Li/MgO Catalysts:
The first catalyst which was tested in a fluidised bed reactor was the 7 wt% Li/MgO catalyst prepared according to method 1. It has a good performance when used in a fixed bed reactor. According to the classification of Geldart (Ref. 12) the catalyst is an A/B powder and should fluidise well. And indeed, at room temperatures it does. But, under reaction conditions the Li_2CO_3 phase is liquid and acts as a glue between the catalyst particles. Conglomerates of several, former individual, particles are formed, which are too large to fluidise. Actually, the Li/MgO catalyst particles consist under reaction conditions of small stable MgO particles which are imbedded in a matrix of Li_2CO_3 that is molten. Pure Li_2CO_3 has a melting point of 723 °C. This liquid phase is not stable at 800 °C, it should be converted into the oxidic form see Figure 6.2.1, but its existence is enabled by the carbon dioxide formed during oxidative coupling of methane. The fluidisability of these catalysts could be improved by preparing catalysts with lower lithium contents and by dilution of the catalyst bed with quartz particles. In the latter case, the quartz acts as a lithium sink under formation of solid, stable lithium meta silicate, see Figure 6.2.2, which actually results in a lower lithium loading of the magnesium oxide. Catalysts that fluidised for a maximum of 24 hours were prepared.

Samarium oxide catalysts:
From literature (Ref. 13), it is known that samarium oxide, not being as good as Li/MgO, could be used as a catalyst for the oxidative coupling of methane. Calcium oxide and potassium oxide used as dopants increase the stability of these catalysts. The problem of these catalysts is the fact that the mechanical strength of the fluidising particles is terribly low. Most of the catalysts have been prepared by method 2 and

resulted in porous catalysts. Neither of the oxides used melts during the preparation. Therefore, these catalysts do not have a binding component comparable to Li_2CO_3 in the Li/MgO system and they consist of small particles which easily break down into very fine powder. It is not possible to calcine these catalysts at higher temperatures to melt the oxides, for samarium oxide is converted from the cubic structure to the less active monoclinic structure at about 850 °C.

Sodium/calcium oxide catalysts:
The $NaOH/Ca(OH)_2$ catalysts were prepared via the wet impregnation method and are easy to fluidise when carefully dried. A heat treatment in a helium atmosphere restores fluidisation, which again stops when the catalyst material has absorbed too much reaction water (usually after about 100 operating hours). With this catalyst, selectivities of up to 60% can be reached at CH_4 conversions of about 12%. In Figure 6.2.3 these catalysts are indicated as "pure catalysts". The stability of this type of catalysts is good.

Performances of the catalysts on carriers.

In order to reduce the attrition in the fluidised bed, the mechanical strength of the catalysts has been increased by putting the catalytic active components on carriers. Three kinds of carrier materials have been tested: silica, alpha and gamma alumina. They have been impregnated with the 7 wt% Li/MgO and Sm_2O_3. All these materials fluidise very well under reaction conditions for long periods of time. However, the catalyst carrier has a significant influence on both the methane conversion and the C_{2+} selectivity, which is clearly shown in Figure 6.2.3 in which the catalysts are ordered to their carrier material.

And α alumina supported catalysts have a rather low performance with C_{2+} selectivities of under 30% and methane conversions of up to 10%. SiO_2 supported catalysts can achieve a high selectivity of up to 80%, but only at poor CH_4 conversions (<5%). At high CH_4 conversions (20%) that selectivity drops to just 20%! The highest yield (5%) is achieved at a CH_4 conversion of 12% and a C_{2+} selectivity of 40%. From Figure 6.2.3 it is clear that the more acidic the carrier material the worse the catalytic performance is. Besides those acidic sites on the pure carrier the Li/MgO catalyst is less active on these carriers. Lithium reacts with the carrier itself and forms lithium aluminates and lithium silicates. They are inactive for the oxidative coupling of methane, so, a less active and selective catalyst is the result.

A well performing catalyst is the $Sm_2O_3/Na_2CO_3/CaO/\ -Al_2O_3$, in Figure 6.2.3 indicated as "basic alumina". The alumina is used to give the catalyst the necessary strength but the catalyst is not prepared in the usual manner (impregnation of the Na_2CO_3/CaO catalyst doped with samarium oxide on the carrier material) but the Al_2O_3 carrier is co-precipitated, see Chapter 5.2 for the preparation method, with the other starting salts. In this way an active catalyst is made with a good interaction between the basic sodium and calcium sites and the acid alumina, resulting in a neutralization of the acid sites. This could not be obtained when impregnating alumina carrier grains. With XRD, two crystalline phases could be detected: cubic Sm_2O_3 and $CaSmAlO_4$. A yield of 10.5% can be achieved at a CH_4 conversion of 21% and a C_{2+} selectivity of 50% and deactivation of this catalyst is not observed!

Conclusions

The sodium/calcium oxide catalyst systems perform very well in a fluidised bed as catalyst for the oxidative coupling of methane. Periodical drying of those catalysts inside the reactor may be required to remove absorbed water and to restore fluidisation.

Carrier materials like alumina and silica have a good mechanical strength. However, they have acidic sites that assumably attribute to the combustion of hydrocarbons resulting in low selectivities. When the $Sm_2O_3/Na_2CO_3/CaO/\ -Al_2O_3$ catalysts are made by co-precipitation, a good mechanical strength is remained, but also a good selectivity is obtained.

6.3. MOLTEN SALTS IN A BUBBLE COLUMN REACTOR AS CATALYSTS FOR THE OXIDATIVE COUPLING OF METHANE.

Introduction

Among many materials that have been reported to be catalytically active for the oxidative coupling of methane (Refs. 4,14,15,16,17,18,19), lithium doped magnesium oxide especially has attracted the attention of many researchers (Refs. 8,9,18,19,20). In earlier reported work (Ref. 21) it appeared possible to use pure Li_2CO_3 supported on ZrO_2 as a catalyst with a similar behaviour as Li/MgO, albeit that its stability appeared very limited. It was proposed that Li_2CO_3 is an active catalyst or catalyst precursor in Li/MgO. As to the Li/MgO catalyst, the C_2 selectivity has an optimum with respect to the amount of lithium loading as shown in Figure 6.3.1. This optimum shifts to higher loadings when the reaction temperature is increased. It is of interest to know if this tendency continues. Therefore, the catalytic activities of lithium carbonate, pure and doped with minor amounts of magnesium oxide, have been tested.

Lithium carbonate melts at 723°C, which makes it impossible to investigate the catalytic activity of pure lithium carbonate or heavily doped Li/MgO catalysts in a fixed-bed reactor at higher temperatures. The lithium carbonate would just melt and trickle downwards in the reactor. Therefore, a bubble column reactor was developed in our laboratory in order to investigate liquid catalyst systems.

Results & Discussion

The reactions were carried out in a micro-flow reactor system operated at atmospheric pressure, described in Chapter 5.1, in which the fixed bed reactor is replaced by a bubble column reactor. The carbon dioxide partial pressure inside the reactor was kept at 0.01 bar by addition of CO_2 to the feed. This was sufficiently high to keep the lithium in its carbonate form, in agreement with thermodynamic calculations. Lithium carbonate (Merck extra pure) and MgO (Merck p.a.) were used as the starting materials for the catalysts, which were made by slurrying the solids in water followed by evaporation, drying and grinding (Ref. 8). No calcination took place before reaction. Conversions and selectivities were calculated on carbon bases.

Table 6.3.1 shows the catalytic performance of solid and liquid lithium carbonate (18 g) as a function of temperature. The methane conversion decreases slightly, but the oxygen conversion increases with temperature which is accompanied by a dramatic loss of hydrocarbon selectivity. From 700°C to 800°C the C_2 selectivity drops from 55 % to only 2.4 %. Qualitatively this is in agreement with the reaction mechanism proposed (Ref. 8). At higher temperatures, consecutive reactions, i.e. the oxidation of C_2 hydrocarbons, become more important and cause the selectivity drop. Despite the decrease in specific surface when Li_2CO_3 melts, the activity, in terms of oxygen conversion, increases.

To investigate the influence of magnesium oxide on the catalytic behaviour of lithium carbonate, catalysts with different MgO/Li_2CO_3 ratios were prepared. Under reaction

conditions, magnesium oxide is present as a solid powder, suspended in the liquid. The presence of magnesium oxide has a significant effect on the selectivity, particularly at the high concentration level (compare Table 6.3.2 and Table 6.3.1). This proves that the Li/MgO catalyst is not just a carrier covered with a molten Li_2CO_3/Li_2O phase, but that magnesium oxide plays an essential role. Former investigations (Ref. 7) have shown that deactivation of the lithium doped magnesium oxide catalysts occurred in a fixed-bed reactor, but deactivation was not observed here. This can be explained by two facts. First of all there is no loss of Li or segregation of Li and MgO possible in the slurry system, in which there is an abundance of liquid Li_2CO_3. So, the composition is not changing. Secondly, the co-feed of CO_2 might also be important, as Korf et. al. (Ref. 10) have shown that it stabilizes these catalysts.

Conclusions

In conclusion, it can be said that minor amounts of higher hydrocarbons were obtained from molten lithium carbonate. However, addition of magnesium oxide to lithium carbonate is very beneficial for the production of ethane and ethylene and opens the possibility of the creation of (new) active centres. These centres could be mainly responsible for the catalytic coupling activity, as it is known that only a small part of the total Li-content in Li/MgO causes the high activity observed during methane coupling (Ref. 21). In this respect, it can be said that the interaction of Li with Mg is essential for a high C_2 yield. For reasons of heat removal, a bubble column reactor might be a suitable reactor for a methane oxidative coupling process. However, further research in order to develop improved catalysts has to be done.

7. REACTION MECHANISM AND KINETICS OF THE OXIDATIVE COUPLING OF METHANE OVER Li/MgO.

7.1. COMPARISON BETWEEN CATALYTIC AND NON-CATALYTIC METHANE CONVERSION.

Introduction

Methane can be converted to ethylene with the aid of oxygen over Li/MgO catalysts. At the reaction temperatures used (800°C) non-catalytic reactions cannot be excluded. The role of the catalyst is therefore not yet clear. Investigation of both catalytic and non-catalytic methane conversion can clarify the reaction mechanism of the process and elucidate the role of the catalyst.

Results and discussion

Experiments were carried out in the quartz micro fixed bed reactor operated at atmospheric pressure described previously. Figure 7.1.1 shows the product selectivity of a deactivated Li/MgO catalyst diluted with quartz particles as function of the oxygen conversion. In the same figure also the product selectivity of pure gas phase oxidative coupling is plotted. As can be seen a remarkable resemblance between gas phase oxidation and catalytic activation exists concerning product selectivity at the same oxygen conversion. The catalytic experiment needs much shorter contact times to reach a high conversion level compared to the non-catalytic experiment. This is due mainly to the difference in surface area in contact with the gas phase. This picture confirms that the catalytic oxidative coupling of methane at 800°C always consists of a homogeneous and a heterogeneous part. However, this picture could also imply that a catalyst is not needed. When on the other hand the gas phase coupling is compared to a fresh Li/MgO catalytic performance the beneficial effect of the catalyst can be seen (Figure 7.1.2). With the non catalytic methane coupling the C_{2+} yield is tied to a maximum of about 7% while with Li/MgO catalyst the C_{2+} yield which can be reached (with the same gas feed) is at least a factor 2 to 3 larger (18%). The contact time can be very short due to the high activity. For gas phase methane activation the contact time has to be longer to reach high conversion levels resulting in product oxidation. This explains the high selectivity observed over Li/MgO.

Conclusions

1. Both non-catalytic and catalytic conversion of methane to ethylene is possible, although the C_{2+} yield is much higher with than without a catalyst.

2. The catalytic conversion of methane cannot be separated from the non-catalytic reactions. Homogeneous gas phase reactions play an important role in the reaction mechanism.

7.2. INFLUENCE OF THE PROCESS CONDITIONS.

Introduction

The influence of the oxygen partial pressure, the helium partial pressure and the size of the pre- and post-catalytic spaces on the oxidative methane coupling catalyzed by Li/MgO will be successively discussed in this section.

Influence of the oxygen partial pressure.

The influence of the oxygen partial pressure was determined at a total flow of 125 Ncm^3/min, W/F = 0.48 gs/Ncm^3 and a constant methane partial pressure of 0.6 bar. Figure 7.2.1 shows an optimum in the ethylene selectivity at an oxygen partial pressure of 0.03 bar. At low oxygen partial pressures, the carbon monoxide and carbon dioxide selectivities approach zero. This is to be expected, since only pyrolysis reactions can occur without oxygen and, therefore, only ethane, ethylene and acetylene can be formed. The proposed reaction mechanism, shown in Figure 7.2.2, also suggests that ethane is the only product at low oxygen partial pressures. When more oxygen is present, a consecutive reaction to ethylene can take place on one hand, while the methyl radicals can react in the gas phase to form carbon oxides on the other hand.

With increasing amounts of oxygen in the feed, the combustion reactions become more and more predominant. Finally, mainly CO and CO_2 are observed. In summary; the results of this experiment fit the proposed reaction mechanism.

Influence of the helium partial pressure.

The influence of the helium partial pressure was determined at a steady total flow of 120 Ncm^3/min and a constant methane/oxygen ratio of five. From Figure 7.2.3, it appears that a larger helium partial pressure, which means a dilution to a higher extent, results in higher selectivities to ethane and ethylene and lower selectivities with respect to CO and CO_2.

Otsuka (Refs. 4 and 22) owes many of the high yields he obtained to the high degree of dilution he used in his experiments. However, his production, in terms of absolute mole C_2H_4 per weight of catalyst per second, was very small.

This can be explained by the fact that the formation of ethylene and ethane is of a different and lower reaction order than the production of carbon oxides. Dilution with an inert gas is thus responsible for the formation of less CO and CO_2.

Variation in the sizes of the pre- and post-catalytic spaces.

It is clear from Figure 3.1.4 that gas phase reactions taking place before the reaction mixture has reached the catalyst bed, i.e. reactions in the pre-catalytic space, can be

minimized by shortening the (corresponding) residence time. Now, it will be very interesting to know what happens after the bed. Figure 7.2.4 shows an experiment in which the space after the catalyst bed, which was heated at the same temperature as the catalyst bed itself, was varied in a way described in Ref. 7. The process conditions were carefully chosen so that the conversion in the pre-catalytic zone was negligible and that the oxygen, which was in short supply, became completely converted within the catalyst bed.

It can be clearly seen in Figure 7.2.4, that the methane conversion is constant. So, evidently, methane is not reacting in the absence of oxygen. Furthermore, selectivities with respect to the carbon oxides are hardly influenced by changing the post-catalytic space, which means that the water gas shift reaction, (water and hydrogen are present as reaction products), is rather slow compared to the cracking reactions. The most important reaction that takes place is the conversion of ethane into ethylene. This means that, in a commercial process, a large empty space after the catalyst bed (fixed, bubbling or fluidised) can have the beneficial function of an ethane cracker which improves the ethylene yield and utilizes part of the excess heat of the oxidation reactions.

Quite different results were obtained when similar experiments were carried out at conditions where the oxygen is only partly consumed in the catalyst bed. The remaining oxygen appears to react for a great deal with other molecules than methane, as shown in Figure 7.2.5. As a result less ethylene and ethane and much more CO is produced.

Combining the conclusions from this paragraph enables the definition of optimal conditions for the production of ethylene from methane by oxidative coupling. These conditions can be qualitatively defined by:

-a short residence time
-a low oxygen partial pressure
-a small pre-catalytic space
-complete conversion of oxygen within the catalyst bed
-utilization of the post-catalytic space as an "ethane cracker"

7.3. HOMOGENEOUS GAS PHASE EXPERIMENTS IN A CSTR.

Introduction

The experiments that will be presented here concern homogeneous gas phase reactions in a well mixed reactor (=CSTR). See Chapter 5 for a description of the set-up and the recycle reactor. The latter is operated in the CSTR mode. The advantage of this type of operation is that no concentration gradients are present inside the reactor. The concentrations in the reactor can be adapted by adding extra feed gases or changing feed ratios. A number of experiments have been carried out in which the effect of CO_2, water, hydrogen and ethane on the oxidative coupling of methane is investigated.

In all the experiments the following conditions have been chosen:

Reactor temperature:	1073 or 1173 K
Reactor pressure:	1.10 - 1.25 bar
Reactor volume:	10 cm^3
Integral feed:	50 - 60 Ncm^3/min
Differential feed:	1700 - 2600 Ncm^3/min
Recycle ratio:	30 - 50

Results and conclusions

The effect of carbon dioxide on the gas phase reactions has not yet been reported, whereas its effect on the catalytic reactions is extensively described in literature (Ref. 10). In Figure 7.3.1 an experiment is shown, in which the carbon dioxide partial pressure in the reactor is varied by adding CO_2 to the other feed gases. The residence time is kept constant by diminishing the helium feed with the same amount as the CO_2 added. It is clear from this figure, that carbon dioxide has no effect at all. No changes occur in the partial pressures inside the reactor. This is in agreement with the model developed to simulate the homogenous gas phase reactions (Ref. 23). The formation of carbon dioxide in the gas phase is rather slow, but its decomposition is still much slower.

By cooling the recycle stream in a condenser kept at 273 K, the main part of the water was removed and so its effect on the oxidative coupling of methane could be observed. A higher water partial pressure increases both the methane and oxygen conversion. This is not caused by higher partial pressures of methane or oxygen, because these are equal and lower respectively, see Figure 7.3.2. The net production rates of ethylene and propylene are hardly influenced by the water partial pressure. The net production rate of ethane decreases a little bit, whereas the CO_2 formation rate increases due to an increased CO concentration. So, the C_{2+} selectivity drops when the water concentration in the reactor rises.

Figure 7.3.3 depicts the effect of the addition of hydrogen to the feed at a constant residence time. The water production and the oxygen consumption are accelerated. So, the hydrogen is burned to water, which causes a lower C_{2+} and a higher CO and CO_2 selectivity, compare Figure 7.3.2 with 7.3.3. The effect of water and hydrogen are indeed

similar.
Ethane is added to the primary feed of the reactor to investigate its effect on the reaction rates. The partial pressures of methane and oxygen in the reactor are kept constant by increasing their feed flows. The residence time is kept constant by using the helium as a balance. At the chosen conditions, T = 1073 K, the effect is tremendous, see Figure 7.3.4. The conversion of methane is increased 12 times and that of oxygen by 10 times. As a result the concentrations of especially ethylene, and, to a smaller extent, CO and CO_2 are higher, whereas the propylene concentration drops in contradiction to what is expected. This experiment proves without doubt that ethane can be dehydrogenated much more rapidly than methane. Ethane is converted into radicals relatively easily and it therefore acts as an initiator for the oxidative coupling of methane.

7.4. LOW PRESSURE CATALYTIC REACTIONS

Introduction

The aim of low pressure experiments is to further clarify the gas phase and catalytic reaction steps in the oxidative coupling of methane. The pressures used lie around 100 Pa and this means that the reaction rates are lowered by at least a factor of 100. The advantage is that consecutive reactions can be distinguished and that second order reactions are hardly occurring.

Results and discussion

Figure 7.4.1 and 7.4.2 show the oxidative coupling of methane with and without a 7 wt% Li/MgO catalyst at a total pressure of 60 Pa with a gas flow rate of 10^{-7} mole/s as a function of the reaction temperature. As expected the presence of a catalyst hardly matters at the short contact times applied. At low pressure the reaction rates are lowered so longer contact times are needed to detect conversion. This can be done by carrying out batch experiments and follow the course of the reaction over a long period. Figure 7.4.3 and 7.4.4 show the methane batch oxidation with and without the presence of the Li/MgO catalyst. Again without catalyst almost no conversion can be detected during 1 hour reaction at 800°C. With catalyst clearly methane activation is occurring. Surprisingly, the C_{2+} product fraction is very low and the dominant products are the total oxidation products CO and CO_2. This means that coupling products are not formed in a first step or rapidly converted to total oxidation products at the catalyst surface. More likely however is that at the low pressure applied the methyl radicals formed by hydrogen abstraction of methane can only react at the catalyst surface and cannot combine in the gas phase. For coupling they must loose their energy and this is (at low pressure) only possible at the catalyst surface. The chance of being oxidized at the catalyst surface is greater than coupling with another methyl radical. This theory is confirmed by atmospheric experiments with varying diluent gas concentration. Figure 7.2.3 shows the change in product selectivity as function of the helium diluent concentration during oxidative coupling of methane carried out at 100 kPa and 800°C. Clearly one can see the beneficial effect of more diluent on the C_{2+} selectivity. The partial pressures of methane and oxygen are lowered as in the low pressure experiments, but the total pressures remains at 100kPa. This means that gas phase coupling of methyl radicals is favoured. High concentrations of inert gas reduces the oxidation of the radicals in the gas phase but improves the coupling efficiency. This means that the homogeneous radical gas phase reactions play a very important part in the C_{2+} selectivity which can be reached. This also lays constrains on the comparison of different coupling catalysts. A different diluent concentration can mean a large difference in the C_{2+} selectivity.

From atmospheric experiments it was concluded that the reaction mechanism of the methane coupling to ethylene occurred via a model of consecutive reactions (Ref. 24). Methane is first converted to a methyl radical by a hydrogen abstraction step occurring at the catalyst. These methyl radicals react further in gas phase to ethane which in turn is dehydrogenated to ethylene. The ethylene is burned to CO and the CO is catalytically converted to CO_2. In order to test this reaction mechanism and to eliminate gas phase

contributions we carried out ethane and ethylene oxidation experiments at low pressure.

Therefore a $C_2H_6/O_2/Ne$ (5/5/1) was fed to the low pressure reactor. Figure 7.4.5 and 7.4.6 show the ethane oxidation with and without catalyst as function of the temperature. Again gas phase oxidation does not occur but with Li/MgO catalyst oxidation sets in between 600°C - 800°C. Beside total oxidation products ethylene is formed. Hydrogen abstraction and formation of ethylene takes place at the catalyst surface. This confirms our ideas about the consecutive model. We also carried out the same experiments with an ethylene oxygen mixture. The results were as we expected: total oxidation to CO and CO_2. (Figure 7.4.7).

The best way of showing the that the consecutive model is correct is done by carrying out an ethane batch experiment. Figure 7.4.8 shows the product distribution of an ethane oxygen batch experiment over Li/MgO. Clearly the fraction of ethylene is coming up first followed by CO_2. The fraction of CO is nearly constant during the whole time. This means that it is converted relative rapid to CO_2. This last reaction is catalyzed by the Li/MgO catalyst because the same experiment without catalyst shows that CO and C_2H_4 are the main products (Figure 7.4.9).

Conclusions

Low pressure experiments can give substantial information on the reaction mechanism of the catalytic oxidative coupling of methane. It makes discrimination between homogeneous and heterogeneous reactions possible. The role of the Li/MgO catalyst during oxidative coupling of methane is that of a methane activator which produces methyl radicals which couple preferentially in the gas phase. The ethane and ethylene formed are rapidly oxidized to CO and CO_2 at the catalyst surface. A high diluent concentration in the gas phase strongly influences the C_{2+} selectivity by favouring the gas coupling of methyl radicals and preventing their oxidation.

7.5. PLASMA EXPERIMENTS

Introduction

Beside the micro fixed bed and fluidized bed reactors used to carry out catalytic experiments in our laboratory also a completely different type of reactor was developed in cooperation with the Physics Department of our University. It concerns a plasma reactor which seems suitable to study radical reactions occurring during methane conversion to ethylene. The advantage of this kind of reactor is the possibility of making a controlled amount of radicals which can be brought into contact with the catalyst.

The plasma used for chemical reactions usually contains neutral atoms and molecules, ions, electrons, and photons. The desired atomic or molecular species are obtained through the various interactions that the neutral species undergo with energetic electrons and/or photons. Figure 7.5.1 shows the evolution of the voltage with the current intensity for various kinds of discharges (Ref. 25).

The plasma that we apply is the normal glow discharge which consists of zones with different properties. Figure 7.5.2 shows the potential versus the distance between the cathode and anode. As can be seen the potential difference is large close to the cathode, whereas in the positive column hardly no potential difference exists. By placing the gas inlet directly in the positive column we eliminate the influence of high energy electrons taking part in the reaction and cracking all the methane. The radicals produced in the positive column are formed by interaction of metastables (Ar^* or H_2^*) with methane leading either to CH_3 or CH_2 radicals. The energy of the metastables lies around 11.5 eV being enough for abstraction of two hydrogen atoms from methane but not for more (C-H bounding energy = 4.5 eV). The radicals formed can only react at the reactor wall because of the low pressure in the reactor (320 Pa). By change of the reactor wall the influence of a surface on the radical reactions can be studied.

Results and discussion

Figure 7.5.3 shows the product distribution of the light hydrocarbons as function of the gas inlet position in the reactor.
Ethane is the primary product followed by propane, butane etc. Acetylene is formed via the coupling of two CH_2 radicals by loosing two hydrogen atoms. Direct ethylene formation from the coupling of two CH_2 radicals is energetically not favoured. Its energy of formation is too high:

$$CH_2 + CH_2 \qquad C_2H_4 \qquad dE = 10 \text{ eV}$$

$$CH_2 + CH_2 \qquad C_2H_2 + 2H \qquad dE = 1.1 \text{ eV}$$

Ethylene is produced as a consecutive product from ethane. This is clearly shown by carrying out the same experiment but cooling down the reactor wall (Table 7.5.1).

The once formed ethane sticks to the reactor wall and can only react with radicals from the gas phase. At room temperature ethane returns to the gas phase and is also attacked by metastables. Hydrogen abstraction occurs and ethylene can be formed. Due

to these consecutive reactions all the hydrogens from methane or products can be abstracted resulting in a carbonaceous layer deposited at the reactor wall. The same experiment at liquid nitrogen temperatures prevents the consecutive reactions. Cooling down leads to a polymer layer of saturated hydrocarbons on the reactor wall. The main conclusion from these experiments is that once methane is activated and radicals are formed all coupling reactions can occur easily without any activation needed, even at 77K. The idea is that our Li/MgO catalyst does the same as the plasma does: activation of methane leading to radicals which can react further in the gas phase or on the surface. This is supported by experiments with Li/MgO in the plasma reactor.

Placing the Li/MgO catalyst in the plasma reactor may reveal a possible role in radical coupling reactions. According to Ito et al. (Ref. 20) Li^+O^- centres are the main source for methane activation. These centres are formed at high temperatures in the present of gas phase oxygen. The same centres can also be formed at 100K by UV irradiation. With this technique it is possible to produce the active centres which are responsible for methane activation at high temperatures and study their influence on radical coupling reactions. An effect of the Li/MgO catalyst on radical coupling reactions is investigated by carrying out methane activation experiments with the striated column in the presence of activated Li/MgO. Table 7.5.2 shows the product distribution of a plasma activation experiment with and without activated Li/MgO in the reactor. There are differences in product distribution which can be ascribed to the presence of the Li/MgO catalyst. The catalyst produces more acetylene at the expense of propane, implying that the growth of long hydrocarbons is retarded. The catalyst favours the coupling of $CH_2^{\cdot}$ radicals assuming that acetylene is formed by coupling of two $CH_2^{\cdot}$ radicals, but the effect is not very pronounced. However, between activated and non activated Li/MgO no difference was detected. Probably the number of active sites are too low to detect any difference and during reaction there is no oxygen present, so site regeneration is not possible.

Summarizing the results confirms our general idea of the working of the Li/MgO catalyst in the oxidative coupling of methane: A methane activator which produces a lot of methyl radicals which couple preferably in the gas phase. At the oxidic catalyst no pronounced beneficial effect on radical coupling reactions can detected

Conclusions

The striated column makes it possible to activate methane and produce methyl radicals at low temperature. At the low pressures applied radical reactions take place mainly at the reactor wall. Consecutive reactions are suppressed by freezing the products formed in at the reactor wall. Comparison between a Li/MgO surface and a quartz surface shows that radical reactions are not greatly influenced by the Li/MgO catalyst surface.

7.6. TRANSIENT RESPONSE MEASUREMENTS.

Introduction

An isotope switching experiment, in which one labelled reactant replaces the normal species without disturbing the steady state of reaction is a method which can help to elucidate the reaction path of the oxidative coupling of methane and to give insight in the working mechanism of the catalytic cycle (Ref. 26). We carried out experiments in which we switched from a $CH_4/^{16}O_2/He$ to a $CH_4/^{18}O_2/He$ feed gas mixture. This will elucidate the oxygen pathway over Li/MgO as well as the number of exchangeable oxygen. Analogous experiments with a switch from $^{12}CH_4/O_2/He$ to $^{13}CH_4/O_2/He$ will make it possible to follow the carbon pathway during oxidative coupling.

Results and discussion

Figure 7.6.1 shows the oxygen response as function of the time after the switch. Clearly a fast oxygen response can be seen although it lasts at least 50 seconds before the $^{18}O_2$ reaches its steady state level. This means that oxygen adsorption and/or exchange with the catalyst is occurring and that this must be pretty fast. Also the mixed oxygen form ($^{16}O^{18}O$) is observed but the oxygen scrambling is not at equilibrium. It can be concluded that the O = O bond is broken quite easily at the catalyst surface and that oxygen is incorporated in the bulk of the catalyst. During the course of the reaction the oxygen is incorporated in water and carbon dioxide. The responses of these components were also monitored by scanning the mass numbers (m/e) 20 ($H_2{}^{18}O$), 44 ($C^{16}O_2$), 46 ($C^{16}O^{18}O$), 48 ($C^{18}O_2$). Figure 7.6.2 shows the measured response curves which result in a remarkable difference compared to the oxygen response. It takes at least 200 seconds for the $C^{18}O_2$ to reach its steady state level. This can mean that strong CO_2 adsorption is occurring or that carbonate decomposition is taken place as the decomposition of Li_2CO_3 is believed to be essential in the working principle of the Li/MgO catalyst. Also oxygen scrambling in CO_2 is occurring, because $C^{16}O^{18}O$ is clearly observed, although not at equilibrium. The water ($H_2{}^{18}O$) response is also very slow compared to the oxygen response indicating again water adsorption or fast oxygen incorporation into the lattice.

Table 7.6.1 shows the total rate of product formation before and after the isotopic switch confirming that no isotopic effects are occurring which could alter the total reaction rate. Table 7.6.2 shows the total amount of ^{16}O atoms which is replaced by ^{18}O atoms. These numbers are calculated by integration of the response curves of the oxygen containing products. The sum of these numbers is the total amount of replaced ^{16}O. This number can be related to the number of atomic layers of the catalyst which take part in the oxidation process. Assuming that the catalyst contains about 10^{19} atoms/m^2 and combining this with the surface area (1 m^2/g) and the catalyst amount in the reactor (0.25g) it can be calculated that about 10 lattice layers of the catalyst are exchanged. Probably this is related to 2 -3 carbonate layers which cover the catalyst surface.

The $^{13}CH_4$ switch experiments will give us information about the incorporation of ^{13}C into the catalyst and into the coupling products (C_2H_6,C_2H_4). Figure 7.6.3 shows the CH_4 response after the isotopic switch. Also a trace of Argon was added to the feed to determine whether methane adsorption was occurring. As expected no measurable methane adsorption was occurring because the methane response is identical to the

argon response which does not adsorb. This effect confirms our idea that methane reacts from the gas phase with adsorbed oxygen in a ELEY -RIDEAL mechanism. Methyl radicals are released into the gas phase and couple there to form ethane. This is confirmed by the monitoring of mass (m/e) 26 which results mainly from $^{12}C_2H_4$. The response of this signal is analogous to the $^{12}CH_4$ signal. The coupling products are also not adsorbed at the catalyst surface and react identically as methane. They are formed preferentially in the gas phase via radical reactions. This means that with our equipment with a time resolution of 1 second the actual coupling reactions cannot be followed.
Interesting to know is the carbon dioxide response which is monitored via mass (m/e) 44 ($^{12}CO_2$) and mass 45 ($^{13}CO_2$). Figure 7.6.4 shows the CO_2 response compared to the argon trace. The responses do not differ significantly indicating that CO_2 is hardly adsorbed at 800°C. The $^{13}CO_2$ signal reaches its steady state level within a few seconds indicating that the carbon atom is not incorporated into the lattice of the catalyst. The question now arises how this can be matched with the slow $C^{18}O_2$ response (200 s). This paradox can be explained by the phenomenon that the oxygen in CO_2 is exchanged rather fast and incorporated into the catalyst whilst the carbon in CO_2 is not. The slow $C^{18}O_2$ response can so be brought back to a capacity effect of oxygen exchange of the Li/MgO catalyst. The CO_2 is being formed at the catalyst surface and before it is released into the gas phase the oxygen can be exchanged with oxygen in the catalyst.
Figure 7.6.5 gives a possible oxygen pathway which explains the observed experimental results. The oxygen is adsorbed at the catalyst surface and at the same time partly incorporated into the catalyst lattice. CO_2 is formed from methane or methyl radicals colliding with the active oxygen at the catalyst surface. The CO_2 formed is not strongly bound to the surface but the oxygen in the CO_2 exchanges rather fast with the oxygen from the catalyst. The water which is formed during the methane activation is also desorbed fast into the gas phase. However, also the exchange of the oxygen in the water molecule with the catalyst is rather fast. It can be concluded that the Li/MgO catalyst exchanges the oxygen rather fast. The oxygen in the Li_2CO_3-MgO layer is exchanged rather quickly.
Figure 7.6.6 shows the working principle of the Li/MgO catalyst during oxidative coupling of methane at 800°C. Active centres are created by uptake of oxygen by the Li/MgO catalyst. These centres react with methane from the gas phase to create methyl radicals which combine in the gas phase to ethane. The amount of active centres is very low, but they are very active in methane activation. The high activity of the catalyst can be explained by a fast regeneration of the active centres via a fast oxygen uptake. However, the CO_2 which is also formed can react with the catalyst and form extra Li_2CO_3, which is not active for methane activation. The carbonate is dispersed over the catalyst and in that way protects the oxidation of methyl radicals and products formed. This explains why this catalyst has such an excellent performance in methane coupling. It has a small amount of very active centres and at the same time a large surface which is passive towards total oxidation.

Conclusions

The excellent coupling performance of the Li/MgO catalysts is due to the presence of the Li_2CO_3 phase which is in equilibrium with an oxidic lithium phase which is capable of a fast uptake of gas phase oxygen which is very active in methane activation. The Li_2CO_3 phase prevents the total oxidation of the products formed by covering part of the

Li/MgO catalyst surface. Gas phase oxygen is incorporated into the lattice of the catalyst.

The carbonate in the catalyst is not exchanging fast with gas phase CO_2. Most of the lithium in the Li/MgO catalyst is present in the Li_2CO_3 phase which is a function of the CO_2 partial pressure at 800°C. After a few hours on stream the catalyst reaches the so called stabilization phase which means that the lithium content has become very low (<0.5 wt%) and it is well dispersed over the catalyst. The carbonate is bound quite strongly to the catalyst, because hardly any ^{13}C is built into the catalyst. This means that the active species are not created in a continuous process of carbonate decomposition in the presence of oxygen, but that a small amount of another Lithium phase (e.g. Li_2O) is present, which causes the oxygen uptake and transport into the lattice of the catalyst.

7.7. THE INVESTIGATION OF INDIVIDUAL REACTION STEPS

Introduction

To elucidate the importance of various reaction steps in the oxidative conversion of methane, experiments were carried out with three reaction products: ethane, ethylene and carbon monoxide. These products were studied separately in oxidation experiments with and without a catalyst. Moreover, the effect of admixing them to a methane/oxygen feed was investigated. All experiments were carried out in a micro flow tubular quartz reactor which was either empty or filled with lithium doped magnesium catalysts at a temperature of 800 °C. The reactor set-up is described in Chapter 5.1. Conditions were chosen similar to those used in methane oxidative coupling experiments.

Results & Discussion

First, experiments were carried out in an empty reactor. The results are shown in Figure 7.7.1. It appears that ethane is oxidized much easier than methane, which starts to be converted at a much higher temperature (A figure is not shown; the temperature difference is more than 150 °C). The main product is ethylene. Ethylene is oxidized even faster than is ethane, the main product being CO. The difference in oxidation rate between ethane and methane correlates with the difference in C-H bond strength in these molecules (CH_4: 104 ± 1 kcal/mole, C_2H_6: 98 ± 1 kcal/mole (Ref. 27)), and the fact that hydrogen abstraction undoubtedly is the rate determining step. The high reactivity of ethylene must be due to the fact that oxygen or oxygen-containing radicals attack the double bond. The fact that the conversion level of ethylene is lower than that of ethane is not reflecting kinetics. The only reason is that oxygen consumption is complete in both cases and that the oxidation of ethylene consumes much more oxygen per hydrocarbon molecule than does that of methane.

Similar experiments were next carried out in a reactor filled with the lithium/magnesium oxide catalyst. The results are surprisingly similar to those just described, except for a remarkable shift in the selectivities with respect to the carbon oxides, as shown in Figure 7.7.2. The oxidation of CO to CO_2 is apparently strongly accelerated by the catalyst. Additional evidence stems from a similar shift that was observed during the deactivation of the catalyst in the methane oxidation experiments (Figure 7.7.3).

Direct proof of the activity of the catalyst for CO oxidation is produced by separate CO oxidation experiments, as shown in Figure 7.7.4. Initially, very high rates are achieved with a catalyst. Significant deactivation occurs, which may be explained by poisoning of the catalyst by CO_2, as proven by Korf et al. (Ref. 10). However, even after catalyst deactivation, the conversion level of CO is an order of magnitude larger than in the absence of the catalyst.

Although the oxidation of ethane and ethylene separately fed to the reactor gives valuable information, cofeeding with methane is even more interesting. Ethane is present in natural gas, and moreover, recycling of the ethane is of interest to improve the ethylene yield. Cofeeding of ethylene is particularly useful to obtain more reliable data

on its stability (its relative reactivity with respect to methane) under actual reaction conditions. The results of ethane and ethylene cofeeding (Figure 7.7.5) show remarkable similarities. All the corresponding curves in these figures have practically the same shape. It seems to make no difference whether ethane or ethylene is fed to the methane/oxygen flow. Apparently, ethane is rapidly converted into ethylene, maybe even before methane oxidation starts.

The top diagrams in Figure 7.7.5 show the actual concentrations of methane and hydrogen, corrected for the small changes in the total volume that occurs. The feed gas contains 45 mole% of methane; the shaded area therefore represents the methane conversion. It is clear that the addition of C_2's to the feed stream decreases the methane conversion, because part of the oxygen available is consumed by the C_2's added. The two extra hydrogen atoms of ethane, in comparison to ethylene, cause somewhat higher hydrogen and water concentrations at the outlet of the reactor than in the case of ethylene addition. Furthermore, it is shown that the more C_2 is added, the more carbon monoxide is produced, which is in agreement with the ethylene experiments; see Figure 7.7.1. This CO is oxidized further to CO_2, the production of which also increases. However, at high added mole fractions, the oxygen is used by C_2's before CO can be oxidized, and this results in a diminished CO_2 production.

The C_3 concentrations are shown a hundred-fold magnified in Figure 7.7.5. No C_4-products could be detected. The C_3 production is enhanced by C_2 cofeeding, but the amounts formed remain relatively small. Methane oxidation thus appears to be a rather selective process for the production of ethylene, particularly if ethane is recycled. One should realize however, that the net C_2 production rapidly decreases when ethane is added. It is already zero at an added mole fraction ethane of 2 %.

Conclusions

It is believed that the oxidative methane coupling mainly occurs via radicals and that an appreciable part of the reaction sequence takes place in the homogeneous gas phase. A simplified scheme is shown in Figure 7.7.6. The bold arrows indicate the main reaction path, as emerges from our results.

The catalyst plays an essential role in at least two reaction steps: besides the initiation reaction, the oxidation of CO to CO_2 is also catalyzed, as is established in this work. As it is known that high initial ethane selectivities can be achieved (Refs. 4 and 22), CH_3· radicals apparently first combine to ethane. This ethane is then very rapidly converted into ethylene, which is further oxidized into carbon monoxide either directly or via formaldehyde. The C_3 products play a minor role in this mechanism due to their low formation rates. Calculations with a computer simulation program, see Ref. 23, have confirmed this.

In conclusion, it can be said that the conversion of methane to C_2 is relatively slow in comparison to the oxidation of C_2 into CO. This puts serious constraints on the maximum attainable yield. A graphical representation of the attainable yield as a function of conversion is given in Figure 7.7.7, this is calculated according to the simplest parallel-consecutive reaction scheme, and assumes that all reactions are first order with

respect to hydrocarbon and the have the same order with respect to oxygen (Ref. 28). The data points in Figure 7.7.7 show that the catalyst studied here corresponds to k2/k1 = 0.25 (initial selectivity = 80%) and k3/k1 = 3. Both excellent initial selectivities and low relative combustion rates of ethylene are required to obtain high selectivities at a reasonable conversion level. The relative combustion rate of ethylene, in particular, deserves more attention in catalyst evaluation studies.

7.8. DIFFERENTIAL KINETIC MEASUREMENTS IN A FIXED BED REACTOR

Introduction

Differential kinetic measurements will result in kinetic parameters with which the methane coupling over Li/MgO can be described. This is essential for the reactor design and the process development. Before kinetic measurements of a catalytic reaction can be carried out it has to be verified whether transport limitations and catalyst deactivation are occurring. Therefore experiments were done to determine the stability of the catalyst when changing the process conditions and to find out whether transport limitations, internal or external, were playing an important role at the reaction conditions applied in the kinetic measurements.

Catalyst stability and transport limitations experiments.

Catalyst stability. The stability of the catalyst was investigated by varying the process conditions for 15 minutes and returning to the standard conditions to check what the influence of the changes were. The standard conditions are: Temperature 800°C, $CH_4/O_2=5$, $CH_4/He=1.25$, $W/F= 0.30$ g.s/ml(s.t.p.) and quartz dilution (50% on weight basis) of the catalyst bed.
Figure 7.8.1 shows the influence of changes in process conditions on the conversion and product selectivity. The following changes were applied:

- Temperature rise to 900°C
- Feed gas composition change to helium and to oxygen/helium
- CH_4/O_2 change from 2 to 10

From Figure 7.8.1 it its clear that the process condition changes applied do not influence the steady operation of the catalyst. In this way the catalyst is suited for kinetic measurements. In Figure 7.8.2 the influence of cool off and start up on the catalytic performance has been investigated. This means that the catalyst has been cooled down to room temperature and has been heated-up to 800°C again after 16 hours. It is shown that the normal catalytic behaviour is not influenced by such an operation. However, catalyst deactivation does occur, caused by lithium loss as described previously. This is a slow but continuing process even after prolonged reaction time. It is therefore necessary to carry out kinetic measurements within the shortest possible time range. The most accurate experiments are carried out within the time range of a few hours. Even then repeated experiments at standard conditions are required to measure deactivation and account for it in the interpretation of the results, which might otherwise lead to erroneous results.

Transport limitations. Transport limitations regarding solid catalysts are divided into two areas: internal and external.
Internal diffusion limitation is related to the pore structure of the catalyst. The catalyst particle size determines the pore length over which the gaseous reactants have to diffuse. The time the reactants spent in the pores in relation to the their reactivity is a measure for the occurrence of internal diffusion limitations. This can have effects on the product

selectivity. The occurrence of internal transport limitations was investigated by carrying out catalytic experiments with varying catalyst particle size (0.1 to 0.8 mm). The desired catalyst particle sizes were obtained by grinding and sieving a batch of calcined catalyst into the desired fractions.
Figure 7.8.3 shows the conversion as function of time on stream for different catalyst particle sizes. Only the smallest catalyst fraction behaves differently : it deactivates more strongly. This can be explained by the fact that the smallest particle size has the highest specific surface area from which lithium components can volatilize more easily due to the lowest diffusional resistance path for lithium salts to diffuse to the outer surface. Effects on the product selectivity are not present as shown in Figure 7.8.4. where the product selectivity is plotted against the oxygen conversion. This confirms transport limitation calculations which also predict the absence of pore diffusion.
External diffusion limitations were tested by varying the linear gas velocity at constant contact time (W/F). Figure 7.8.5 shows the conversion as function of the total gas flow at constant W/F. It clearly shows that there is no effect of flow on the activity of the catalyst, at least at the linear gas velocities used here. Effect on the selectivities are also not present as shown in Figure 7.8.6.

Differential kinetic measurements.

This paragraph describes the results of differential kinetic measurements carried out in a micro fixed bed reactor as described previously. The aim is to determine the overall reaction order in methane and oxygen during oxidative coupling of methane over a Li/MgO catalyst.
The process conditions applied were : temperature 800°C, pressure 1 bar, total flow rate = 8.33 Nml/s, catalyst weight = 0.25 g. The fresh catalyst contained 4.27% Li/(Li+MgO) and the particle size used was 0.25 - 0.30 mm.
The reaction rate was measured after the deactivation rate had been decreased to an acceptable level (approximately after 40 hours on stream). The reaction rate was measured for four different methane and oxygen concentrations in the feed gas mixture. The exact compositions are shown in Table 7.8.1.
The reaction rate (r_m) was calculated as mole/kg cat. s. :

$$rm = F_m/W * X_m \qquad (7.8.1)$$

W = Catalyst weight (kg)
F_m = Flow rate in mole CH_4 /s
X_m = Methane conversion

Figure 7.8.7 shows the reaction rate as function of methane and oxygen partial pressure respectively. Correlating this result with the simple power rate equation leads to:

$$r_m = k * [pCH_4]^a * [pO_2]^b$$

a = 0.91 ± 0.12
b = 0.62 ± 0.13
k = 0.145 ± 0.015

with pressures in bar.

One can conclude from these data that the overall reaction rate is first order in methane and half order in oxygen. The order 0.5 with respect to oxygen can be explained in two ways: 1) Oxygen is rapidly and reversibly dissociated into "active surface atoms". The adsorption is weak, hence the concentration of surface oxygen atoms is proportional to the oxygen pressure. As a result the power law is correctly describing the kinetics. 2) Molecular oxygen is involved in the rate determining process. It is relatively strongly adsorbed. This may result in an apparent reaction order of 0.5, although an Eley Rideal equation should fit the data better. Indeed it appears possible to fit our data to the following equation:

$$r_m = k_1 * [pCH_4] * [pO_2]/(1+bO_2*[pO_2])$$

$k_1 = 0.45$
$bO_2 = 5$

with pressures in bar.

Unfortunately, it was not possible to discriminate between the two models suggested. Some deactivation inevitably occurred in the time between the methane variation at constant oxygen pressure and the oxygen variation experiment at constant methane pressure. The high accuracy required for a reliable choice could therefore not be achieved.

Conclusions

The Li/MgO catalyst performance is not influence by periodic short variations in process conditions. However, catalyst deactivation is a continuous process, which limits the time scale on which the kinetic measurements should be performed.
There are no transport limitations at the reaction conditions applied. This is also predicted by transport limitation calculations.
The overall kinetics of the oxidative coupling of methane over Li/MgO catalyst were determined by differential measurements. The results can be summarized:

$$r_a = 0.145 \pm 0.015 * pCH_4^{0.91\pm0.12} * pO_2^{0.62\pm0.13} \text{ mole } CH_4/\text{kg. s.}$$

pressures in bar.

The kinetics can be well described with an ELEY-RIDEAL kind of mechanism in which methane from the gas phase reacts with adsorbed oxygen on the catalyst surface.

7.9. KINETICS OF THE "PARTIAL" OXIDATION OF ETHANE AND ETHYLENE.

Introduction

The main reaction path of the oxidative coupling of methane over Li/MgO catalysts goes via methane to ethane to ethylene and finally to carbon oxides, see Ref. 24. As is stated in Chapter 7.7, the main selectivity loss at high methane conversion levels is caused by combustion of the ethylene produced. Therefore, the formation of ethylene and its decomposition are of utmost importance. So, the kinetics of ethane and ethylene oxidation have been investigated.

Results & Discussion

All the experiments described in this chapter were carried out with a micro flow reactor set-up, which is described in Chapter 5.1, in combination with the specially developed reactor (which has a "block-form" temperature profile), described in the same chapter.

Ethylene oxidation

For both the homogeneous and heterogeneous ethylene oxidation the kinetic parameters were determined, see Table 7.9.1. The reaction orders have been determined with an accuracy of ± 0.4. For both the homogeneous gas phase and the catalytic reaction the order in oxygen is higher than it of the oxidative coupling of methane, which partly explains why a low oxygen partial pressure favours the C_2 hydrocarbon selectivity. The two activation energies derived from the experiments are both lower than the literature values of the initiation reactions of an ethane/oxygen gas mixture, see Table 7.9.2. This is to be expected, since part of the ethylene is converted by the propagation reactions, having low activation energies and also because the catalyzed reactions are expected to have lower activation energies. At 746 °C and at an oxygen and an ethylene partial pressure of both 0.2 bars, the ratio of the heterogeneous and homogeneous reaction rates is almost 3 $m^3_{\text{gas phase}} / m^3_{\text{catalyst bed}}$.

Ethane oxidation

Kinetic parameters of ethane oxidation have been determined for the homogeneous gas phase only. Direct oxidation of ethane into carbon oxides is not an important reaction, since the initial selectivity with respect to ethylene is nearly 100%. The reaction order in oxygen is 0.96 and for ethane it is 0.19. This reaction is strongly pressure dependant (a small pressure increase from 1.2 to 1.8 bars results in an ethylene selectivity drop of over 40% and an increase in ethane conversion from 28 to 85 %), which makes it interesting to compare homogeneous and heterogeneous reaction rates at slightly elevated pressure. In Table 7.9.3 this comparison is shown and it is evident that the Li/MgO is active in converting ethane. Of course this is not surprising, since methane and ethane are molecules of the same kind. Under the conditions applied, the

heterogeneous reaction is a factor one and a half times faster.

Conclusions

The Li/MgO catalyst activates both the conversion of ethane into ethylene and the oxidation of ethylene into carbon oxides. This opens the opportunity to develop a catalyst in such a way that it activates the methane and ethane only. The ethylene oxidation can than be minimized, which will results in high selectivities even at high methane conversion levels.

7.10. ELEVATED PRESSURE EXPERIMENTS

Introduction

The influence of the pressure on the oxidative coupling of methane is not yet extensively investigated. In literature so-called high pressure experiments have been reported by a group of Japanese workers (Refs. 29,30,31) for the homogeneous gas phase reactions. The reactor pressure amounted to 16 bars. However, more than 84% of the feed consisted of nitrogen, so the actual pressure of reactants was only 2.5 bars. Catalytic experiments described by Labinger (Refs. 32 and 33) do not exceed 3 bars. In our laboratory, preliminary experiments showed that especially for the oxidative dehydrogenation of ethane the pressure influence was large, see Chapter 7.9. Therefore, a set-up has been designed and constructed, as is described in Chapter 5.1, to measure under elevated pressures.

Results and discussion

Experiments have been carried out with an empty reactor and with the Li/MgO catalyst. Figure 7.10.1 shows the conversions and selectivities for the empty reactor. At 4 bars the reactions are ignited; the methane conversion is greater than zero. An increase in pressure results in increased conversions. The selectivity shifts from ethane to ethylene to carbon monoxide. The carbon dioxide partial pressure is rather low. This is in agreement with the simulations of Chapter 7.11. that show that the oxidation of carbon monoxide in the gas phase is a relative slow process.

The influence of the pressure on the catalytic reactions is shown in Figure 7.10.2. The lithium doped magnesia used was aged for 5 days to get a stable catalytic performance. By changing the flow rate with pressure, the residence time in the reactor was kept constant. The methane conversion is not influenced by changing the pressure as was the case for the homogeneous gas phase reactions, see Figure 7.10.1. An increase in pressure results in lower C_{2+} selectivities and higher CO_x production rates, but the effects are not detrimental.

Conclusions

It is feasible to carry out the oxidative coupling of methane under elevated pressures without oxidizing all the desired C_2 products. The heat production per unit of volume of the reactor increases more than linear with pressure, which easily results in heat transfer limitations and can result in hot spots or even run-away of the reactor. This most probably has limited the amount of articles that are concerned with real (= no dilution with inerts) elevated pressure experiments.

Economically, it is very interesting to work at higher than atmospheric pressures. Smaller, and thus cheaper, process equipment can be used and especially the expensive compressor, see Chapter 8.1, can be replaced by a much cheaper one.

7.11. KINETIC MODELLING

As is shown in Chapter 7.1, oxidative coupling of methane can occur in the homogeneous gas phase. A computer program has been developed to simulate and analyze those reactions. The program is based on a combination of a reaction and a reactor model. The latter is modelled as an one dimensional ideal plug flow reactor. The gas phase reactions take place according to a complex free radical mechanism which can be described by a set of elementary reactions, see Table 7.11.1. Each of these reactions is characterized by an extended Arrhenius expression for the reaction rate constant: $k = A \cdot T^b \cdot \exp(-Eact/R \cdot T)$

In which	A =	frequency factor	
	b =	non-linearity coefficient	[-]
	T =	absolute temperature	[K]
	Eact =	energy of activation	[kJ/mole]
	R =	gas constant	[kJ/(mole.K)]
	$A \cdot T^b$	for a first order reaction	[s^{-1}]
		for a second order reaction	[m^3/(mole·s)]
		for a third order reaction	[m^6/($mole^2$·s)]

An important feature of the model developed is its option for a kinetic sensitivity analysis. It determines the influence of each elementary reaction on the product distribution. The principle of the method is that the frequency factor of each reaction in turn is divided by a constant, for example 10, and that new concentrations resulting from the calculations are used to compute integral sensitivity factors. These are defined as $s_{ij} = \delta \ln c_i / \delta \ln k_j$, in which c_i = concentration of component i and k_j = rate constant of reaction j. A set of over 400 reactions, see Figure 7.11.1, could be reduced to the 164 reactions of Table 7.11.1 (Refs. 34,35,36,37,38,39,40,41,42,43,44) by omitting all the reactions which had no significant contribution to the product distribution. In this way, for example the formation of methanol and reactions in which a methyl dioxygen radical is involved were skipped. This simplifies the reaction network but at the same time limits the applicability to conditions relevant for the methane oxidative coupling. The product distribution turns out to be highly sensitive towards reactions no. 6, 13, 15, 16, 46, 54, and 70. A reasonable fit between the model and experimental data (Ref. 45) was obtained (see Figure 7.11.2), using the kinetic constants from the literature. Only minor changes (within reported accuracy limits) were applied for some of the most sensitive constants. Note that the ethylene selectivity predicted by the model is too low. This requires further attention. The negative ethylene selectivities at low methane conversion are caused by (calculated) conversion of traces of ethylene present in the feed.

Another powerful tool of the model is the integration of individual reaction rates over the reactor, thus demonstrating the most important reaction pathways. It appears that H, OH, HO_2, and CH_3 are the most reactive species. After an induction period in which the radical concentrations are built up, they stay fairly constant at typical concentrations of 10^{-7} - 10^{-4} mole/m^3. Figure 7.11.3 shows the main reactants and reaction pathways of carbon containing compounds. The thickness of the arrows corresponds to the contribution of the respective reaction. It may be obvious that the C_2-oxygenates, CH_2, CH, CH_3OH and other omitted species are unimportant. The most important initiation reaction no. 2, in which oxygen reacts with methane, appears to contribute very little to the methane conversion, and the same applies to other initiation reactions. The

formation of CH_3 radicals from methane appears in the scheme as a rapid system of equilibrium reactions in which various radicals are involved. In agreement with experimental results, the quantities of C_3-products are very limited, not because they are oxidized very fast, but because of their low rate of formation, see Figure 7.11.3. The C_2-species prefer to undergo hydrogen abstraction rather than coupling with methyl radicals. Ethane and ethyl radicals are hardly oxidized and the formation of CH_3 from C_2H_6 is negligibly small, which implies that extremely high initial ethylene selectivity of ethane oxidation should be achievable. This is confirmed, although not shown here, experimentally.

The trends of the effects of temperature, dilution and CH_4/O_2 on the selectivity of the reaction are very similar for both homogeneous gas phase reactions and the Li/MgO catalyzed reactions. We therefore assume that the reaction scheme is valuable for the catalytic reactions as well. A major difference is the formation of CH_3 radicals, the key component for a good C_{2+} selectivity, see Figure 7.11.3. A catalyst favours the (irreversible) formation of this radical (Ref. 46), involving oxygen and resulting in much higher levels of CH_3 radicals. Thus higher rates and higher coupling efficiencies may be achieved using a catalyst. In Table 7.11.2 simulations and experiments are shown, for both catalyzed and homogeneous gas phase reactions. The catalyst is simulated by a set of reactions that equals the overall reaction: $4\ CH_4 + O_2 \dashrightarrow 4\ CH_3 + 2\ H_2O$. As is shown, indeed the higher CH_3 radical formation rate results in a higher reaction rate and a higher ethane selectivity. The decrease in reaction time is however too large compared to the experimental value. Therefore, it is assumed that the catalyst also acts as a radical sink. Radicals collide with the surface and react to less active molecules. This lowers the radical concentrations and slows down the conversions of methane and oxygen.

Conclusions

The model developed simulates the experiments correctly. The main carbon reaction path goes via CH_3, C_2H_6, C_2H_5, towards C_2H_4, that is oxidized rapidly into CO. The most active reaction species in the homogeneous gas phase are the radicals H, OH, CH_3 and OH_2. C_3-hydrocarbons are hardly produced due to their low rate of formation. Simulations have made clear that the Li/MgO catalyst cannot be described as a methyl radical producer only: probably it also acts as an (aselective) radical consumer.

8. PROCESS DESIGN AND ECONOMIC EVALUATION STUDIES

8.1. ETHYLENE FROM NATURAL GAS BY DIRECT PARTIAL OXIDATION. A technical and economic evaluation study.

Summary

A new process has been designed for the production of ethylene from natural gas; methane, the main component of natural gas, is directly partially oxidized into ethylene by oxygen. In an economic evaluation, this process can be compared to naphtha cracking which is the most important commercial process for ethylene production presently. For the direct partial oxidation process, three different reactor types: a multi-tubular, a multi-stage and a fluidised-bed have been designed. The performance of the catalyst used was based on both data from literature and experiments. On the basis of a designed flow sheet, the investments and profitability have been estimated and compared with their equivalents of the naphtha cracking process based on a simplified flow sheet for an existing plant. A yearly ethylene production of 350,000 tons was assumed and the same plant location were chosen for both processes. It turned out that the direct partial oxidation process is technically feasible, and that it can be very attractive economically when better catalysts are developed. In conclusion, it is a very promising new method for the production of ethylene.

Introduction

Ethylene is the most important chemical from the petrochemical industry. In 1983 its total production was 34 million tons (the Centrally Planned Economies excluded). Oil is by far the most important source of ethylene. Most other feed stocks (see Figure 8.1.1), except for ethane that originates from natural gas, are of less interest economically, and when they are used it is often for political reasons. However, when the R/P ratios (proven reserve divided by annual consumption) of oil and natural gas are compared, see Figure 8.1.2 (Ref. 47), it is evident that the latter will be available for a longer period of time. Furthermore, remote natural gas fields and the excess natural gas from oil production call for a process to convert the gas into useful chemicals. Methanol, being an alternative for ethylene, has the disadvantage that its production route via synthesis gas (a mixture of CO and hydrogen) is rather expensive, whereas direct partial oxidation of natural gas into methanol is far from a commercial proposition, see Ref. 48. Great research efforts are being used nowadays on the oxidative coupling of methane and they are justified for the reasons mentioned above and the fact that a profitable process based on the oxidative coupling of methane may soon within reach. Indeed, it was reported in 1986 that the prospects of this new process are very good (Ref. 49).

In Figure 8.1.3, the performance of the best catalysts and results of non-catalytic experiments, as found in the literature, are shown. A complete list of the catalysts is given in Ref. 50. For the present feasibility study, two starting points have been chosen arbitrarily: Case A (30% methane conversion) and Case B (50% methane conversion) as indicated in Figure 8.1.3 by the triangles.

The reaction mechanism of the oxidative coupling of methane actually comprises a very complex set of catalytic reactions and gas phase radical reactions (Refs. 8 and 22). However, an extensive kinetic study with a Li/MgO catalyst, carried out in our laboratory, has pointed out that simple simplifications could be made which do not alter the basic kinetic diagram. In the calculations, only C_2H_x (ethane and ethylene in a fixed ratio of 2/3) and CO_x (carbon monoxide and carbon dioxide in a fixed ratio of 1/1) were considered as the reaction products and only three reactions, representing the main reaction paths (Ref. 8), were taken into account. The kinetic data used is shown in Figure 8.1.4 and give the selectivity-conversion relationship as is shown in Figure 8.1.3, with an ideal plug flow reactor.

Reactor and process design

Designs were made for a plant capacity of 350,000 tons of ethylene per annum. Oxygen and Dutch North Sea Gas (so-called Balgzand natural gas) and were taken as the feed stocks, see Table 8.1.1. The natural gas was purified to remove the higher hydrocarbons and sulphur containing components before it entered the coupling reactor. The feed conditions in all Cases were 700°C and 1 atmosphere pressure. Elevated pressures were not considered, because some preliminary calculations and experiments showed a dramatic loss of ethylene selectivity with high pressures.

Three reactor types were considered: a multi-tubular packed bed reactor, a multi-stage reactor (a series of adiabatic fixed beds with interstage cooling and oxygen feeding), and a fluidised bed reactor.

The multi-tubular reactor, although capable of giving 80% C_{2+}selectivity at 30 % CH_4 conversion and 50% C_{2+}selectivity at 50 % CH_4 conversion, was not attractive, as it appeared to be very sensitive for both runaway and extinction of the reaction. Moreover, the necessary high cooling temperatures demanded a combination of molten salts and water heat-exchangers in series, and ceramic tube wall material, because (stainless) steel is catalytically active in combusting the hydrocarbons. The impracticable great number of 100,000 tubes (diameter = 0.025 m, length = 1 m) filled with catalyst is required in order to produce 350,000 tons of C_2H_4/year.

A multi-stage reactor, see Table 8.1.2, cooled to 700°C between the stages, is much more flexible. The packed length of each stage was set after 200°C temperature rise or complete oxygen conversion; rather short beds (lengths of 5-10 cm) were found. For Case A: 5 stages with the oxygen feed split over stage 1 and 3 and for Case B: 11 stages were needed. Much higher ethylene selectivities than those in Figure 8.1.3 could be obtained if the number of stages was increased, see Figure 8.1.5; this caused a more even spread of the oxygen feed and a better temperature control. However, in order to slow down the aselective gas phase reactions, the oxygen had to be mixed very rapidly with the reactor gases in between the beds and this could be a problem in practice.

A fluidised bed reactor seemed to be the most suitable for this process. The design was based on an ideal dense phase mixing and plug flow bubble phase. Much better selectivities than those in Figure 8.1.3 were obtained, see Table 8.1.3; the low oxygen concentration in the dense phase being responsible. A great advantage of the fluidised bed was its nearly homogeneous temperature which is easy to control. Cold reactants could be fed into the reactor in order to prevent undesirable combustion reactions during preheating. Moreover, an aged catalyst could be easily replaced, even in continuous operation. Details of the fluidised bed designs for Cases A and B are shown

in Table 8.1.3.

Figure 8.1.6 shows the process flow sheet, including temperatures and pressures used in Case A (30% CH_4 conversion, 80% C_{2+} selectivity). The reactor feed was preheated by heat exchange with the product gas for the fixed bed reactor. A second reactor downstream of the coupling reactor, in which also a recycled ethane stream was injected, was an ethane cracker. This auto-thermal reactor, operated on the energy produced in the coupling reactor; it could be either a separated reactor or integrated into the coupling reactor as a post-catalytic zone (Ref. 7). Ethane was converted into ethylene (conversion = 60%, selectivity = 82%, a by-product was methane (Ref. 51)). About 85% of the water produced was quenched in a water stream at 34°C. The product gas was compressed from 1 to 40 bars by a three-stage compressor with cooling and water separation in between the stages. The gas flow entered the separation section at 40 bars together with the natural gas feed at 40 bars. A Catacarb unit removed most of the carbon dioxide and molecular sieves reduced the water and CO_2 content to ppm levels. Further product separation occurred in a cold box with three distillation columns, one gave the product ethylene and a small recycle stream of ethane, another produced the methane recycle stream and some fuel gas, including inert components. The methane recycle cooled down the cold box feed and the released energy provided by expansion of this stream was used in the compression section. Specifications of the process equipment for Case A is given in Table 8.1.4, further information can be found in Ref 49.

Investment estimate

The capital cost of the proposed new plant and an existing naphtha cracker (production capacity of 350.000 tons of ethylene a year) were estimated using Miller's method with a claimed accuracy of 25% (Ref. 52). That method is based on the costs of the main process items, to be derived from flow sheets; Figure 8.1.6 was used for Case A, a similar flow sheet for Case B, and for the cracking process, a flow sheet was used from an existing cracker. The differences in investments for the three types of coupling reactors did not justify further separated treatment. In Figure 8.1.7, the investment costs are broken down, extended information can be founded in Ref 49. Land, and working capital to a lesser extent, do not contribute much to those costs. The total capital investment amounts to US$ 479 millions for the cracker, to 168 for Case A, and to 207 for Case B at January 1989 price levels. So, the coupling process requires a substantially lower total capital investment due to its lower equipment and construction costs because it is a less complex plant.

Profitability analysis

Profitability analyses are needed to decide whether the projects are viable or not; they were carried out using Holland's method (Ref. 53). By-product credits were taken into account in all cases, they are of major importance in the naphtha cracking process. The net annual profits were US$ 9.5, 70, and 30 millions for the cracker, for Case A and Case B, respectively. Evidently, the designed new process would be more profitable than the cracking process. The higher profitability of Case A proves that a high selectivity was preferred to a high conversion level. The break-down of the production cost for ethylene

using the oxidative coupling process are shown in Figure 8.1.8. Indeed, it can be seen that the direct manufacturing expenses, which mainly consist of raw materials, contribute to more than half of the production costs. The credits for the by-products: electricity, that would be produced from the excess reaction heat, and the fuel gas, (see Figure 8.1.6) would reduce the production cost only slightly, especially for Case A.

The sensitivity of the ethylene price to major cost factors was investigated too. Figures 8.1.9 and 8.1.10 show its dependence on the raw material costs. The ethylene production cost is more sensitive to both the price of natural gas and oxygen for Case B, due to its lower raw material efficiency compared with Case A. Note that the ethylene bottom price (when the natural gas is available free of charge) is US$ 200/ton. Air could be used as the oxidizing agent instead of pure oxygen. The process equipment would expand due to the inert nitrogen present and it results in an ethylene production price of US$ 452 per ton (Case A). This would be slightly higher than when using pure oxygen at its standard oxygen price, see Figure 8.1.10. So, a small saving would be gained if the nitrogen was removed from air at the beginning of the process (before feeding to the coupling reactor) instead of at the end (in the cold box).

The ethylene production cost for the oxidative coupling process is seen to vary for Case A, from US$ 300 to US$ 600 with an average of US$ 446 per ton; for Case B these values are US$ 300 - 800 and US$ 566 respectively.

Figure 8.1.11 is most interesting, because it gives an impression of the performance required of a catalyst. It shows that a minimal selectivity of 65% is required for a profitable process at a C_2 yield of 25%. So, those figures should be one of the targets for the development of new catalysts.

Conclusions

In conclusion, it must be said that the oxidative coupling of methane is a very promising process. It is technically feasible and can be economically attractive. But, because of the short lifetimes of existing catalysts, more stable catalysts will have to be developed, so that they combine a high conversion with a high selectivity.

8.2. METHANOL FROM NATURAL GAS. PROVEN AND NEW TECHNOLOGIES.
A process design and economic evaluation study.

Summary

The world methanol consumption has surpassed 25 million tons per annum and is still growing steadily, indicating an increasing importance of methanol in the bulk chemicals market. At present, methanol is produced in a two step process: steam reforming of a hydrocarbon feedstock, followed by synthesis gas conversion into methanol.

Single step methanol production by partial oxidation of methane is a promising new catalytic process providing new opportunities for natural gas utilization. To study the economic perspective of such a new process and to set targets for further research, a process design study was carried out, based on literature data with respect to kinetics and yields. This study included investment and production cost estimates relative to those of existing plants.

The results prove that the new process is less economic, unless extremely selective catalysts are developed. Using the present data, the investment is of a similar level, while the variable costs are much higher due to the lower carbon efficiencies and the consumption of "expensive" oxygen.

Introduction

The world methanol supplies and demands are shown in Table 8.2.1 (Ref. 54). A small surplus in methanol production exists, which has lead to moderate market prices.

Methanol is nowadays produced by reforming (autothermal or steam) of hydrocarbons to synthesis gas which in its turn is converted to methanol. Among the sources of hydrocarbons: petroleum residues, naphtha, coal and natural gas, the latter is by far the most important. The important existing commercial processes: the ICI process and the Lurgi process are more or less equal (Ref. 55).

Historically, about a third of the methanol produced is used to make formaldehyde, see Figure 8.2.1. A large percentage of the formaldehyde is consumed in products for housing and the automotive market. These markets are highly sensitive to changes in the economy, which explains partly the major gains and losses in the methanol production. Fast growing consumers of methanol are the acetic acid production and the production of gasoline octane improvers such as Methyl-Tert-Butyl Ether (MTBE). A promising area is the direct use in fuels or a feedstock in Mobil's MTG (Methanol To Gasoline) process. Also promising is the production of Single Cell Proteins which can be used as animal food additives.

Besides the above described processes, a new not yet existing one is indicated by a dashed arrow in Figure 8.2.1. It is the direct partial oxidation of methane, the main component of natural gas, to methanol.

The direct oxidation of methane to methanol and formaldehyde has been investigated by several authors. Recent reviews have been published by Foster, Gesser and Hunter, and Edwards and Foster (Refs. 56,57,58). Oxygen, air and dinitrogen oxide have been proposed as oxidants and a wide range of materials have some catalytic activity (Ref. 59). However, high selectivities to methanol or formaldehyde are only

possible at very low conversion levels of methane, see Figure 8.2.2, resulting in poor yields.

However, in the future new better catalysts will be developed. In a US patent (Ref. 60) 80% methanol selectivity at 20% methane conversion is already claimed without the use of a catalyst. Therefore, starting points as stated in Table 8.2.2 were chosen for the present study.

Oxygen was chosen as the oxidizing agent, for it is relatively cheap. Because the methane conversion per pass is low, the surplus of methane has to be recycled. To prevent an enormous nitrogen recycle or an expensive separation of nitrogen/oxygen and methane in the recycle, pure oxygen is used.

Reactor design

A multi tubular fixed bed was chosen as the reactor, as it is easily scaled up. Preliminary calculations showed that heat removal from this reactor would not create serious problems. The following reactions in the catalyst bed have been taken into account:

$$CH_4 + 1/2\ O_2 \text{ ---> } CH_3OH$$

$$CH_4 + \quad O_2 \text{ ---> } CH_2O + \quad H_2O$$

$$CH_4 + 2\ O_2 \text{ ---> } CO_2 + 2\ H_2O$$

Because the literature provides very little kinetic data for these reactions, simple kinetics were assumed. The total rate has been based upon the kinetics of the first reaction only, which was assumed to be first order in both methane and oxygen concentrations. The yields of CO_2 and formaldehyde were derived from the selectivities; CO formation has been omitted since no information about the CO selectivity was available. Temperature dependence of the rate constant was estimated according to Arrhenius' law from published data. Relevant data are summarized in Table 8.2.3 (Ref. 61).

The reactor dimensions (tube length and diameter, and number of tubes) were determined by numerical simultaneous integration of the differential heat and mass balances. Heat removed through the tube walls is used to produce superheated steam at a pressure of 120 bars. Precautions were taken to prevent radial temperature profiles and pore diffusion limitation.

The basic design criterion was an approximately zero oxygen concentration in the reactor outlet to prevent consecutive oxidation reactions behind the catalyst bed. The reactor was to produce 400,000 tons/y of methanol, assuming 8000 operating hours a year.

More details are reported elsewhere (Ref. 62).

As an example of calculation results Figures 8.2.3 and 8.2.4 present the conversion and temperature profiles respectively inside the reactor for case A; the number of tubes is used as a parameter, while the tube diameter is fixed at 6 cm. A decrease of the number of tubes means an increasing superficial velocity. Correspondingly, a longer reactor must be used. Table 8.2.4 shows relevant reactor data that meet the demands of the design for case A.

Process design

A process flow diagram has been developed, a general outline of which is presented in Figure 8.2.5. Calculations were made using the flow sheet simulation program "Process" (Ref. 63).

So-called Balgzand gas is taken as feed for the plant; its composition is shown in Table 8.2.5. The higher hydrocarbons are assumed to be burned inside the reactor. Oxygen and natural gas are supposed to be delivered to the plant at 40 bar pressure.

Unconverted reactants are separated from the reactor effluent and recirculated to the reactor. Therefore, the stream leaving the reactor is cooled down to 300 K. In a vessel T1, liquid methanol is in equilibrium with and separated from a gas, which is subsequently washed with water in tower A1 for further methanol removal. Most formaldehyde is taken away with the water as well. The off-gas of the wash tower A1 is split into three: one part goes directly to the recirculation compressor, another part is fed to a Benfield unit for CO_2 removal, and a third part is purged to prevent accumulation of inert gases. The natural gas is directly fed into the Benfield unit to remove CO_2 and H_2S impurities. Before entering the reactor the recirculation stream is heated up to reaction temperature. Simple atmospheric distillation is applied in three columns to recover the methanol product. Detailed information about streams and main process equipment can be found in Ref. 62. The 120 bar steam, produced in the reactor R1 and heat exchanger H2, is used for heating the recirculation stream and for driving both the recirculation compressor C1 and the feed gas compressors C2 and C3.

Investment estimate

The capital investment, that is required for the production of 400,000 tons of methanol per year according to the process described in the previous paragraph, has been estimated, using the well-known Miller method (Refs. 64 and 65). In this method free-on-board-costs of shop-fabricated main process items are used as the starting point for the investment estimate. Additional costs as for installation, instrumentation, services, buildings etc. are calculated using specific factors based on experience. The way of determining such factors has been extensively described (Refs. 64 and 65). Miller's method, having an accuracy of about 25 % is very suitable for selection of the most profitable process from alternative designs. Therefore, the method has been applied to both cases A and B of the new process, as well as to the conventional way of methanol production. For the latter process the necessary information was supplied by Methanor, a large methanol manufacturer in Delfzijl, the Netherlands. A summary of the results of the calculations is presented in Table 8.2.6; more details are given in Ref. 63. It appears from this table that the new single step process does not lead to a considerable reduction of investment capital when compared to the conventional process. The main costs are the distillation section and the large heat exchange batteries, which become expensive, since the limited conversion levels require large capacities, and much recycling.

Profitability

The profitabilities of both the conventional and the direct partial oxidation process were determined using Holland's method (Refs. 65,66,67). This method is based on assumed relationships between costs and plant capacity and complexity. The total expenses are formed by the total manufacturing expenses (= all costs due to production), the depreciations (= 10% of total fixed capital) and the general expenses (= administrative costs, distribution, selling, research & development). The total manufacturing expenses are built up of the direct manufacturing expenses (= sum of raw materials, catalysts, utilities like electricity and water, labour, maintenance, and laboratory charges, minus byproduct credits) and the indirect manufacturing expenses (= overhead, package and storage, local taxes, and insurance). The annual profit after taxes is the revenues from sales minus the total expenses and minus the income taxes that have to be paid.

The natural gas price in the Netherlands is related to the oil price and the amount of consumed gas. Contract prices for large consumers are confidential information. In this study, a price of US $137.25/ton was assumed for gas delivered to the plant at 40 bar.

Oxygen will be supplied from a pipeline, also at 40 bar pressure, for a price of US $ 49.75/ton. Calculations and enquiries proved that the costs for on-site production of oxygen are similar. The number of operators who actually run the plant was calculated to equal 27, including shifts. The vent streams are burned to produce electricity with an efficiency of 50 % and at a price of US $0.05/kWh. Besides electricity, the revenues from sales exist mainly of methanol. Which January 1988 price of US $ 175.6 per ton was used.

In Table 8.2.7 the costs, at January 1988 price levels, are summarized for the conventional process and case A and B of the direct partial oxidation process. The profitabilities of both processes were negative at January 1988. For the conventional process this was confirmed by the Methanor company. However, the profitability of the direct partial oxidation process is even worse than the one of the conventional process. Extra costs for oxygen and a poorer methane utilization account for these differences, see Table 8.2.7, because the raw materials form the major part of the direct manufacturing expenses. For the same reason, a high selectivity per pass is preferred over a high methane conversion per pass, compare case A and B. Figure 8.2.6 shows calculations of the minimum selectivity at complete methane conversion needed for the new process to be profitable if only raw material costs are taken into account. It appears from the figure that an overall methanol selectivity of at least 75% is required. This is a very high selectivity level compared with performances reported in the literature, see Figure 8.2.1. Although the price ratio between methanol and natural gas has increased since January 1988, the targets for a profitable new methane to methanol process will be difficult to reach.

Conclusions

In conclusion, a new production route to methanol by direct partial oxidation of natural gas is chemically a very interesting one, because in principal a 100 % carbon efficiency can be achieved. The process is quite feasible using conventional technologies. However, a much better catalyst performance has to be achieved to meet the selectivity levels required for a profitable process.

9. CONCLUSIONS

The oxidative coupling of methane is a very promising new process to convert natural gas into ethylene. It is technically feasible and economically attractive, when C_{2+} yields of 25% (C_{2+} selectivity>60%) are achievable.

Li doped MgO is a very promising catalyst system for this process with which C_{2+} yields of 19% are reached. Essential for the Li/MgO catalytic mechanism is the presence of the Li_2CO_3 phase without which the catalyst is only little active and selective. Lithium is the active component in Li/MgO. Very small amounts of lithium are sufficient to create an active and selective Li/MgO catalyst. The biggest disadvantage however, is its stability because rapid deactivation occurs by lithium loss which is caused by volatilization of LiOH formed by reaction of Li_2CO_3 and water and by reaction with the quartz reactor wall forming lithium silicates.

From reactor point of view the fluidised bed reactor seems most suitable because of the high exothermicity of reaction. New fluidised bed catalysts have been developed (e.g. Sm, Na, Ca, Al oxides) which have excellent fluidisation behaviour and good catalytic performance.

From reactor design it would be attractive to operate methane coupling under high pressure. Experiments in a high pressure reactor set-up have shown that this is feasible without oxidizing all the desired C_2 products. However, the high heat production easily results in hot spots or even in run-away of the reactor.

The kinetics of the methane coupling over Li/MgO can be described as an Eley - Rideal mechanism in which gas phase methane reacts with adsorbed oxygen species at the catalyst surface. In this way methyl radicals are generated which couple to ethane in the gas phase. Ethane is dehydrogenated to ethylene which in turn gets easily oxidized into CO and CO_2. A kinetic model, which simulates the gas phase methane coupling supports this reaction mechanism and the main role of the catalyst as a methyl radical generator. However, it also makes clear that the catalyst has another role: an aselective radical consumer.

10. ACKNOWLEDGEMENT

The financial support of this research was provided in part by the European Communities in the framework of the Non-Nuclear Energy R&D programme, sub-programme "Optimization of the production and utilization of hydrocarbons", under contract no. EN3C-0038-NL (GDF) and is gratefully acknowledged.

11. LIST OF REFERENCES

1. G. Donat, Proceedings Seminar: "Optimization of the Production of Hydrocarbons", Ed. G. Imarisio, M. Frias and J.M. Bemtgen, Lyon, France, 1988, pp. 419 - 423.

2. G.E. Keller and M.M. Bhasin, J. Cat., 73, 1982, 9-19.

3. W. Hinsen and M. Baerns, Chem.- Ztg., 107, 1983, 223-226.

4. K. Otsuka, K. Jinno, A. Morikawa, Chem. Lett., 1985, 499-500.

5. T. Ito, J.H. Lunsford, Nature, London, 314, 1985, 721-722.

6. J.A. Sofranko, J.J. Leonard and C.A. Jones, J. Cat., 103, 1987, 302-310.

7. J.M.N. van Kasteren, J.W.M.H. Geerts, K. van der Wiele, Ethylene synthesis by catalytic oxidation of methane, Proc. 9th ICC, Ed. M.J. Phillips, Calgary, Canada, 1988, pp. 930-936.

8. J.W.M.H. Geerts, J.M.N. van Kasteren, K. van der Wiele, The investigations of individual reaction steps in the oxidative coupling of methane over lithium doped magnesium oxide, Cat. Today, 4, 1989, 453-461.

9. D.J. Driscoll, W. Martir, J-X. Wang, J.H. Lunsford, J.Am.Chem.Soc., 107,1985, 58-63.

10. S.J. Korf, J.A. Roos, N.A. de Bruin, J.G. van Ommen, J.R.H. Ross, J. Chem. Commun. Chem. Soc., 1987, 1433-1434.

11. J.W.M.H. Geerts, J.H.B.J. Hoebink, K. van der Wiele, to be presented at Boston ACS Meeting, April 22-27, 1990.

12. D. Geldart, Powder Technology, 1, 285, 1973.

13. S.J. Korf, J.A. Roos, J.M. Diphoorn, R.H.J. Veehof, J.G. van Ommen and J.R.H. Ross, Symposium on Direct Conversion of Methane to Higher Hemologues, Presented before the Division of Petroleum Chemistry, Inc., American Chemical Society, Los Angeles Meeting, September 25 - 30, 1988, 437 - 442.

14. K. Aika, T. Moriyama, N. Takasaki, and E. Iwamatsu, J. Chem. Soc. Chem. Commun., 1986, 1210-1211.

15. K. Aika, T. Nishiyama, J. Chem. Soc. Chem. Commun., 1988, 70-71.

16. J. Carreiro, G. Follmer, L. Lehmann, M. Baerns, Proc. 9th ICC, Ed. M.J. Phillips & M. Ternan, Calgary, Canada, 1988, 891-898.

17. C.A. Jones, J.J. Leonard, J.A. Sofranko, US Patent 4,443,644 - 4,443,649 & 4,444,984.

18. K. Otsuka, J. Jpn. Pet. Inst., 30 (6) 1987, 385-396.

19. J.A. Roos, A.G. Bakker, H. Bosch, J.G. van Ommen, J.R.H. Ross, Catal. Today, 1987, 1, 133-145.

20. T. Ito, J-X Wang, C-H Lin, J.H. Lunsford, J. Am. Chem. Soc., 107, 1985, 5062-5068.

21. J.M.N. van Kasteren, J.W.M.H. Geerts, K. van der Wiele, Proc. 1st World Congres, New Developments in Selective Oxidation, Ed. G. Centi & F. Trifiro, Rimini, 1989.

22. K. Otsuka, Q. Liu, M. Hatano, A. Morikawa, Chem. Lett., 1986, 903-906.

23. J.W.M.H. Geerts, Q. Chen, J.M.N. van Kasteren, K. van der Wiele, Thermodynamics and Kinetic Modelling of the Homogeneous Gas Phase Reactions of the Oxidative Coupling of Methane, Presented at 2nd European Workshop on Catalytic Methane Activation, May 1989, In press, Catal. Today, 1990.

24. J.W.M.H. Geerts, J.M.N. van Kasteren and K. van der Wiele, A Mechanistic Study on the Oxidative Coupling of Methane over Lithium doped Magnesium Oxide Catalysts, Proc. EC Congress: "Hydrocarbons: Source of Energy, Ed. G. Imarisio, M. Frias, J.M. Bemtgen, Lyon, France, 1988, 434-440.

25. F.M. Penning, Elektrische gasontladingen, Servire, Den Haag, 1955.

26. J. Happel, E. Walter and Y. Lecourtier, Ind. Eng. Chem. Fundam., 25, 1986, 704-712.

27. D.M. Golden, S.W. Benson, Chem. Rev., 69, 1969, 125.

28. O. Levenspiel, Chemical Reaction Engineering, 2nd edition, John Wiley & Sons, New York, 1972.

29. K. Asami, K. Omata, K. Fujimoto, H. Tominaga, J. Chem. Soc. Chem. Commun., 17, 1987, 1287-1288.

30. K. Asami, K. Omata, K. Fujimoto, H. Tominaga, Energy Fuels, 2, 1988, 574-577.

31. H. Tominaga, K. Fujimoto, T. Hikita, H. Takahashi, Jpn. Patent JP 63/222126, 1988.

32. J.A. Labinger, Catal. Lett., 1, 1988, 371-376.

33. J.A. Labinger, K.C. Ott, J. Phys. Chem.,91, 1987, 2682-2684.

34. W. Tsang, R.F. Hampsen, Chemical Kinetic Data Base for Combustion Chemistry, Part 1 Methane and related compounds, 1986, 1087-1279.

35. W.C. Gardiner (Ed.), Combustion Chemistry, Springler-Verlag, New York Inc., 1984, 197-360.

36. F. Westley, J.T. Herron, Compilation of Kinetic Data for Combustion Chemistry, Part 1 Non aromatic C,H,O,N, and S containing compounds, 1987.

37. J. Warnatz, Hydrocarbon Oxidation at High Temperatures, Ber. Bunsenges. Phys. Chem. 87, 1983, 1008-1022.

38. I.A. Vardanyan, A.B. Nalbandyan, On the mechanism of thermal Oxidation of Methane, Int. J. Chem. Kin., 17, 1985, 901-924.

39. P. Dagaut, M. Cathonnet, J.C. Boettner, Experimental Study and Kinetic Modelling of Propene Oxidation in a jet Stirred Flow Reactor, J. Phys. Chem., 1988, 661-671.

40. G. Rotzoll, Mass Spectrometric Investigation and Computer Modelling of CH_4-O_2-O_3 Reactions from 480 to 830 K, J. Phys. Chem., 90, 1986, 677-683.

41. H.D. Gesser, N.R. Hunter, C.B. Prakash, The Direct Conversion of Methane to Methanol by controlled Oxidation, Chemical Reviews, 85, 4, 1985, 235-244.

42. J. Nicholas, Chemical Kinetics, A Modern Survey of Gas Reactions, Harper & Row Ltd. London, 1976.

43. D.L. Baulch, D.D. Drysdale, D.G. Horne and A.C. Lloyd, Elevated Kinetic Data for High Temperature Reactions, Butterworths, London, 1972.

44. L.F. Albright, B.L. Crynes, W.H. Corcoran, (Ed.), Pyrolysis, theory and industrial practice, Academic Press, 1983.

45. J. Elbers, AKZO, personal communication.

46. D.J. Driscoll, J.H. Lunsford, Gas-Phase radical formation during the reactions of methane, ethane, ethylene and propylene over selected oxide catalysts, J. Phys. Chem. 89, 1985, 4415-4418.

47. B.P. Statistical Review of World Energy, British Petroleum Company PLC, London, 1988.

48. J.W.M.H. Geerts, J.H.B.J. Hoebink, K. van der Wiele, in press Catal. Today, 1990.

49. K. van der Wiele, I² Procestechnologie 1986, 1, 9-14, (in Dutch).

50. J.W.M.H. Geerts, J.H.B.J. Hoebink, Ethylene from natural gas, Internal Report, Eindhoven University of Technology, Eindhoven, The Netherlands, 1989.

51. Kirk, Othmer, Encyclopedia of Chemical Technology, John Wiley & Sons Inc., 1980, 9, 393-431.

52. C.A. Miller, Chemical Engineering, Sep. 1965, 226-236.

53. G.D. Ulrich, A Guide to Chemical Engineering Process Design and Economics, 1984, Wiley and Sons, Chapter 6.

54. Hydrocarbon Process., 65, 5, 1986, 36-37.

55. Hydrocarbon Process., 64, 11, 1985, 144-146.

56. N.R. Foster, Appl. Catal., 19, 1985, 1-11.

57. H.D. Gesser, N.R. Hunter, Chem. Rev. 4, 1985, 85.

58. J.H. Edwards, N.R. Foster, Fuel Sci. Technol., 4, 1986, 365-390.

59. S.T. Sie, Proc. 8th annual AIChE European Colloquium, Scheveningen, The Netherlands, 1987.

60. H.D. Gesser, N.R. Hunter, L. Morton, US Patent 4,618,732, 1986.

61. D.A. Dowden, G. Th. Walker, US Patent 1,244,001, 1968.

62. J.W.M.H. Geerts, J.H.B.J. Hoebink, K. van der Wiele, Methanol from natural gas, Internal Report, University of Technology, Eindhoven, The Netherlands, 1988.

63. Process: Simulation Sciences Inc., Ref. Manual, rev. 1, 1987.

64. C.A. Miller, Chem. Eng., 72, 13, 1965, 226-236.

65. G.D. Ulrich, A guide to chemical engineering process design and economics, J. Wiley & Sons, New York, 1984.

66. F.A. Holland, F.A. Watson, J.K. Wilkinson, Chem. Eng., 80, Aug 20, 1973, 139-144.

67. F.A. Holland, F.A. Watson, J.K. Wilkinson, Chem. Eng., 80, July 23, 1973, 118-121.

TABLES AND FIGURES OF THE REPORT

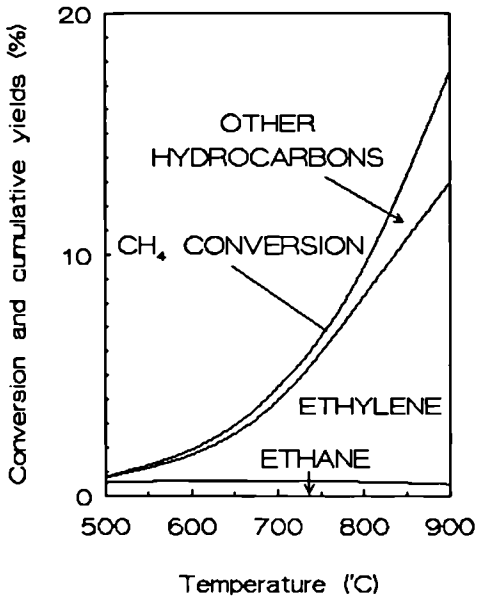

Figure 3.1.1 Calculated equilibrium gas composition of methane pyrolysis, excluding the formation of elementary carbon. P=1 bar.

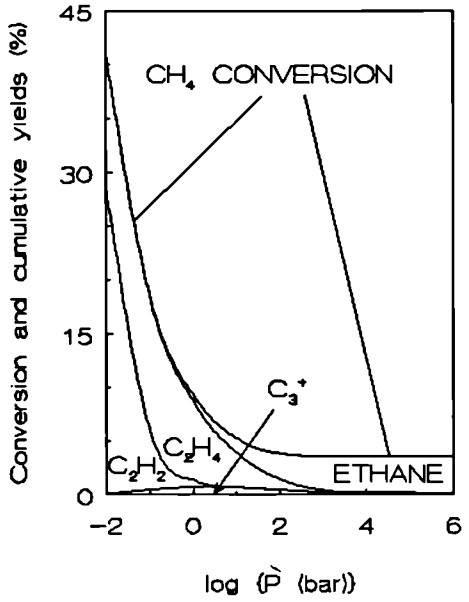

Figure 3.1.2 Calculated influence of the pressure on the equilibrium composition for methane pyrolysis. T=800°C.

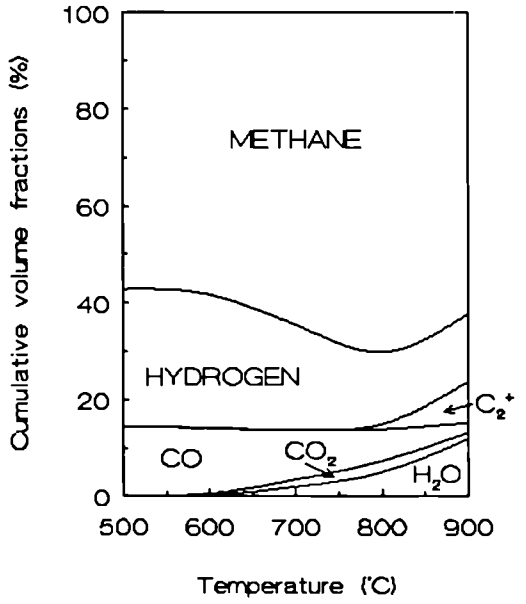

Figure 3.1.3 Calculated equilibrium composition for combined oxidation and pyrolysis of methane. $CH_4/O_2=10$, P=1 bar.

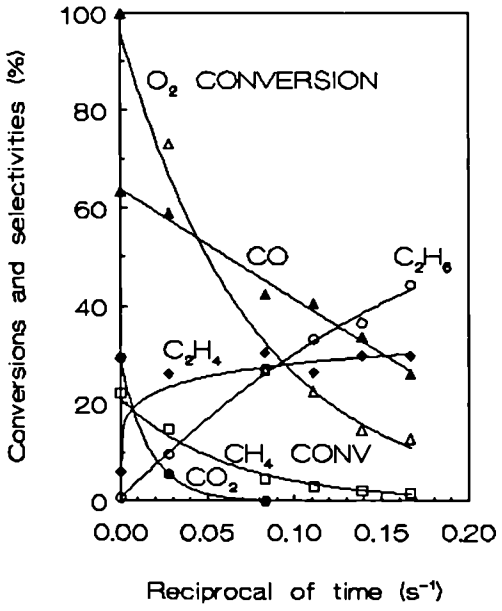

Figure 3.1.4 Influence of the residence time. Gas phase methane oxidation. P=1 bar, T=800°C, $CH_4/O_2=5$, $CH_4/He=0.8$.

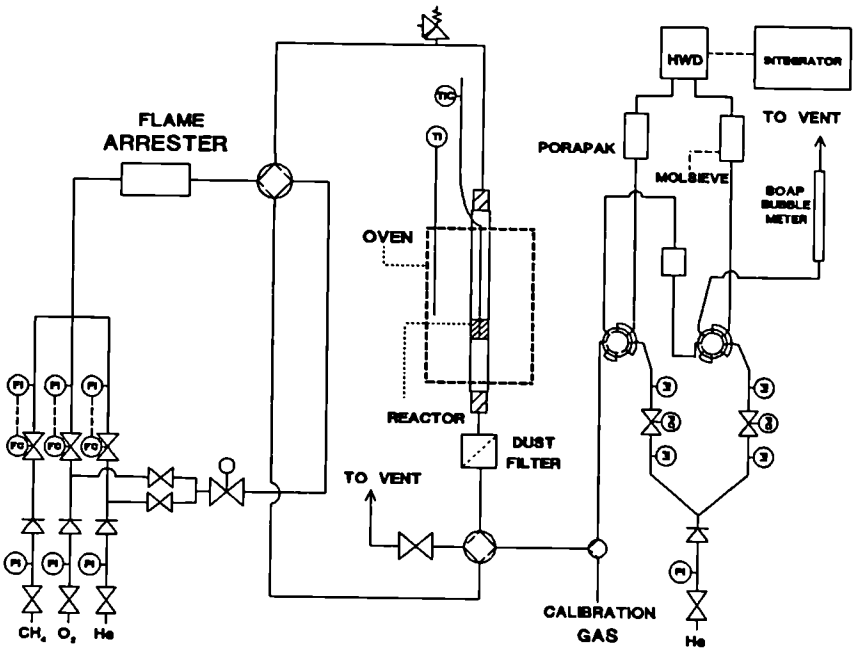

Figure 5.1.1. Reactor set-up for methane coupling experiments in a fixed bed reactor.

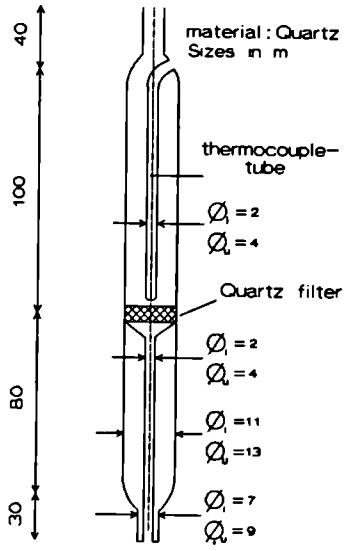

Figure 5.1.2. Quartz micro fixed bed reactor.

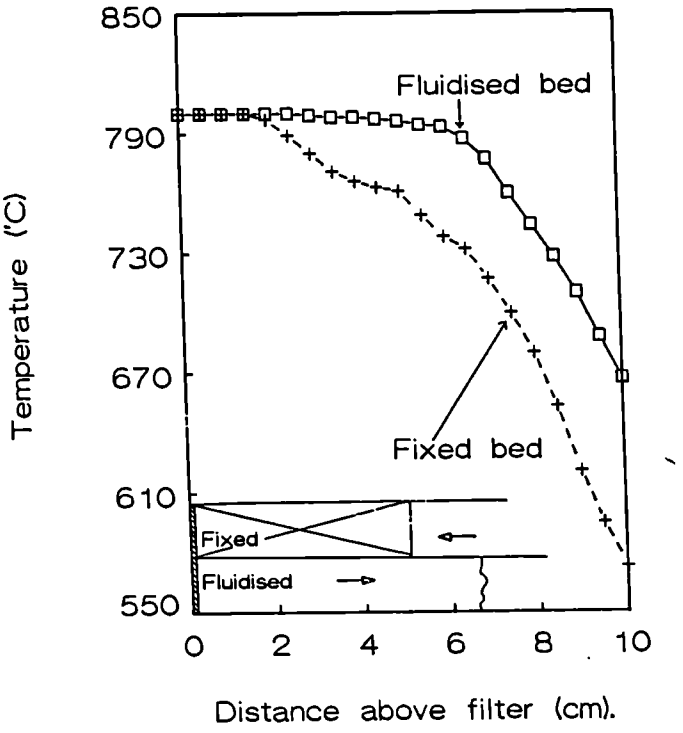

Figure 5.1.3: Axial temperature profiles of a fluidised and a fixed bed measured in the same reactor.

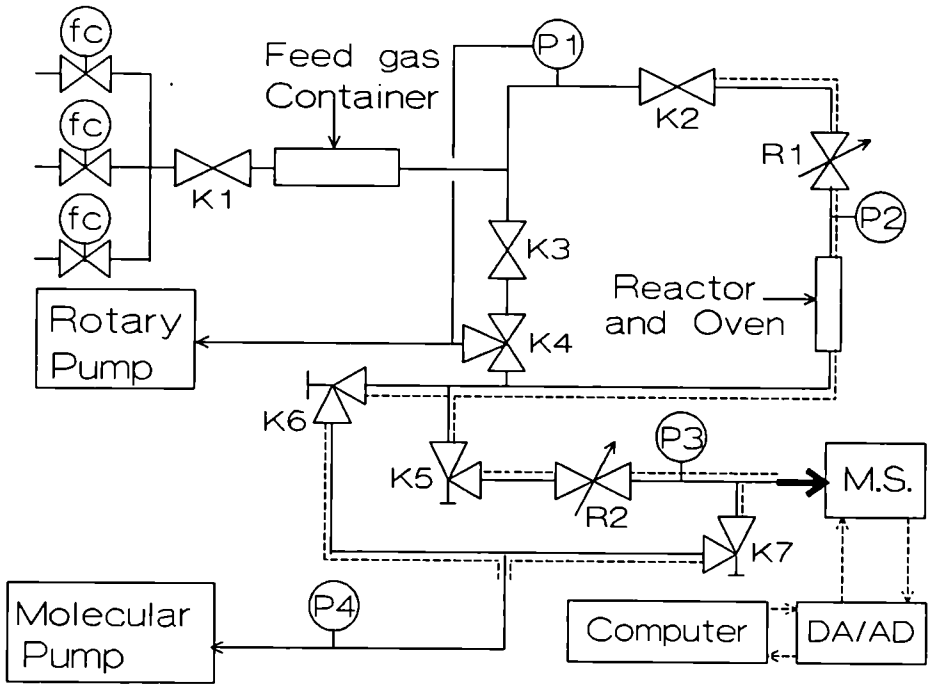

Figure 5.1.4. Reactor set-up for methane coupling experiments at low pressure.

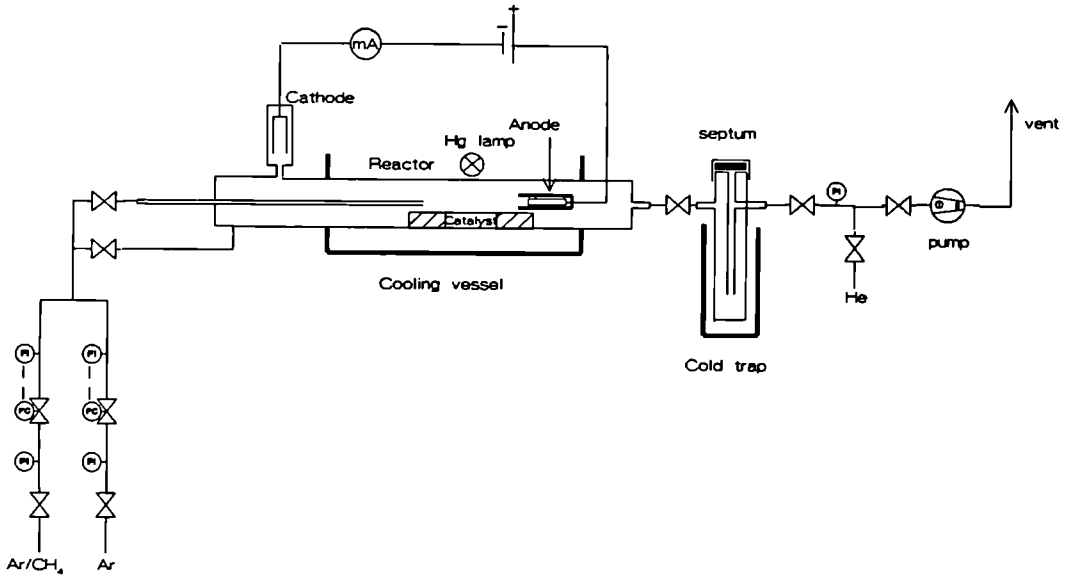

Figure 5.1.5. Reactor set-up for methane activation in a striated column reactor.

Table 5.1.1. Best fit of different feed gases

Composition	Mixture 1		Mixture 2	
	"Prepared"	Fit	"prepared"	Fit
CH_4	22.0	21.7	-	0.1
O_2	19.0	19.6	-	0.0
C_2H_6	-	0.0	16.0	14.0
C_2H_4	59.0	55.1	70.0	63.5
C_3H_8	-	-	19.0	15.2
Others	-	3.6	-	7.0

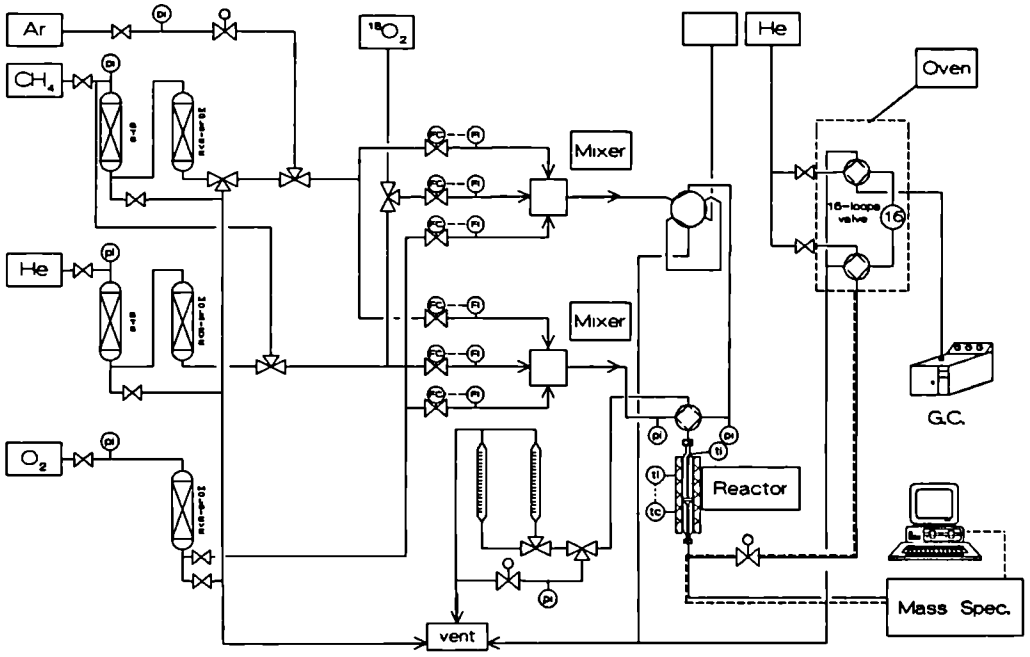

Figure 5.1.6. Reactor set-up for transient kinetic investigations.

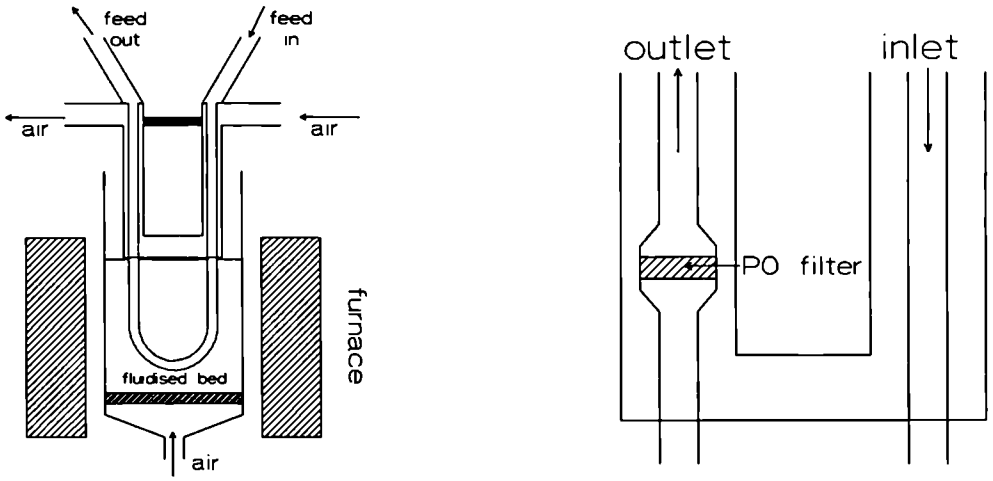

Figure 5.1.7: The new designed reactor in combination with the fluidised sand bed.

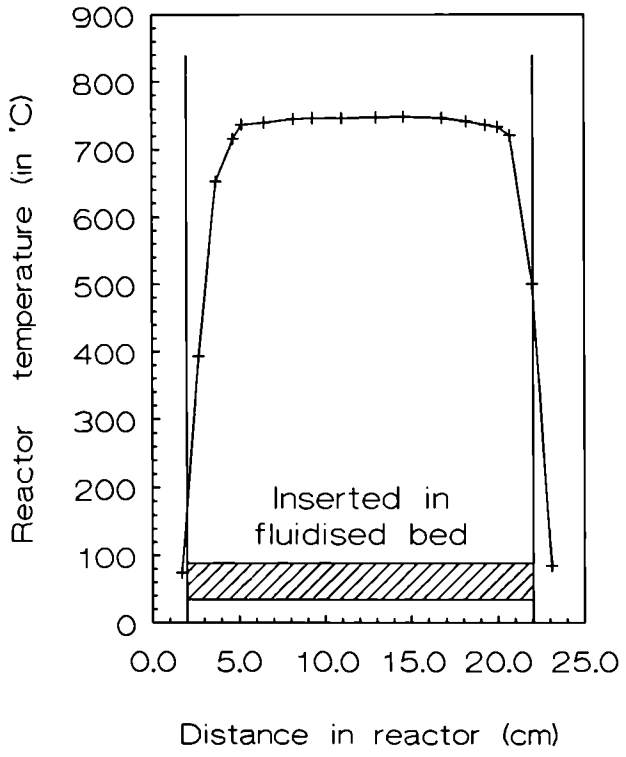

Figure 5.1.8: Axial temperature profile measured inside the new designed reactor which was inserted in the fluidised sand bed furnace.

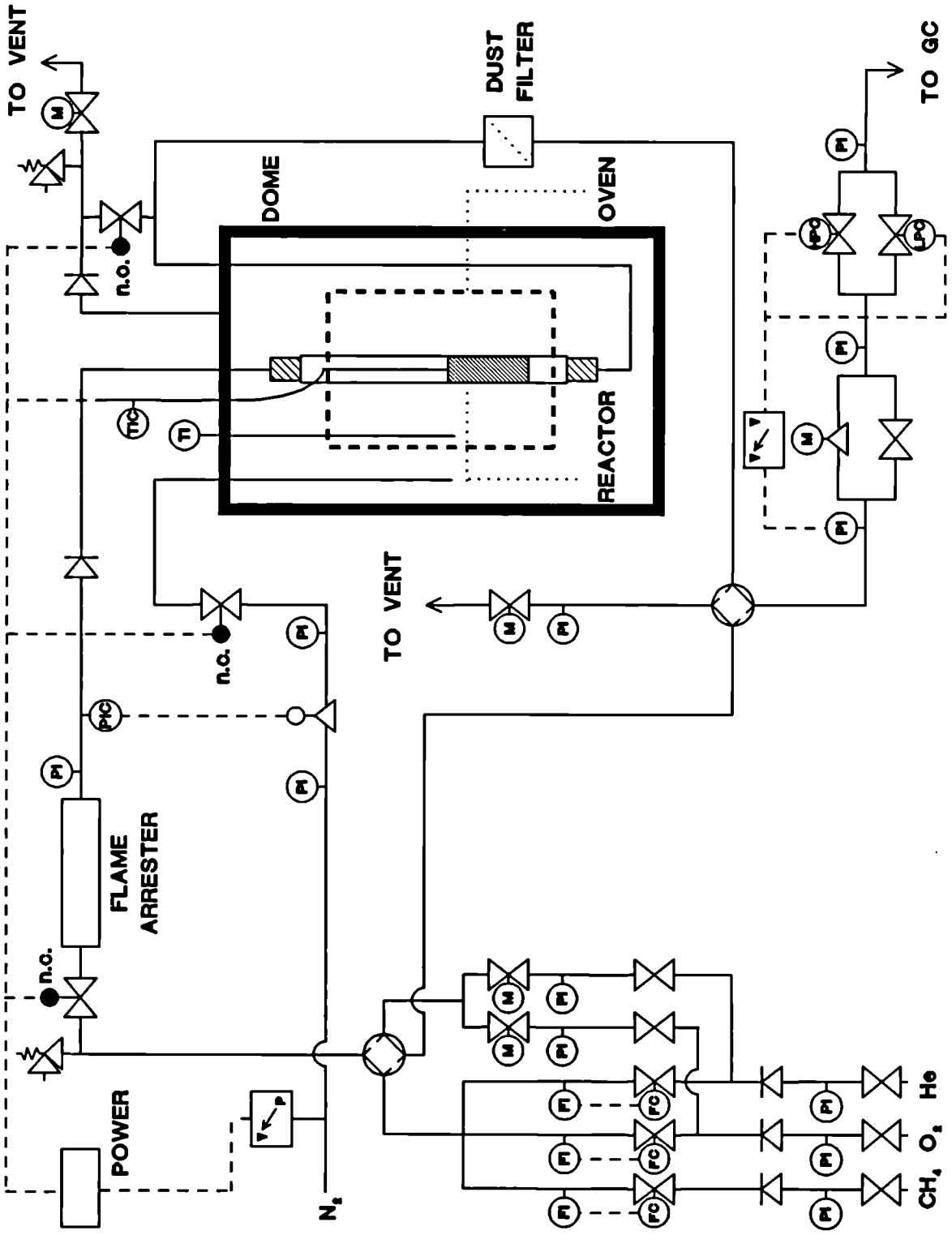

Figure 5.1.9: Flow diagram of the elevated pressure set-up.

Table 6.1.1. Li/MgO catalysts and their pore volume after calcination at 900°C.

Starting Salts	Pore Volume (ml/g)
Li_2CO_3/MgO	0.018
$LiNO_3$/MgO	0.164
LiOH/MgO	0.012
LiF/MgO	0.018

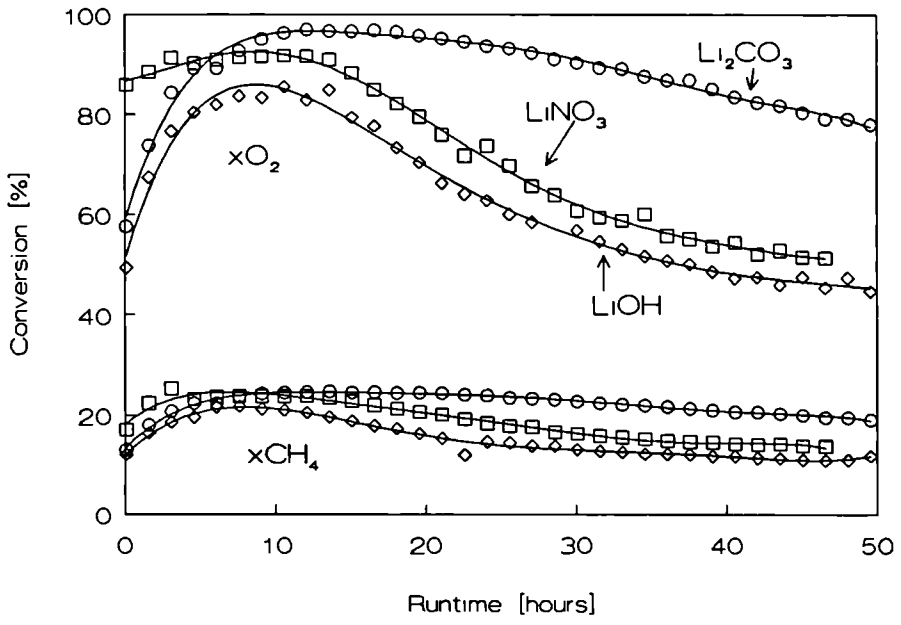

Figure 6.1.1. Methane and oxygen conversion as function of time on stream for different Li/MgO catalysts. T=800°C, CH_4/O_2=5, W/F=0.3 g.s/ml.

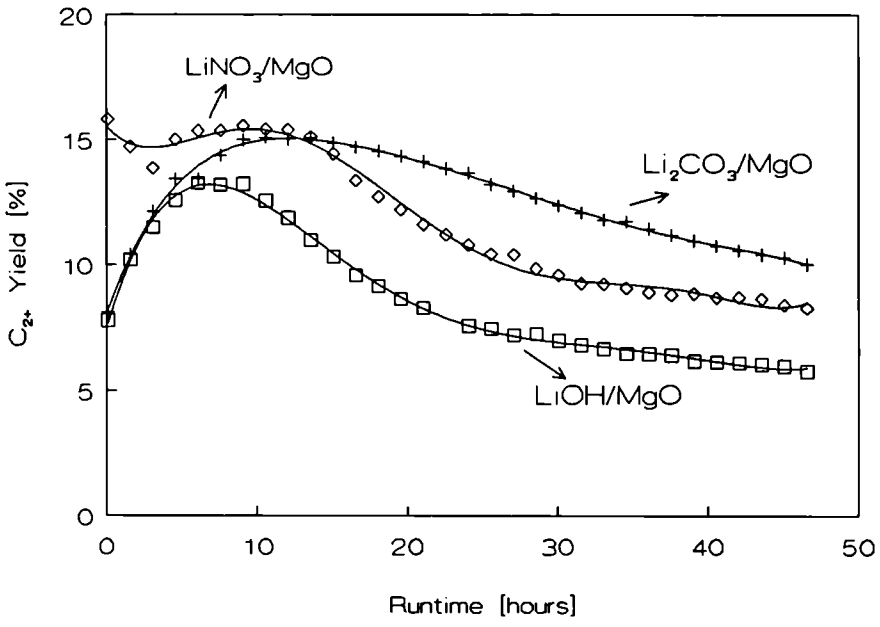

Figure 6.1.2. C_{2+} yield as function of time on tream for different Li/MgOcatalysts. T=800°C, CH_4/O_2=5, W/F=0.3 g.s/ml.

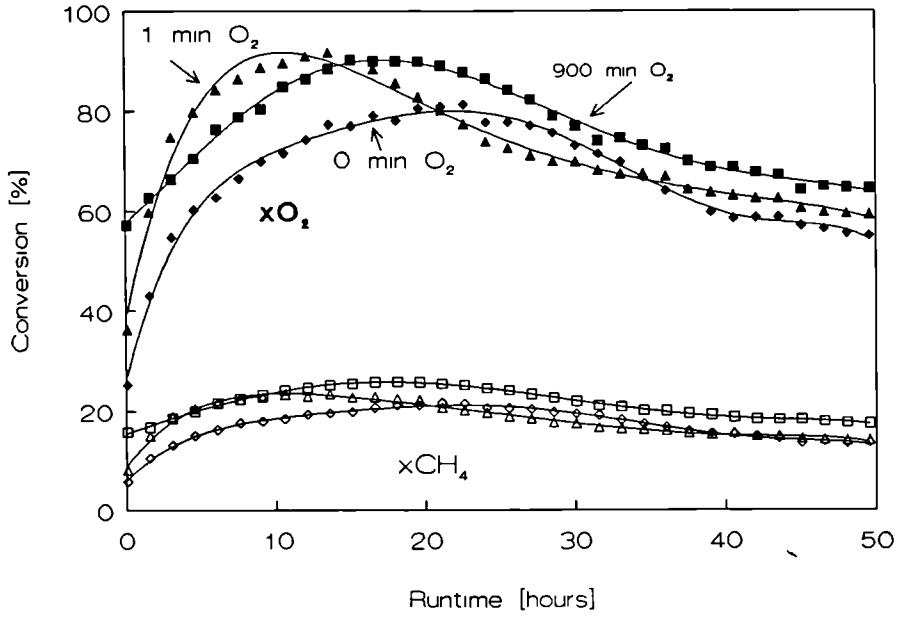

Figure 6.1.3. Methane and oxygen conversion as function of time onstream for different oxygen pretreatment times. Li/MgO catalyst; T=800°C, CH_4/O_2=5, W/F=0.3 g.s/ml.

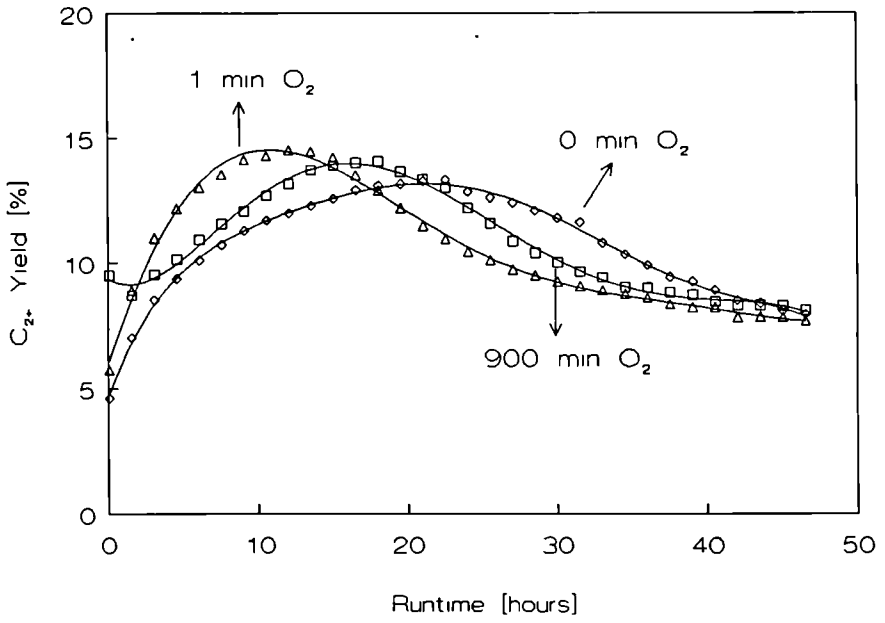

Figure 6.1.4. C_{2+} yield as function of time on stream for different oxygen pretreatment times. Li/MgO catalyst; T=800°C, CH_4/O_2=5, W/F=0.3 g.s/ml

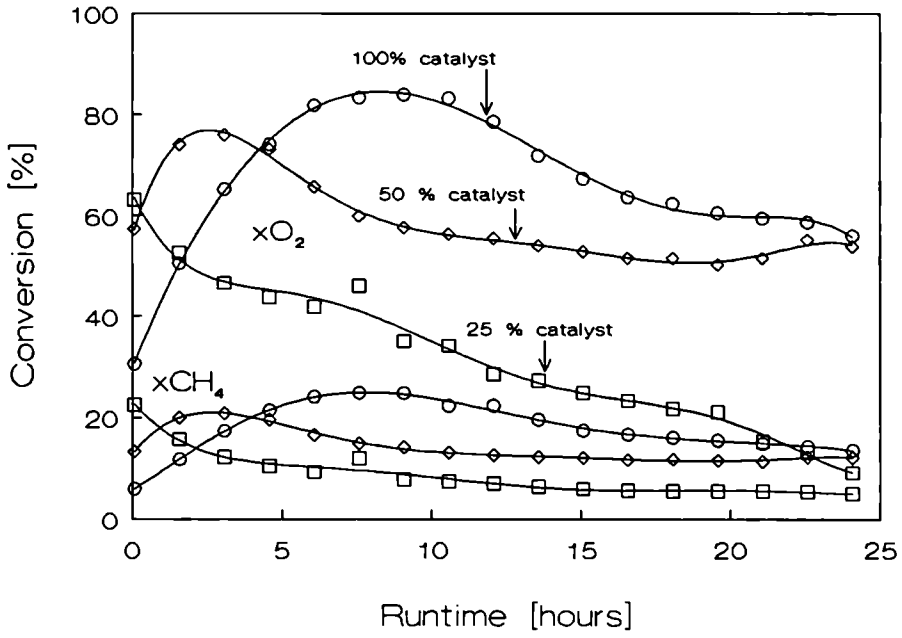

Figure 6.1.5. Methane and oxygen conversion as function of time on stream for different Li/MgO/quartz ratio. T=800°C, CH_4/O_2=5, W/F=0.3 g.s/ml

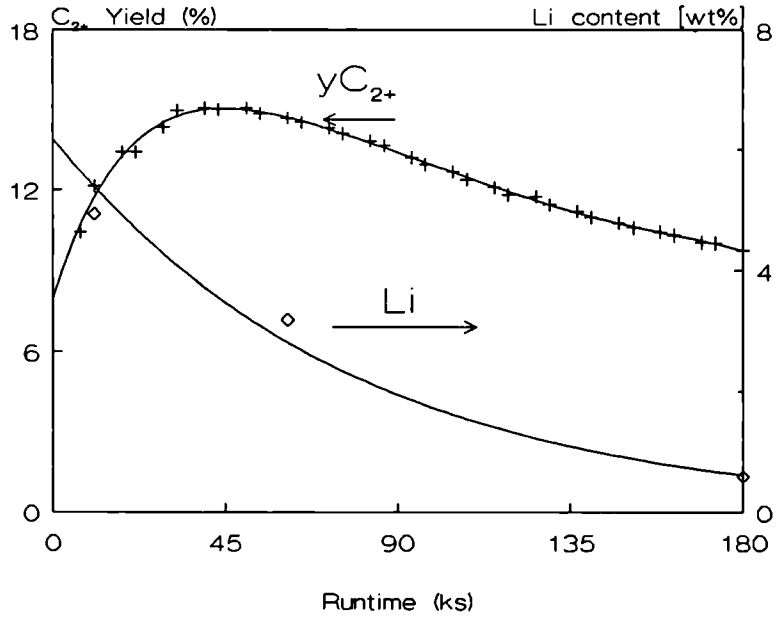

Figure 6.1.6. C_{2+} yield and lithium content of the Li/MgO catalyst as function of time on stream. T= 800°C, CH_4/O_2=5, W/F =0.3 g.s/ml.

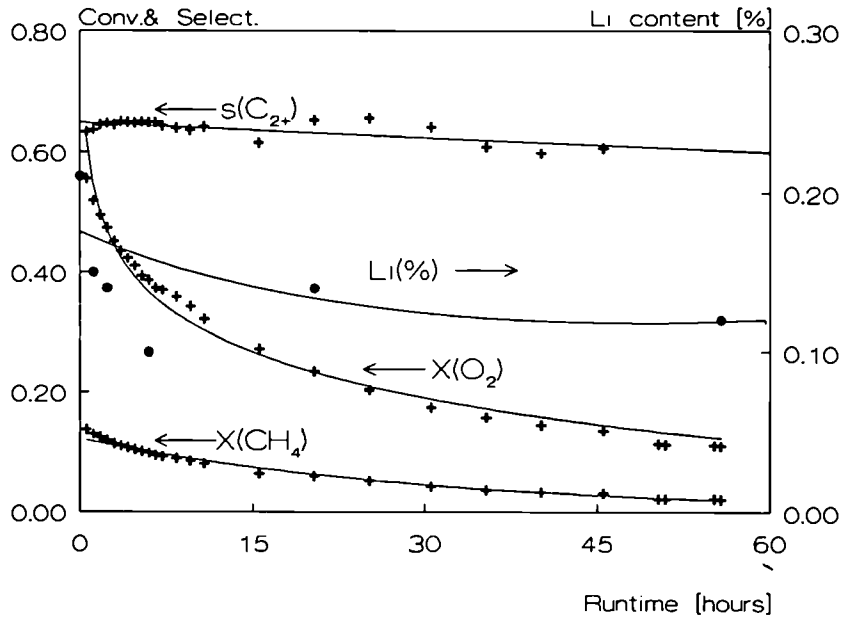

Figure 6.1.7. Methane and oxygen conversion ,C_{2+} selectivity and lithium content of a Li/MgO catalyst as function of time on stream. T=800°C, CH_4/O_2=5, W/F=0.6 g.s/ml.

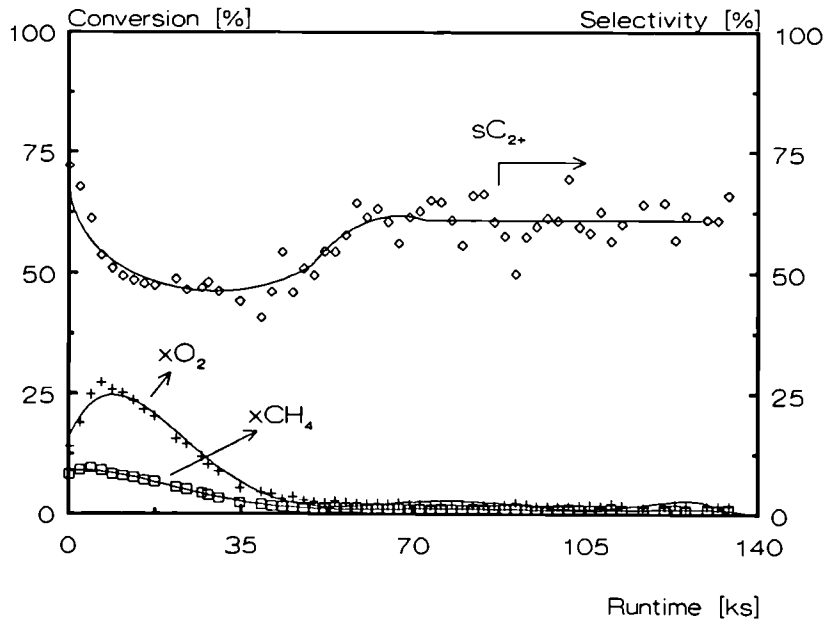

Figure 6.1.8. Methane and oxygen conversion and C_{2+} selectivity during methane coupling over a Li doped ZrO_2 catalyst. T=800°C, CH_4/O_2=5, W/F=0.3 g.s/ml.

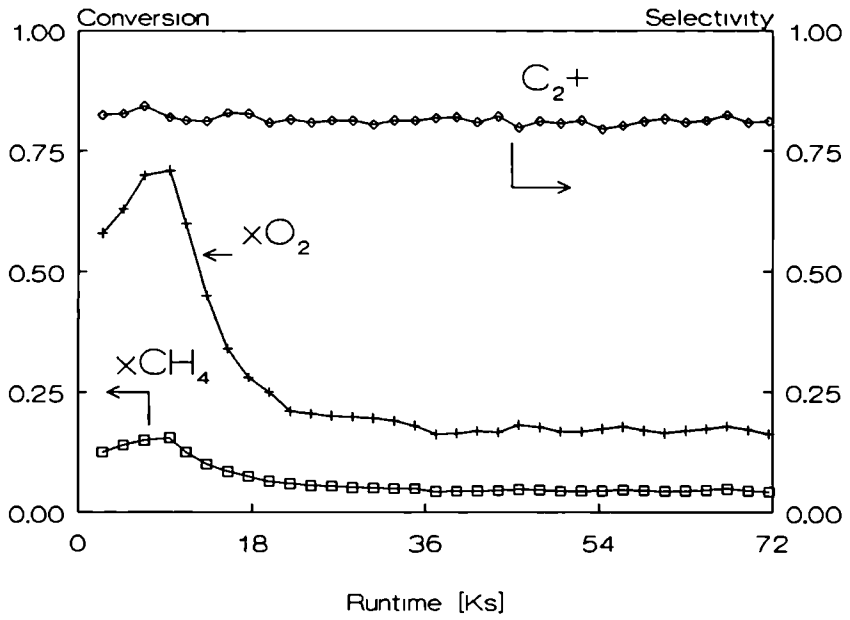

Figure 6.1.9. Methane and oxygen conversion and C_{2+} selectivity as function of time on stream during methane coupling over a Lithium doped Li_2ZrO_3 catalyst. T=800°C, CH_4/O_2=5, W/F= 0.3 g.s/ml.

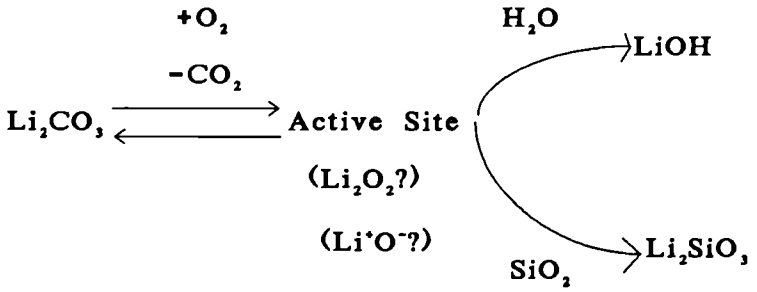

Figure 6.1.10. Working principle of the Li/MgO catalyst.

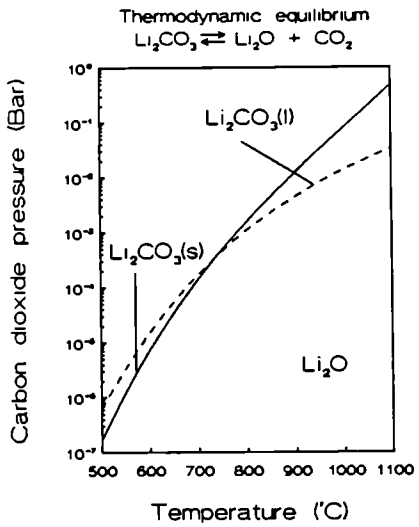

Figure 6.2.1: Calculated thermodynamical equilibrium carbon dioxide pressure of Li_2O as a function of the temperature.

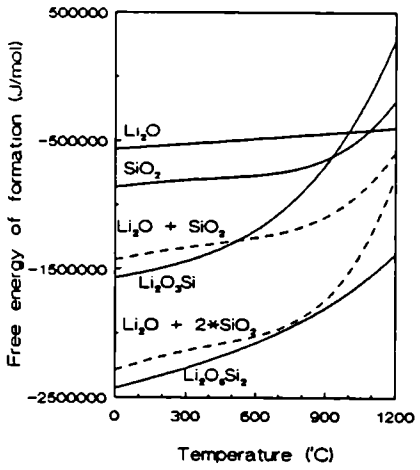

Figure 6.2.2: Gibbs free energies as a function of the temperature.

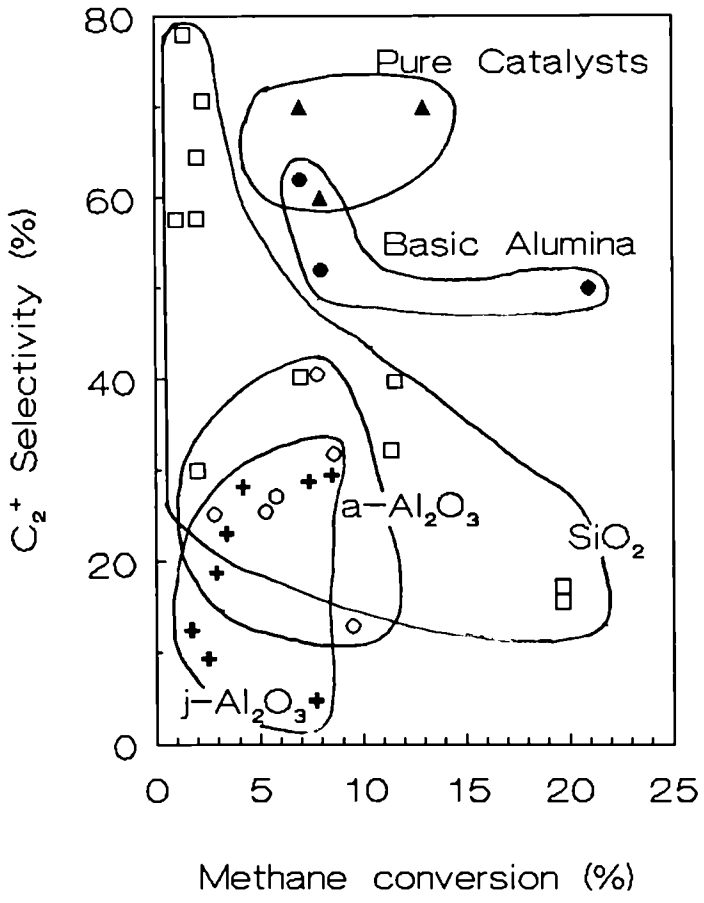

Figure 6.2.3: C_{2+} selectivity as a function of the methane conversion for different catalysts in a fluidised bed reactor.

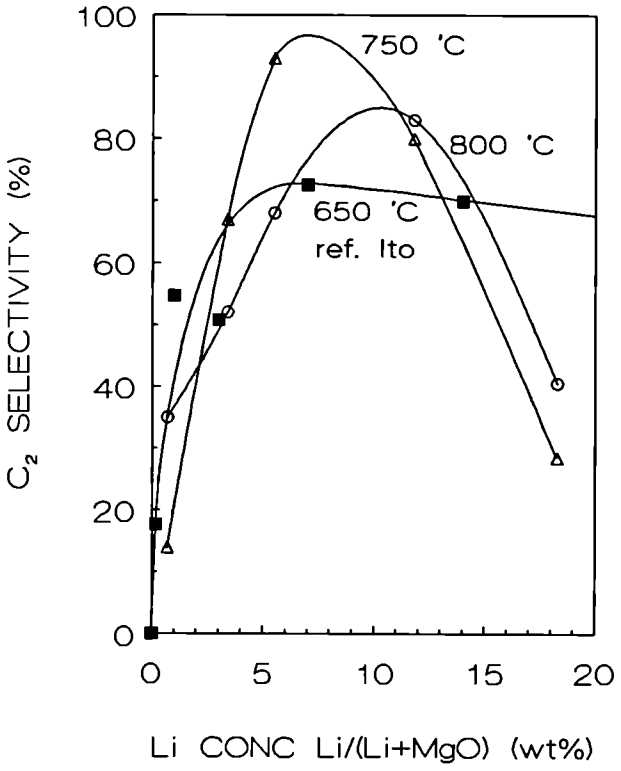

Figure 6.3.1: C_2 hydrocarbon selectivity versus lithium concentration and temperature. P=1 bar, CH_4/O_2=10, W/F=0.5 g s /Ncm^3; data at 650°C see Ref. 9.

Table 6.3.1:
The influences of temperature on the catalytic performance of pure lithium carbonate. P = 1 bar, Feed CH_4:O_2:He:CO_2 = 1 : 4.4 : 1.5 : 44

T (°C)	Conv. (%) CH_4	O_2	Selectivity (%) C_2H_6	C_2H_4	CO	CO_2
700	16.9	82.6	19.4	35.2	5.9	39.4
750	12.6	97.9	2.1	5.5	24.9	67.6
800	12.2	98.5	0.0	2.4	28.4	69.3

Table 6.3.2:
The influences of temperature and wt% MgO in the liquid phase on the catalytic performance. P = 1 bar, Feed CH_4:O_2:He:CO_2 = 1 : 4.4 : 1.5 : 44

MgO (wt %)	T (°C)	Conversion (%) CH_4	O_2	Selectivity (%) C_2H_6	C_2H_4	CO	CO_2
2	750	12.7	96.5	2.4	2.9	40.7	54.0
	800	14.0	96.9	3.8	17.9	19.8	58.5
50	750	17.2	99.6	9.9	33.2	4.3	52.6
	800	16.7	99.6	5.3	36.2	4.3	54.2

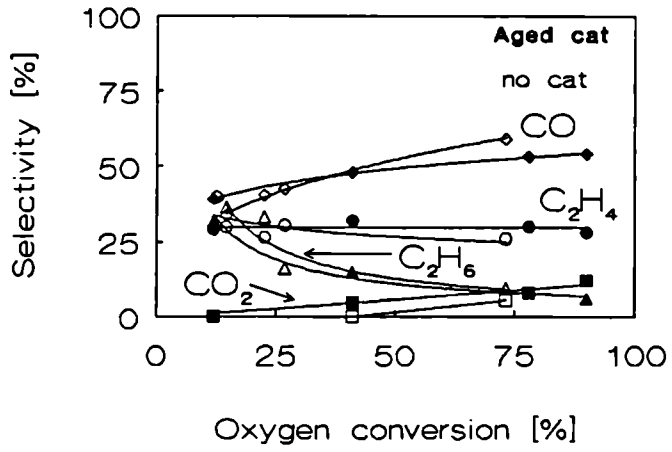

Figure 7.1.1. Product selectivity as function of the oxygen conversion for an aged Li/MgO catalyst and gas phase reaction. T=800°C, CH_4/O_2=5, W/F=0.3 g.s/ml.

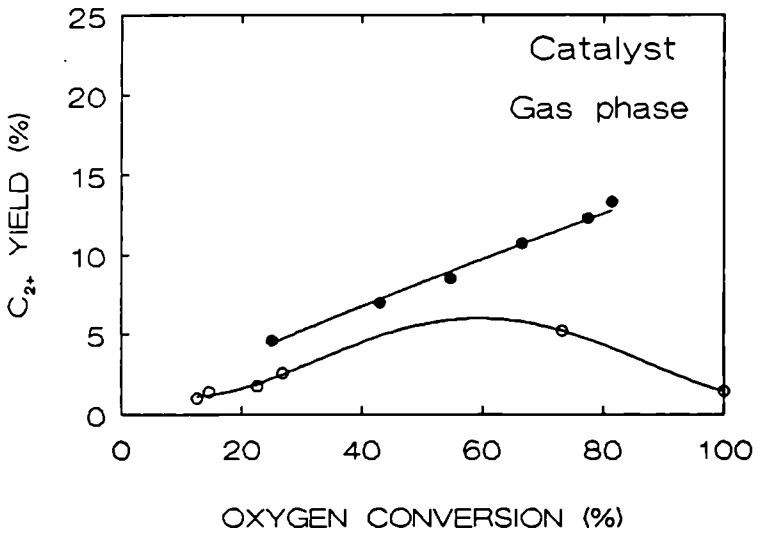

Figure 7.1.2. C_{2+} Yield as function of the oxygen conversion for an fresh Li/MgO catalyst and gas phase reaction. T=800°C, CH_4/O_2=5.

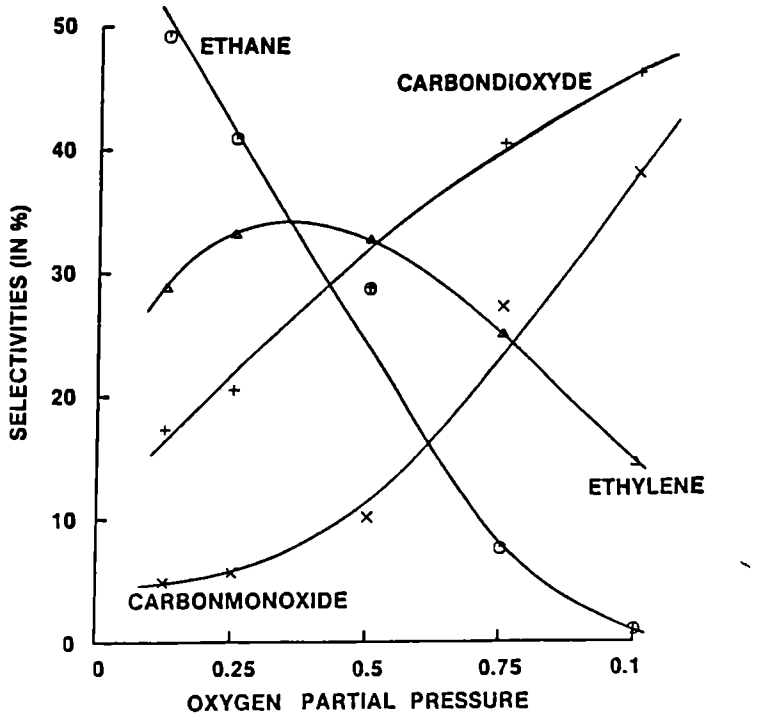

Figure 7.2.1: Selectivities as a function of the oxygen partial pressure. Flow = 125 Ncm^3/min, W/F = 0.48 gs/Ncm^3, P CH_4 = 0.6 bar, T = 800°C.

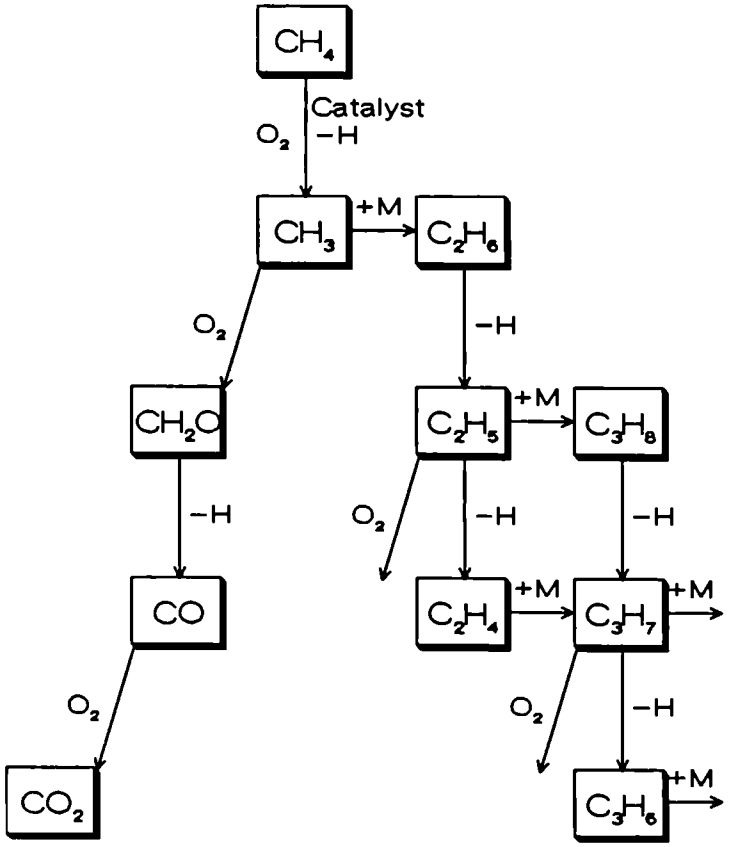

Figure 7.2.2: The proposed reaction mechanism for the oxidative coupling of methane.

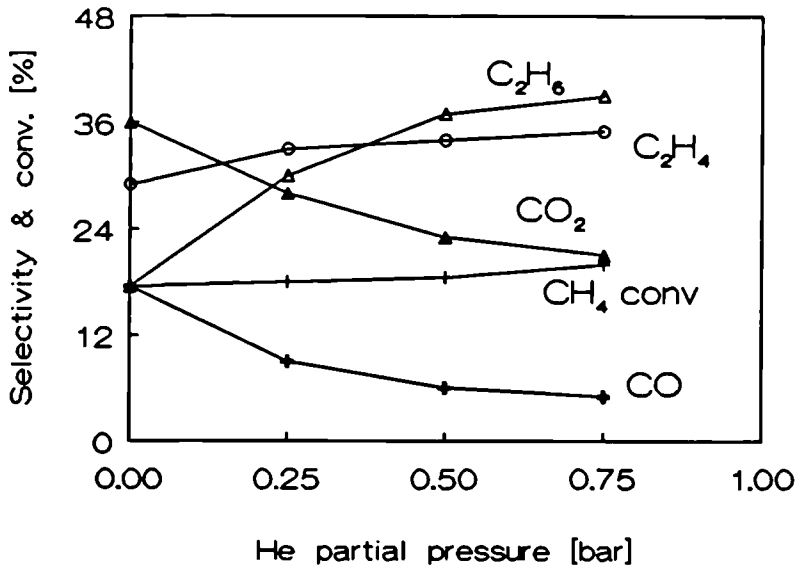

Figure 7.2.3: Selectivities and conversion as a function of the helium partial pressure. Flow 120 Ncm³/min, W/F = 0.6 gs/Ncm³, CH_4/O_2 = 5, T = 800°C, P_{tot} = 1 bar.

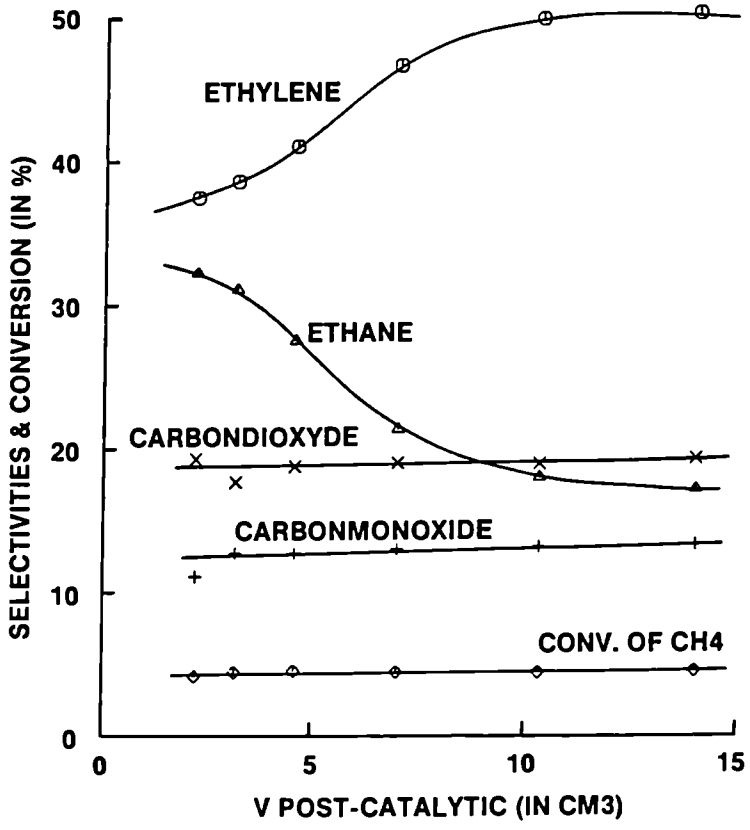

Figure 7.2.4: The dependence of methane conversion and product selectivities on the size of the post-catalytic space for complete oxygen conversion. T = 800 °C, CH_4/O_2 = 10, CH_4/He = 0.8, W/F = 1.2 gs/Ncm³, flow = 67 Ncm³/min.

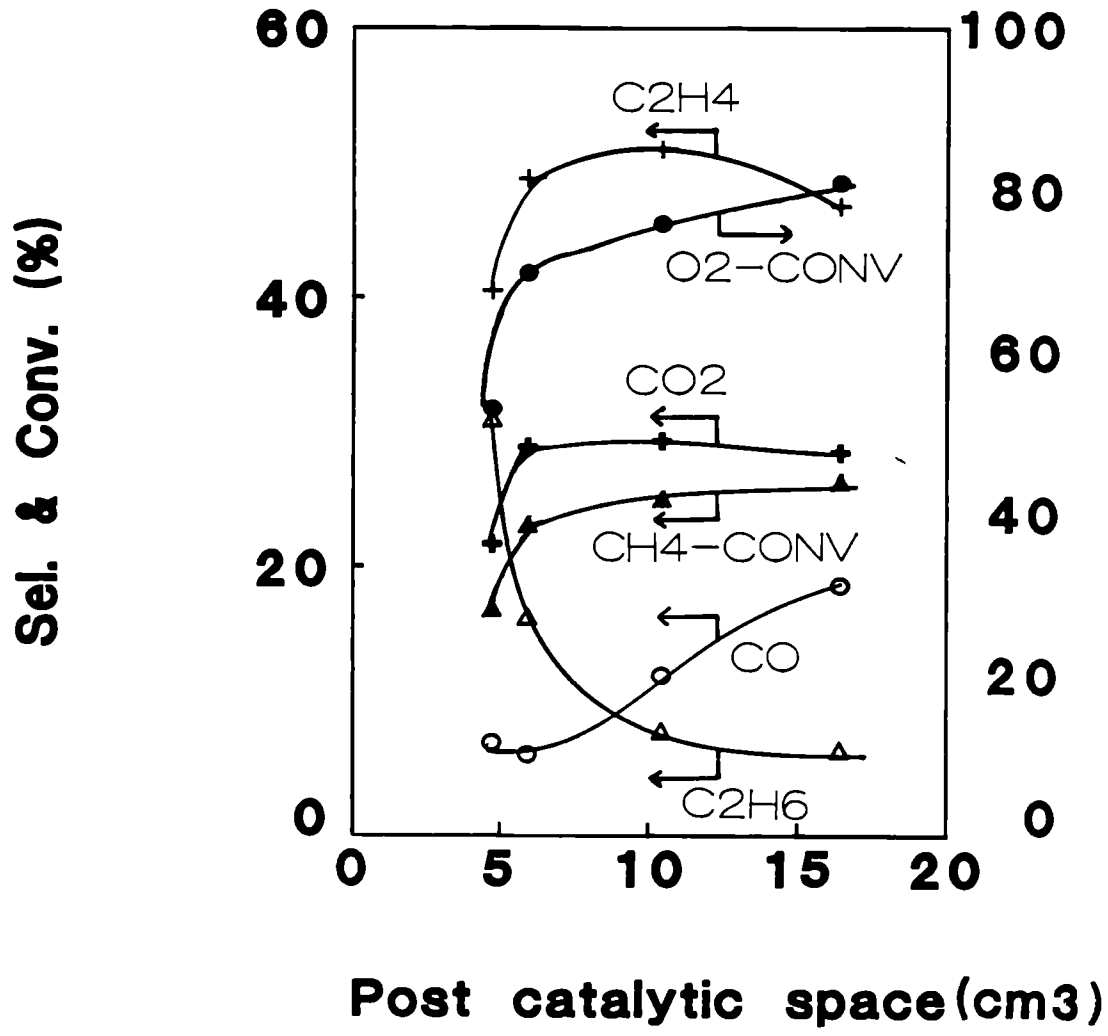

Figure 7.2.5: The dependence of conversions and product selectivities on the size of the post-catalytic space, when the oxygen conversion is not complete. T = 770°C, CH_4/O_2 = 4, W/F = 0.6 gs/Ncm^3, CH_4/He = 0.8, P_{tot} = 1 bar.

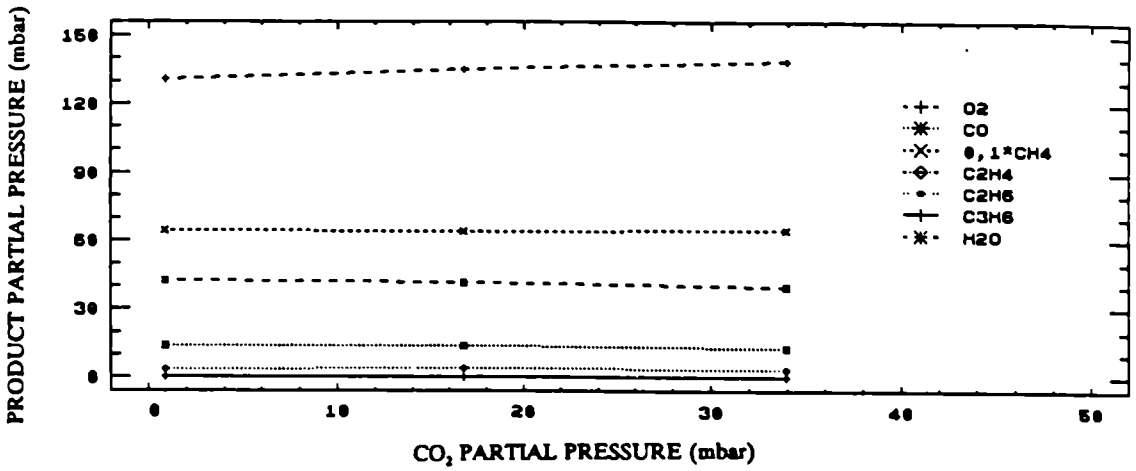

Figure 7.3.1. The influence of carbon dioxide on the oxidative coupling of methane. T = 800°C.

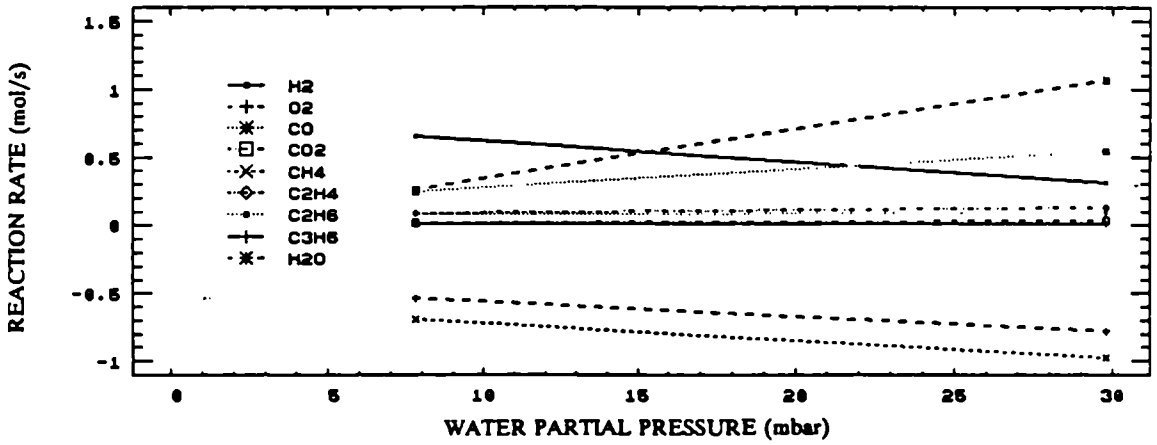

Figure 7.3.2. The influence of the water partial pressure on the integral reaction rates. T = 900°C.

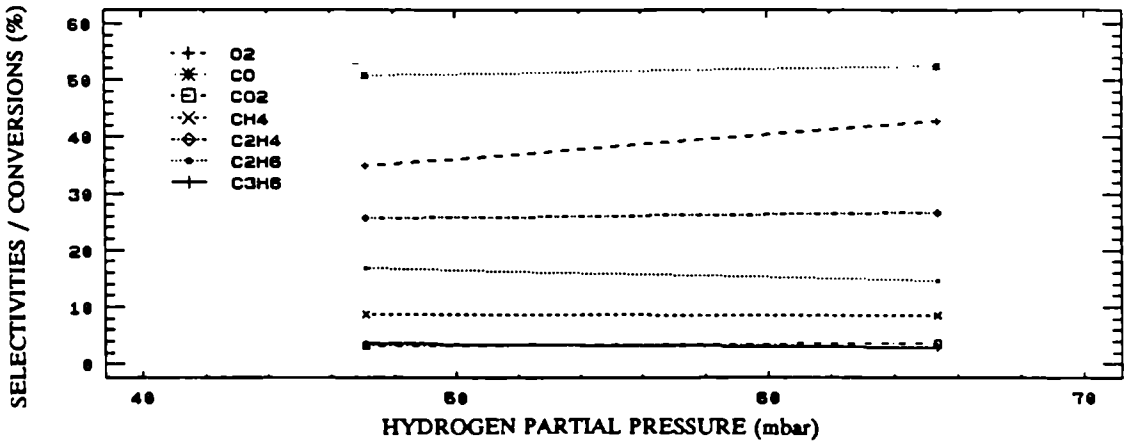

Figure 7.3.3. Influence of the hydrogen partial pressure on the selectivities and conversions (O_2, CH_4). T= 900°C.

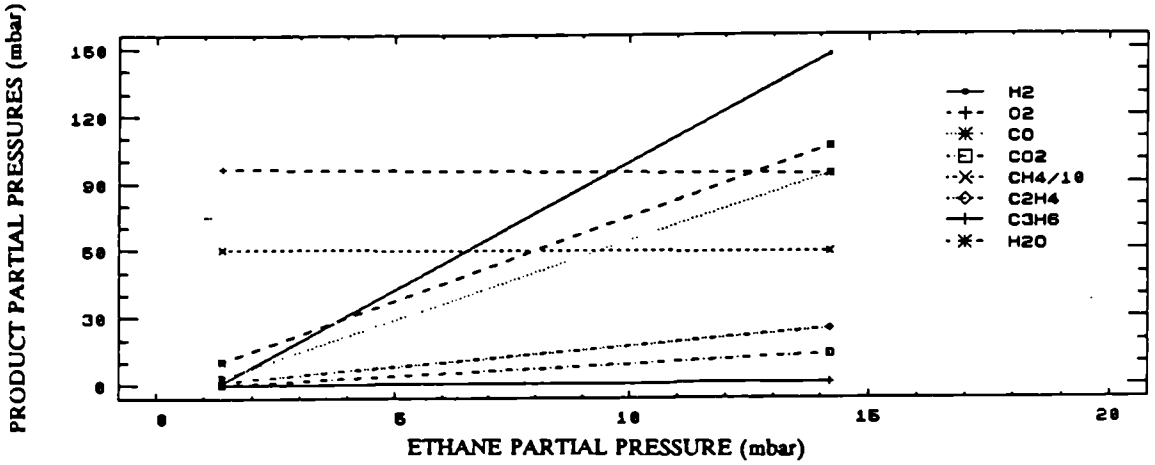

Figure 7.3.4. The influence of the addition of ethane to the feed on the composition of the product gas. The methane and oxygen partial pressures are kept constant. T = 800°C.

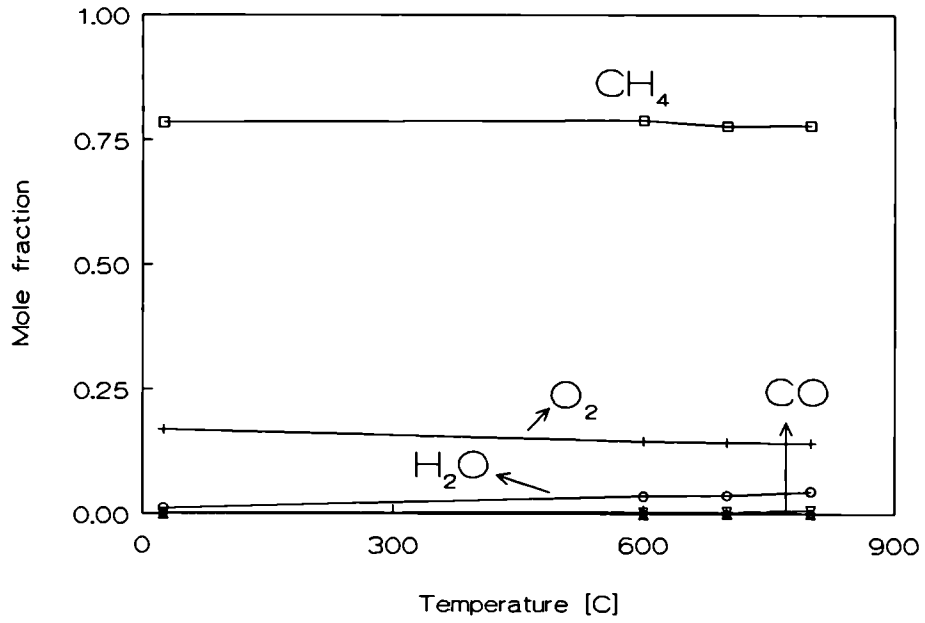

Figure 7.4.1. Product mol fraction as function of the temperature for methane coupling at 33 Pa over Li/MgO. W=0.24g, Flow = 10^{-7} mole/s.

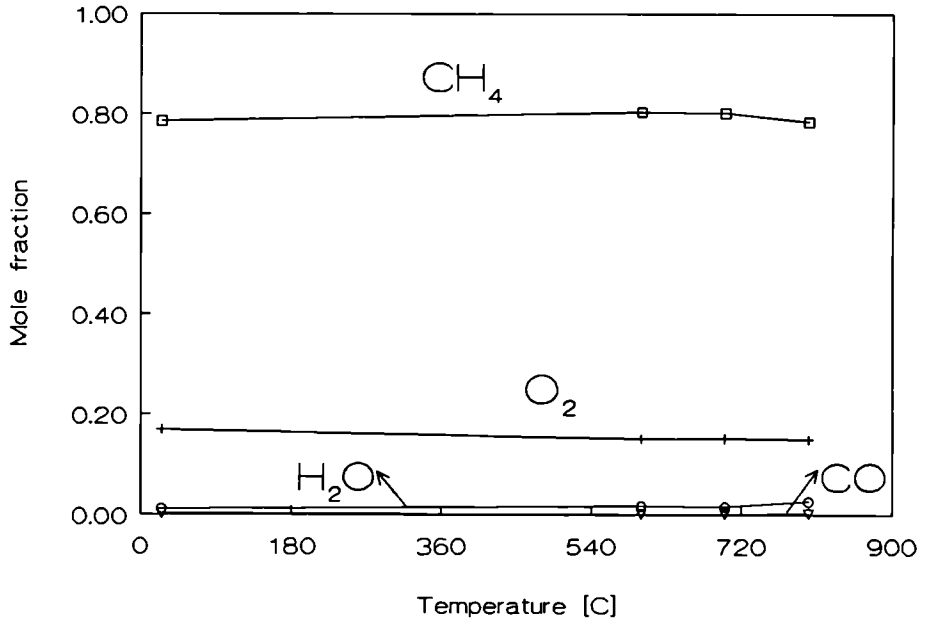

Figure 7.4.2. Product mole fraction as function of the reaction temperature for gas phase methane coupling at 33 Pa. Flow = 10^{-7} mole/s.

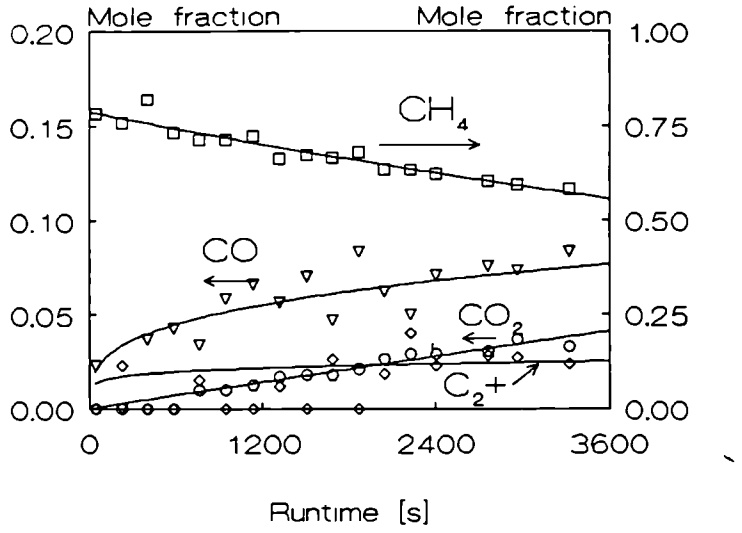

Figure 7.4.3. Product mole fraction as function of the run time for methane coupling over Li/MgO batch reaction. T=800°C, P=138 Pa, w=0.24g.

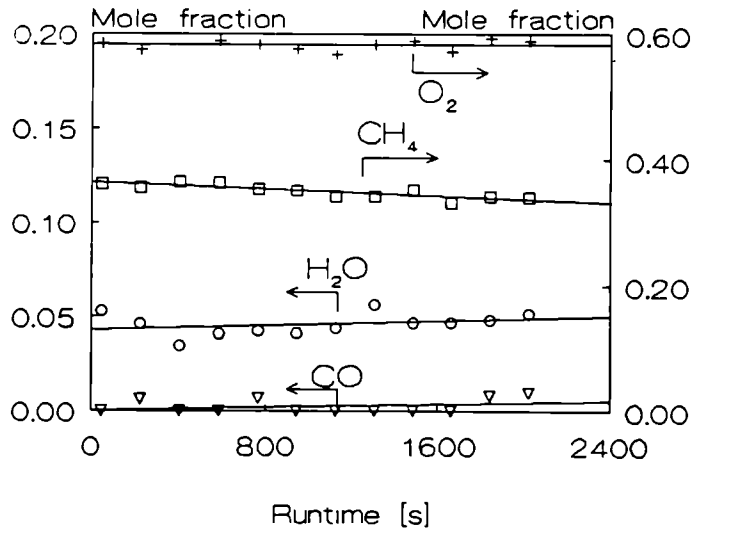

Figure 7.4.4. Product mole fraction as function of the run time for gas phase methane coupling batch reaction. T=800°C, P=65 Pa.

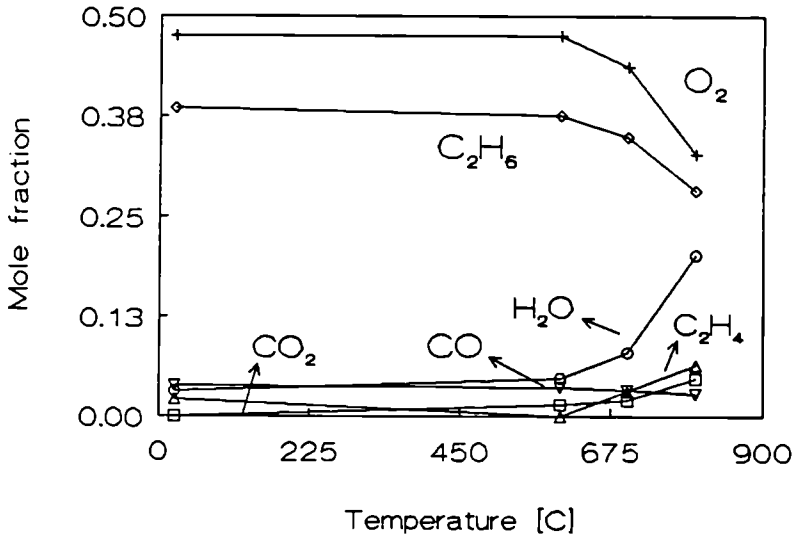

Figure 7.4.5. Product mole fraction as function of the temperature for ethane activation over Li/MgO. T=800°C, P=50 Pa, Flow=$8*10^{-8}$ mole/s, W=0.24g.

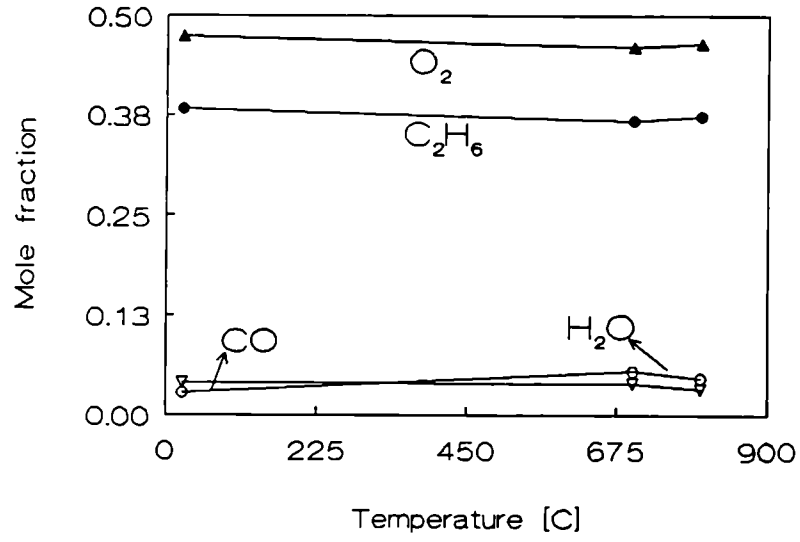

Figure 7.4.6. Product mole fraction as function of the temperature for gas phase ethane activation. T=800°C, P=66 Pa, Flow=$8*10^{-8}$ mole/s.

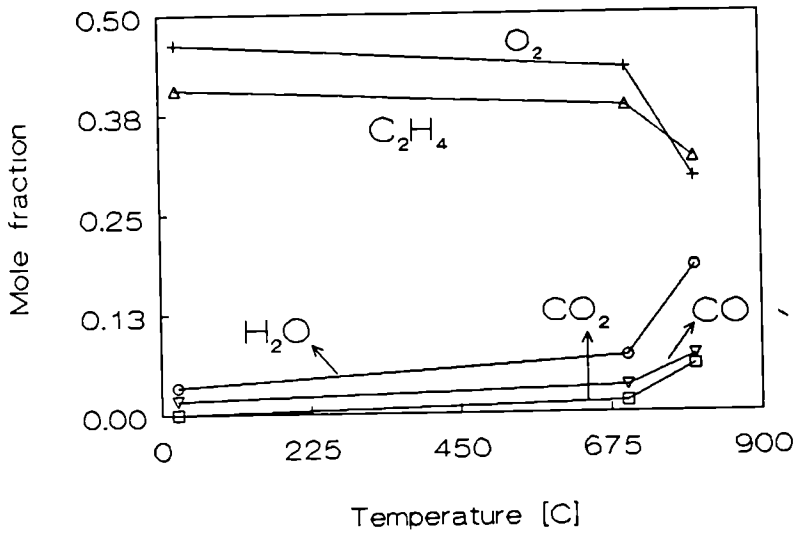

Figure 7.4.7. Product mole fraction as function of the temperature for ethylene activation over Li/MgO. T=800°C, P=50 Pa, Flow=$1.7*10^{-7}$ mole/s, W=1g.

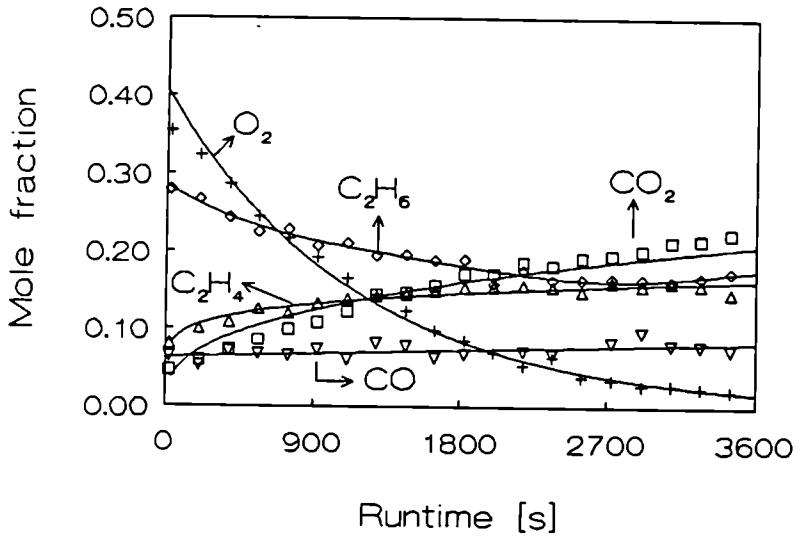

Figure 7.4.8. Product mole fraction as function of the run time for ethane activation over Li/MgO batch reaction. T=800°C, P=133 Pa, W=0.24g.

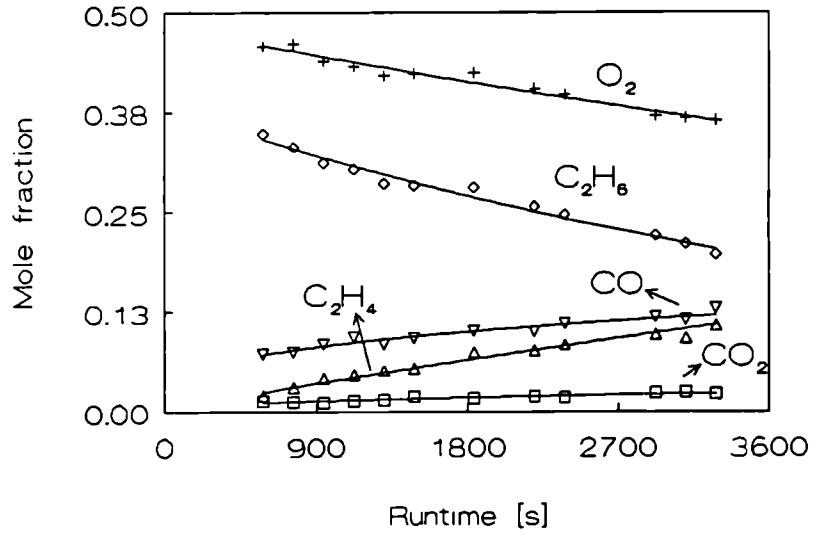

Figure 7.4.9. Product mole fraction as function of the run time for gas phase ethane activation batch reaction. T=800°C, P=65 Pa.

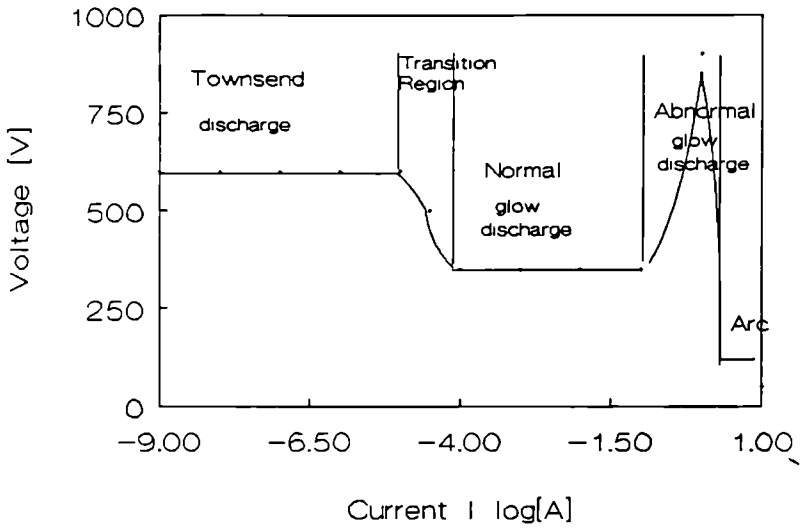

Figure 7.5.1. Plasma discharge classification by potential versus current.

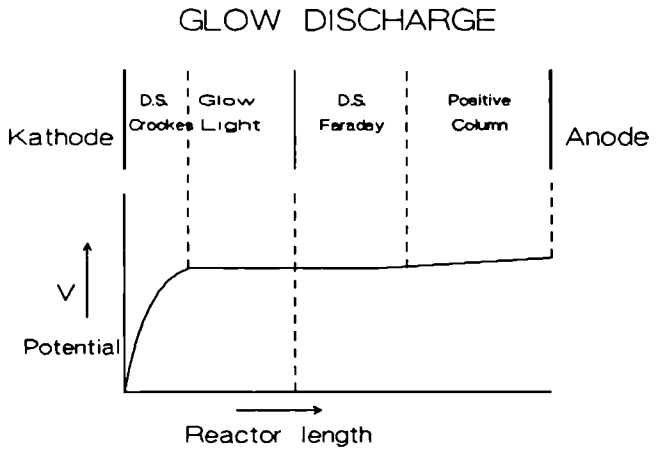

Figure 7.5.2. Potential versus distance between cathode and anode for a glow discharge

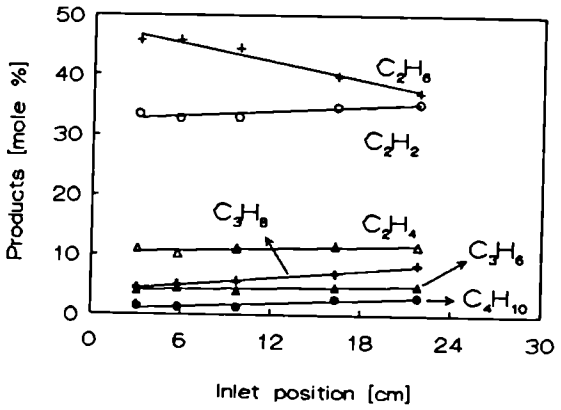

Figure 7.5.3. Product distribution as function of the gas inlet position in the striated column reactor. P=320 Pa, Ar/CH_4=70, T=293 K.

Table 7.5.1. Product distribution as function of the wall temperature.

Temp. (K)	C_2H_6 %	C_2H_4 %	C_2H_2 %	C_3H_8 %	C_3H_6 %	C_4H_{10} %
77	46	1	33	14	2	4
298	44	11	33	6	4	2

Table 7.5.2. Product distribution of plasma reaction with Li/MgO catalyst (mole %). T=77K, Ar/CH_4=70, P=3.2 mbar.

Wall	C_2H_6	C_2H_4	C_2H_2	C_3H_8	C_3H_6	C_4H_{10}
Li/MgO	45	5	41	5	1	3
Li/MgO*	43	3	42	7	1	4
Quartz	46	1	33	14	2	4
Quartz**	44	11	33	6	4	2

*) UV irradiated Li/MgO.
**) T= 293 K.

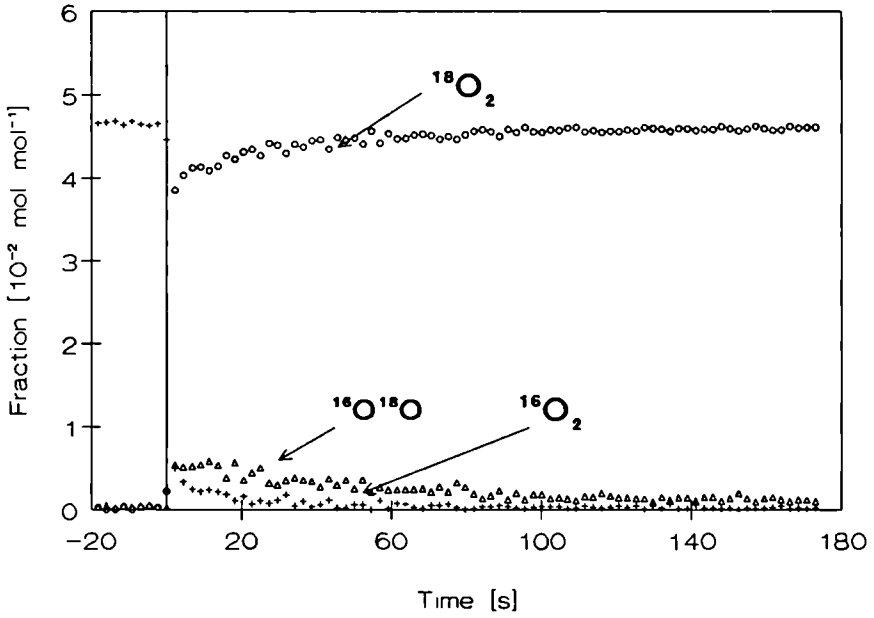

Figure 7.6.1. Oxygen response after a step response of $CH_4/^{16}O_2/He$ to $CH_4/^{18}O_2/He$. T=800°C, CH_4/O_2=1.7, Li/MgO , W/F=0.15 g.s/ml.

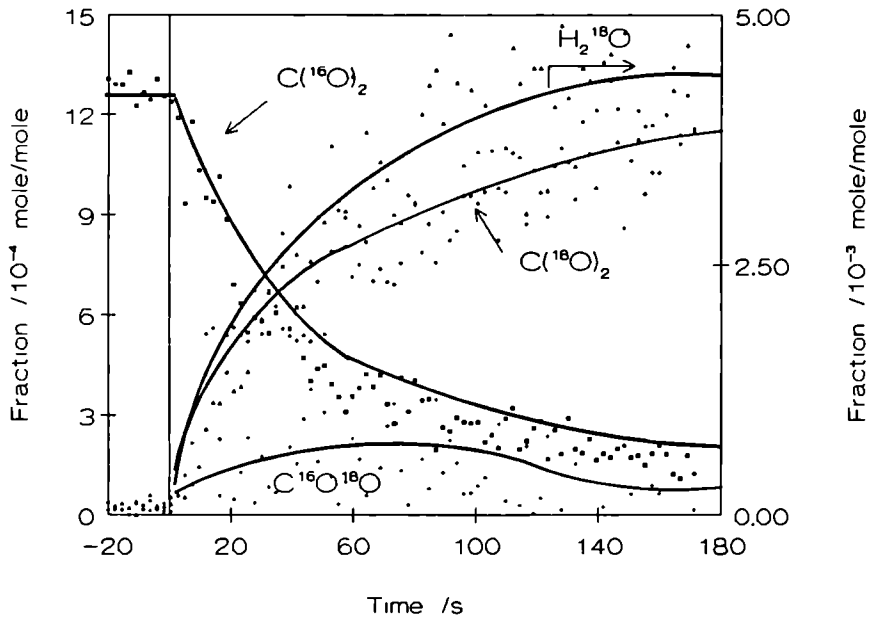

Figure 7.6.2. CO_2 and H_2O response after a step response of $CH_4/^{16}O_2/He$ to $CH_4/^{18}O_2/He$. T=800°C, CH_4/O_2=1.7, Li/MgO catalyst, W/F=0.15 g.s/ml.

Table 7.6.1. Steady state reaction rate of methane and rate of formation of products during methane coupling over Li/MgO before and after the isotopic switch from $CH_4/^{16}O_2/He$ to $CH_4/^{18}O_2/He$. T=800°C, CH_4/O_2=1.7, W/F=0.15 g.s/ml.

Rate of production/ 10^{-4} mole kg_{kat}^{-1} s^{-1}		
	$^{16}O_2$	$^{18}O_2$
CH_4	13	15
C_2H_6	2,8	2,8
C_2H_4	0,5	0,5
CO_2	3	4

Table 7.6.2. Number of exchangeable ^{16}O atoms in the oxygen containing products during methane coupling over Li/MgO. T=800°C, CH_4/O_2=1.7, W/F=0.15 g.s/ml.

molecule	number of ^{16}O-atoms / 10^{19} g^{-1}
$^{16}O_2$	3,0
$^{16}O^{18}O$	2,4
$C^{16}O_2$	1,64
$C^{16}O^{18}O$	0,25
$H_2{}^{16}O$	3,2
total	10,5

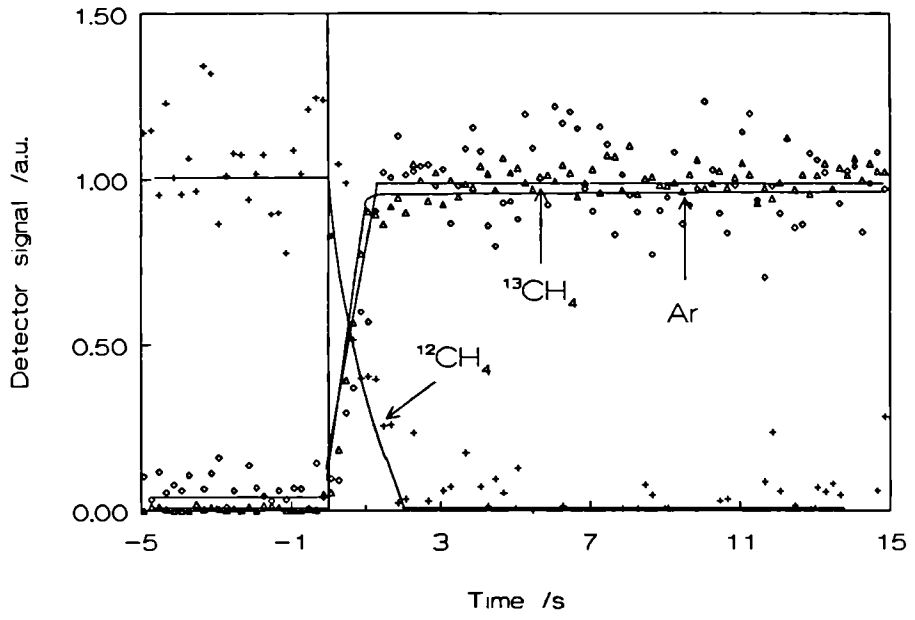

Figure 7.6.3. Methane response after a feed gas switch from $^{12}CH_4/O_2/He$ to $^{13}CH_4/O_2/He$. T=800°C, CH_4/O_2=2, Li/MgO catalyst, W/F=0.25 g.s/ml.

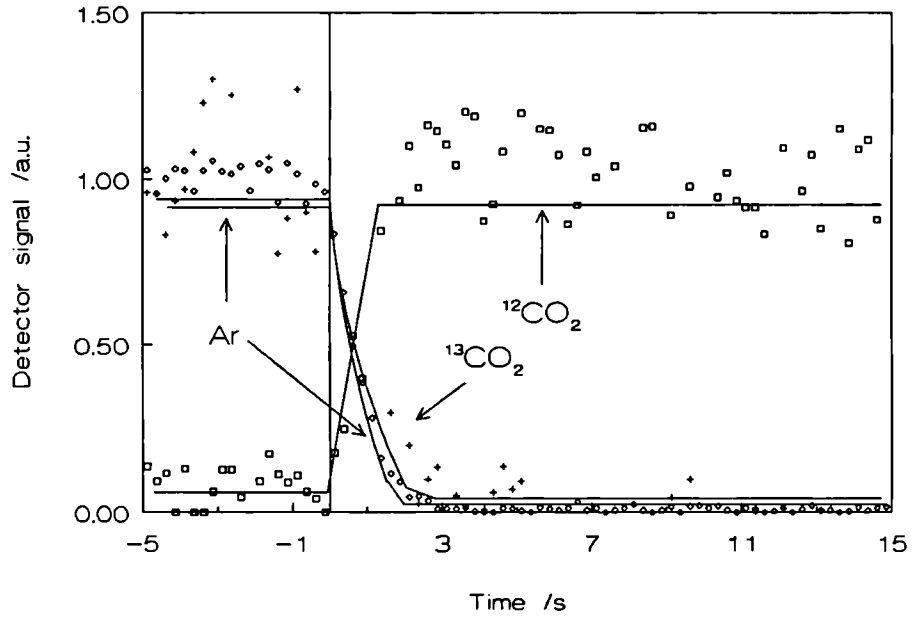

Figure 7.6.4. CO_2 response after a feed gas switch from $^{13}CH_4/O_2/He$ to $^{12}CH_4/O_2/He$. T=800°C, CH_4/O_2=2, Li/MgO catalyst, W/F=0.25 g.s/ml.

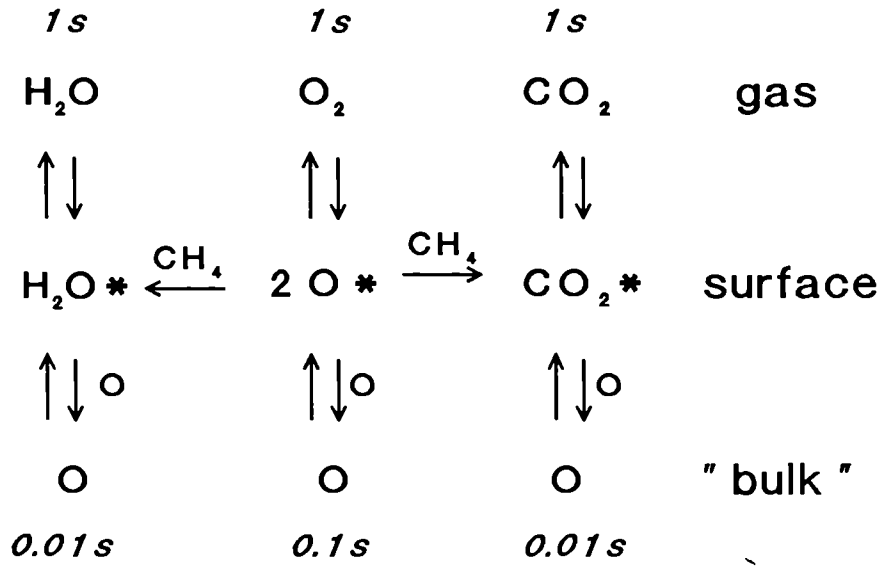

Figure 7.6.5. Oxygen pathway during methane coupling over a Li/MgO catalyst.

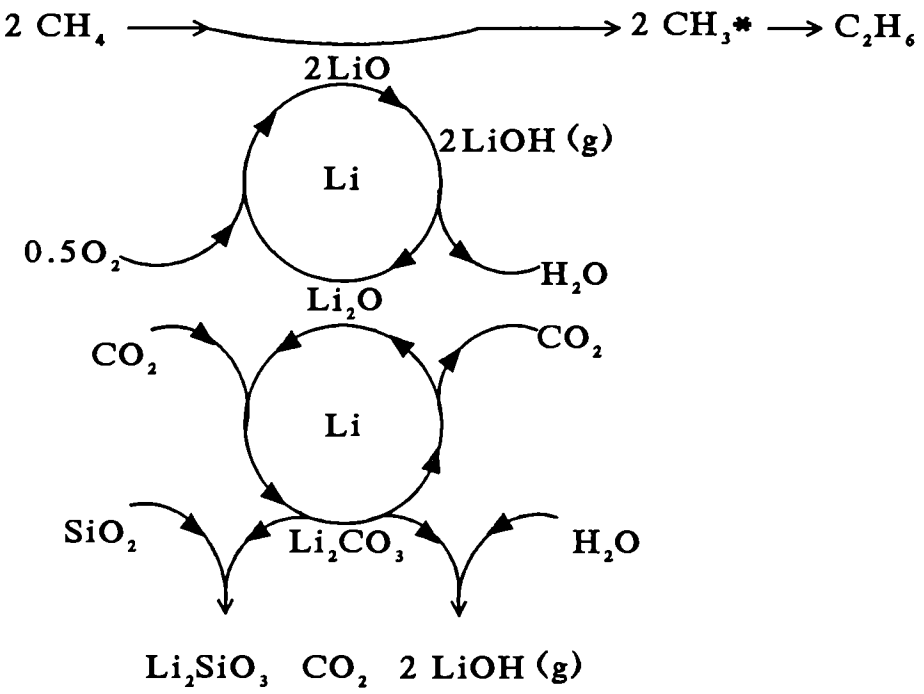

Figure 7.6.6. Working principle of the Li/MgO catalyst during methane coupling.

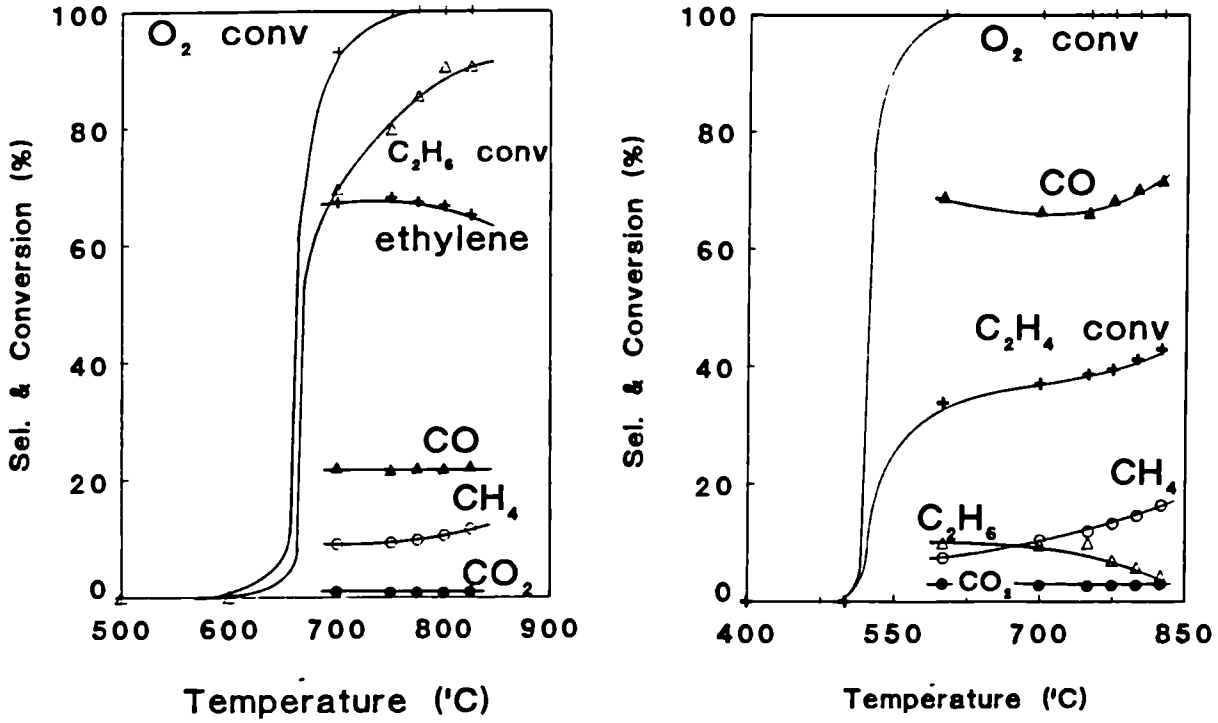

Figure 7.7.1: Ethane oxidation Ethylene oxidation
Selectivities and conversions as a function of the reaction temperature for gas phase oxidation experiments. C_2/O_2=2.2, He/C_2=8.5.

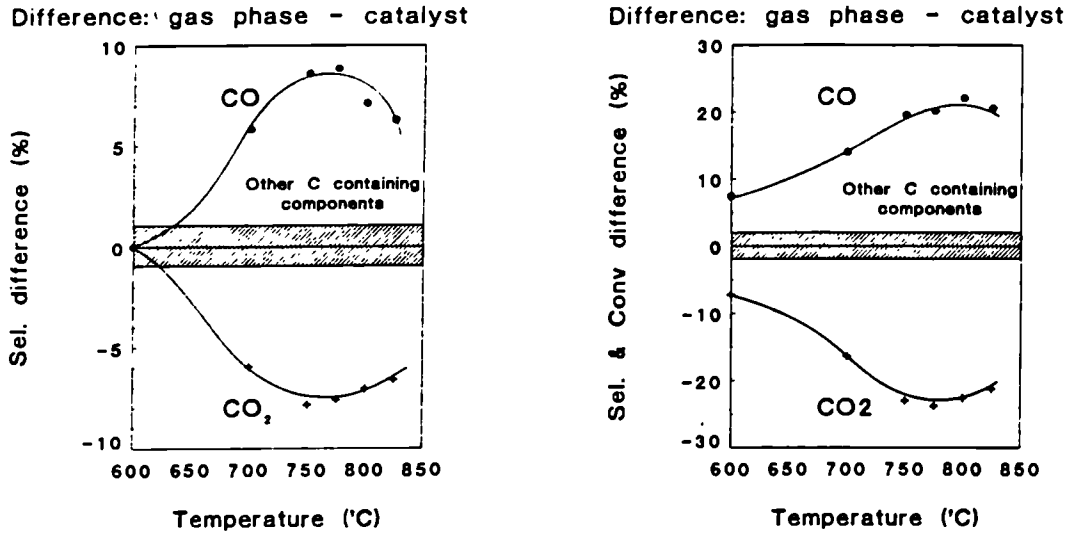

Figure 7.7.2: Ethane oxidation Ethylene oxidation
Differences in conversions and selectivities between gas phase and catalytic C_2 oxidation experiments. C_2/O_2=2.2, He/C_2=8.5, W/F= 0.6 g.s/Ncm^3.

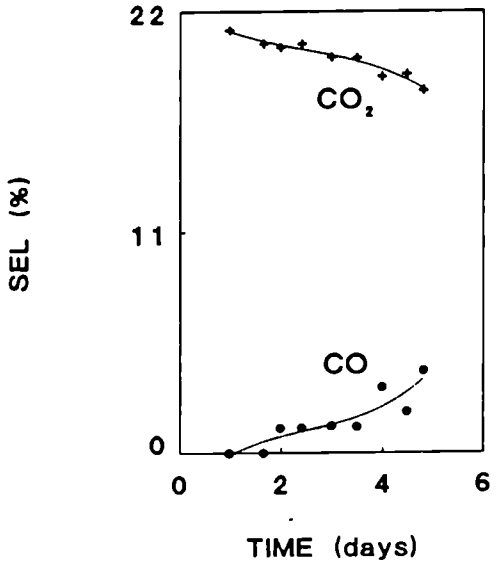

Figure 7.7.3: Catalyst deactivation
Time on stream for a Li/MgO catalyst. T=800°C, W/F=0.6 g.s/Ncm^3, $CH_4/O_2=10$.

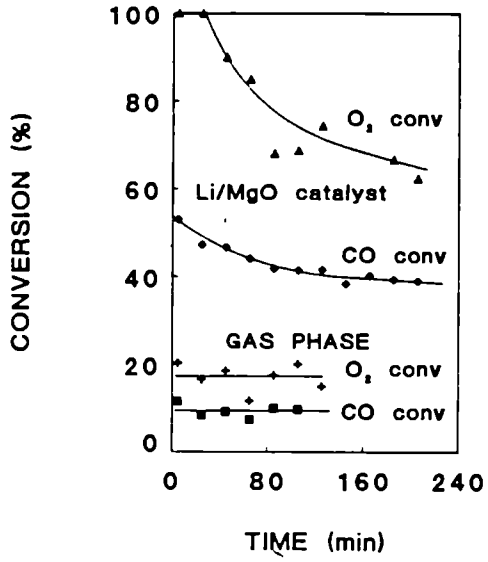

Figure 7.7.4: CO oxidation
Gas phase and catalytic oxidation of CO. T=800°C, W/F=0.3 g.s/Ncm^3, $CO/O_2=4$, $CO/He=0.06$

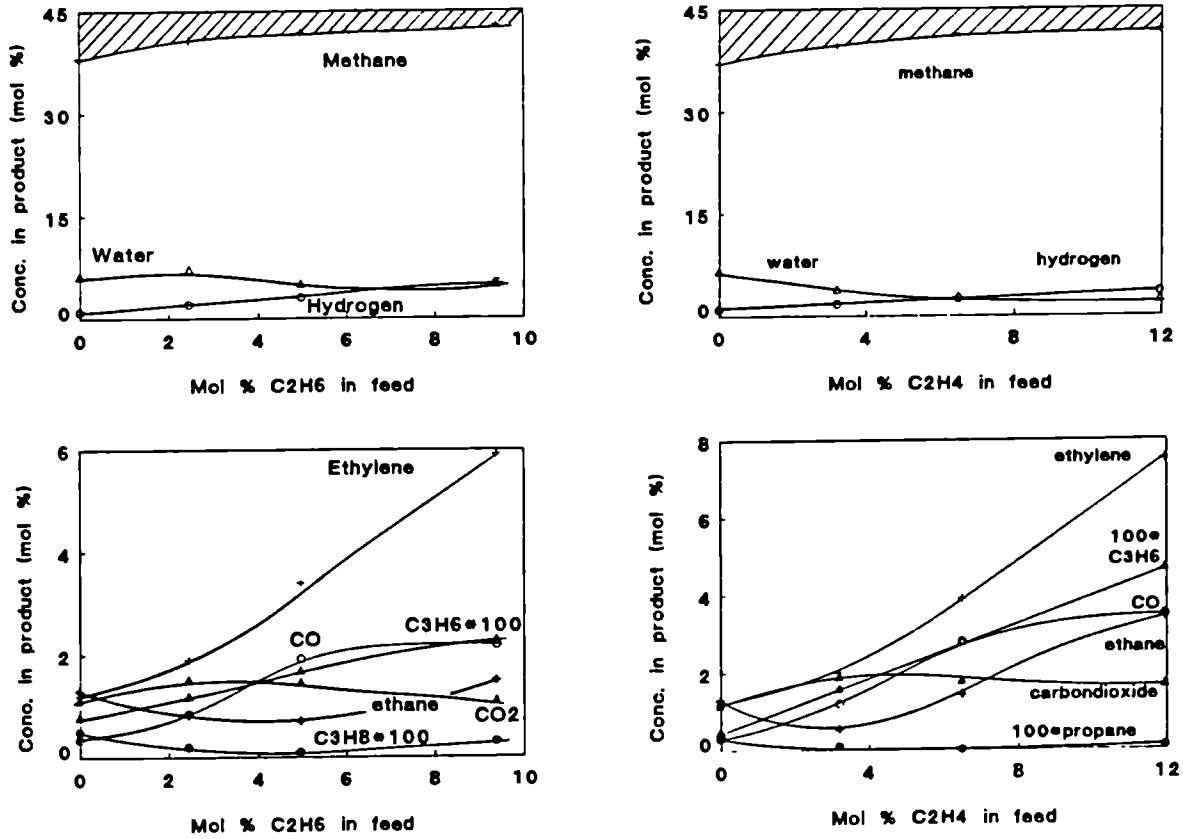

Figure 7.7.5: Addition of ethane Addition of ethylene
Mol fractions at the outlet of the reactor of ;admixing of C_2 to a methane /oxygen/helium mixture, catalysed by Li/MgO. T=800°C, $CH_4/O_2=10$, W/F=0.6 g.s/Ncm^3.

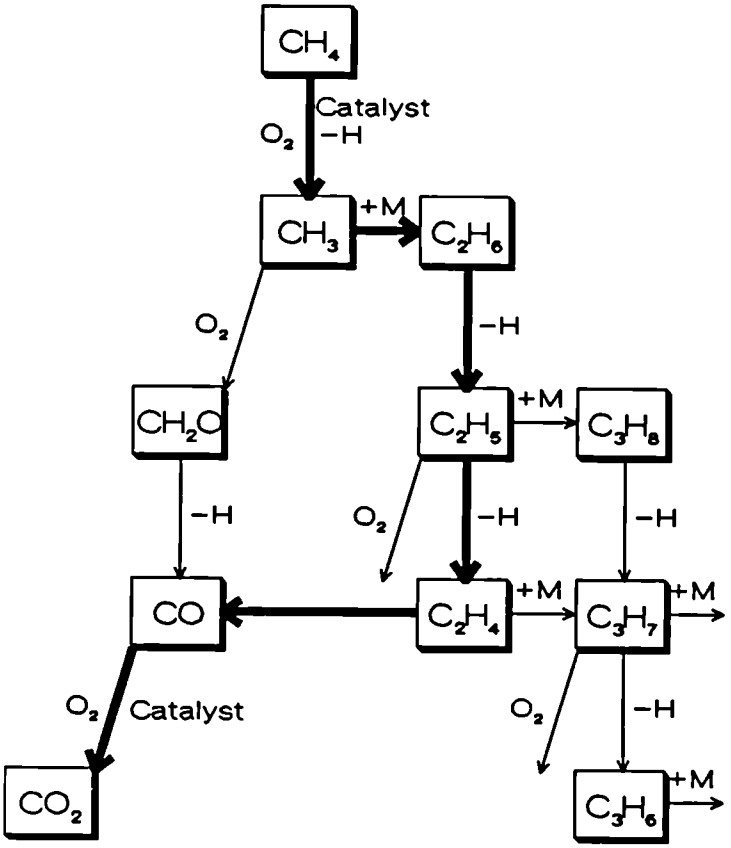

Figure 7.7.6: The proposed reaction scheme. The thick arrows indicate the main reaction path.

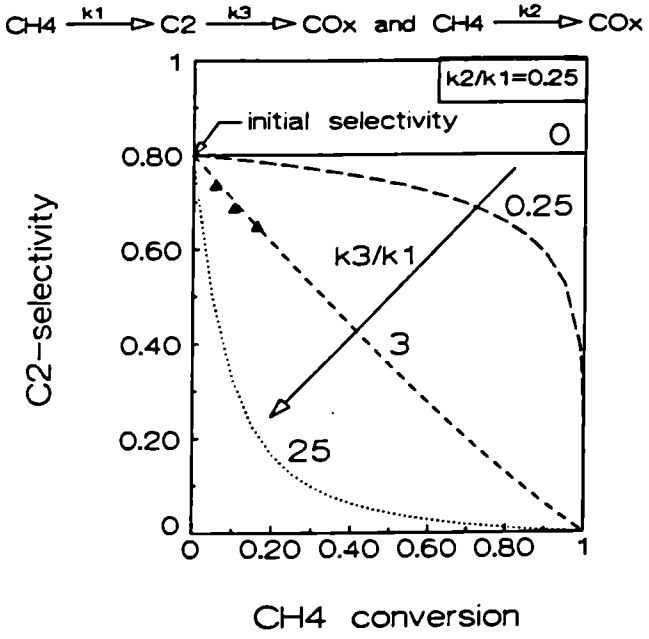

Figure 7.7.7: Selectivity as a function of the CH_4 conversion, for parallel and consecutive side reactions.

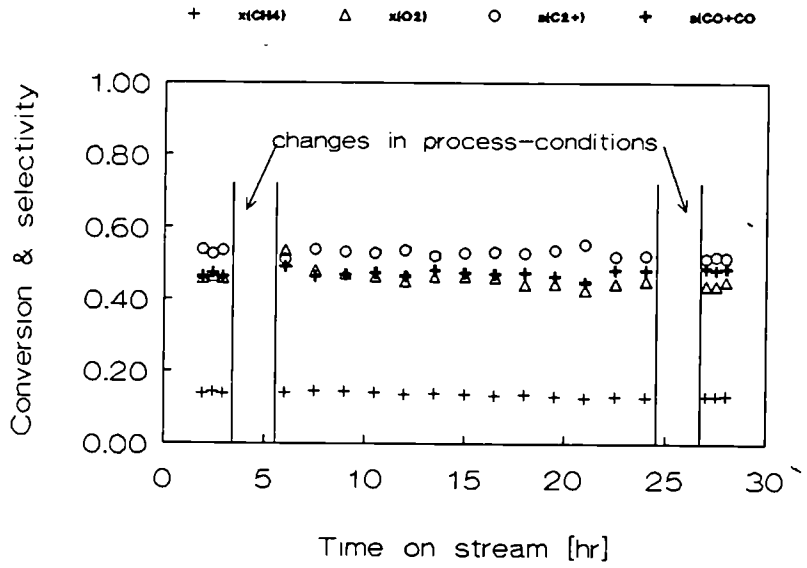

Figure 7.8.1. Influence of short changes in process conditions on Li/MgO catalyst performance. T=800°C, CH_4/O_2=5, W/F=0.3 g.s/ml.

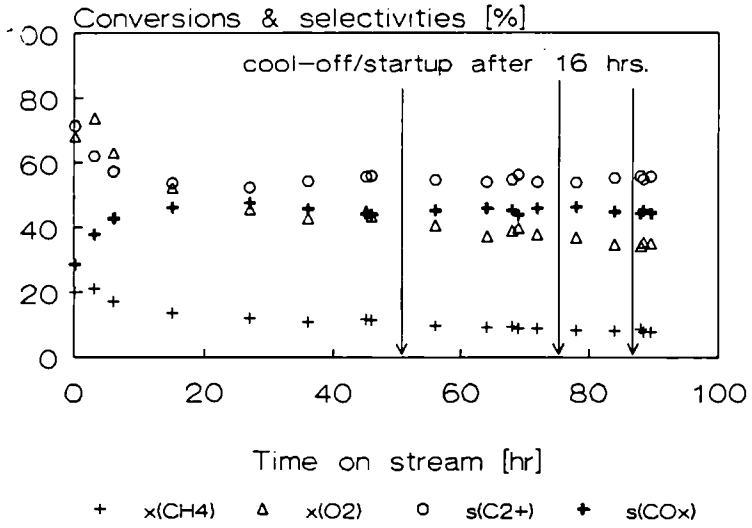

Figure 7.8.2. Influence of cool-off/ startup procedure on Li/MgO catalyst performance. T=800°C, CH_4/O_2=5, W/F=0.3 g.s/ml.

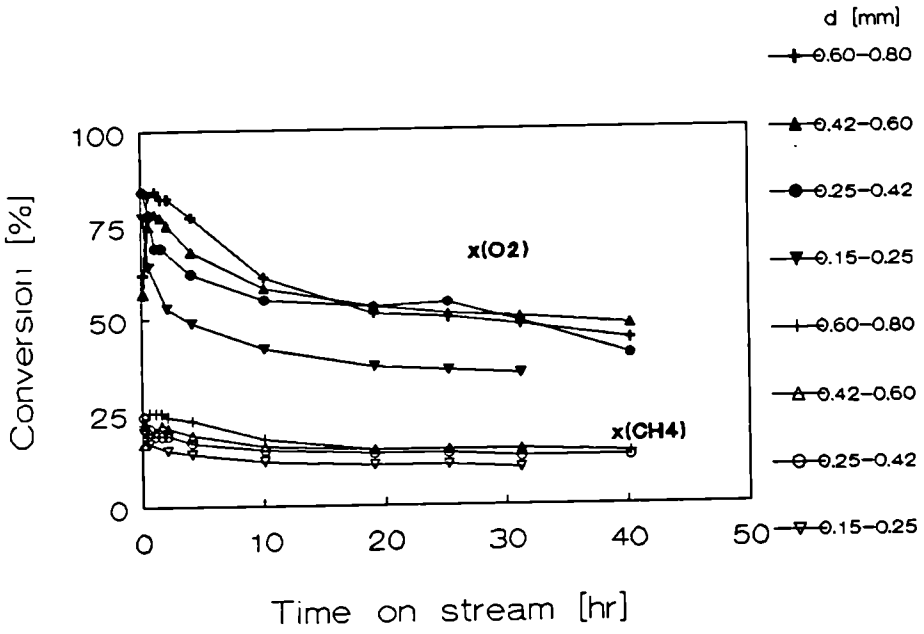

Figure 7.8.3. Conversion versus runtime for different catalyst particle sizes of Li/MgO catalyst. T=800°C, CH_4/O_2=5, W/F=0.3 g.s/ml.

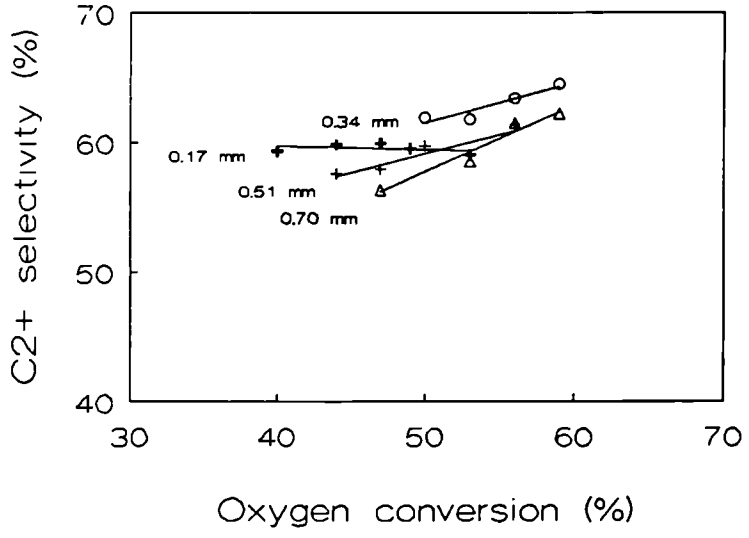

Figure 7.8.4. C_{2+} selectivity versus runtime for different catalyst particle sizes of Li/MgO catalyst. T=800°C, CH_4/O_2=5, W/F=0.3 g.s/ml.

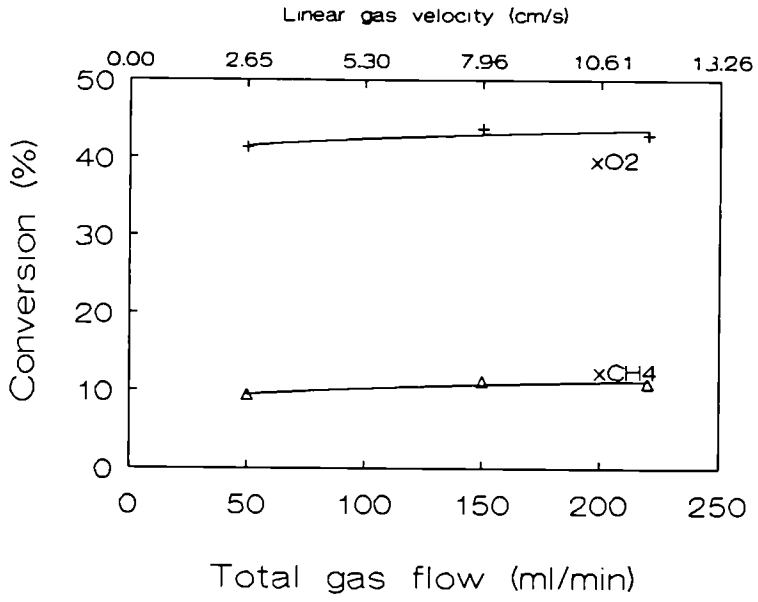

Figure 7.8.5. Conversion versus total gas flow at constant W/F (=0.3 g.s/ml). T=800°C, CH_4/O_2=5.

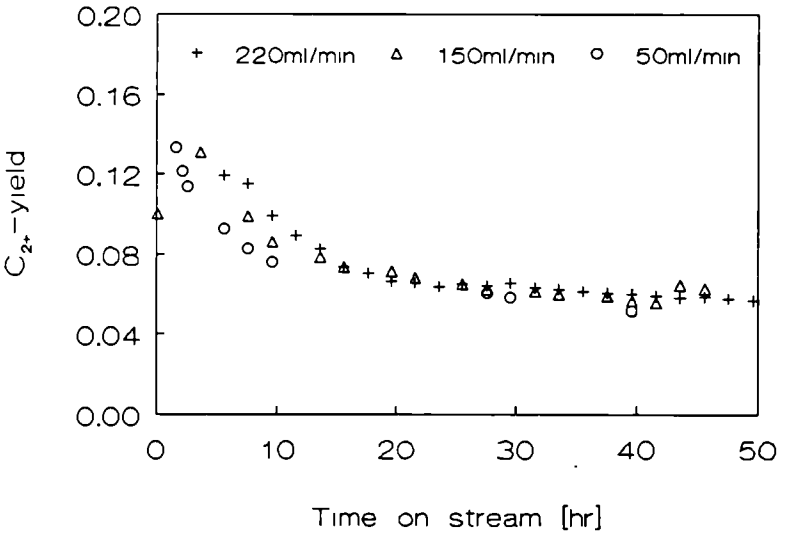

Figure 7.8.6. C_{2+} yield versus runtime for 3 different total flow rates at constant W/F (=0.3 g.s/ml). T=800°C, CH_4/O_2=5, Li/MgO.

Table 7.8.1. Applied feed gas compositions for kinetic measurements.

CH_4 flow Nml/min.	O_2 flow Nml/min.	He flow Nml/min.	CH_4/O_2
50	10	440	5
80	10	410	8
120	10	370	12
160	10	330	16
160	20	320	8
160	40	300	4
160	80	260	2

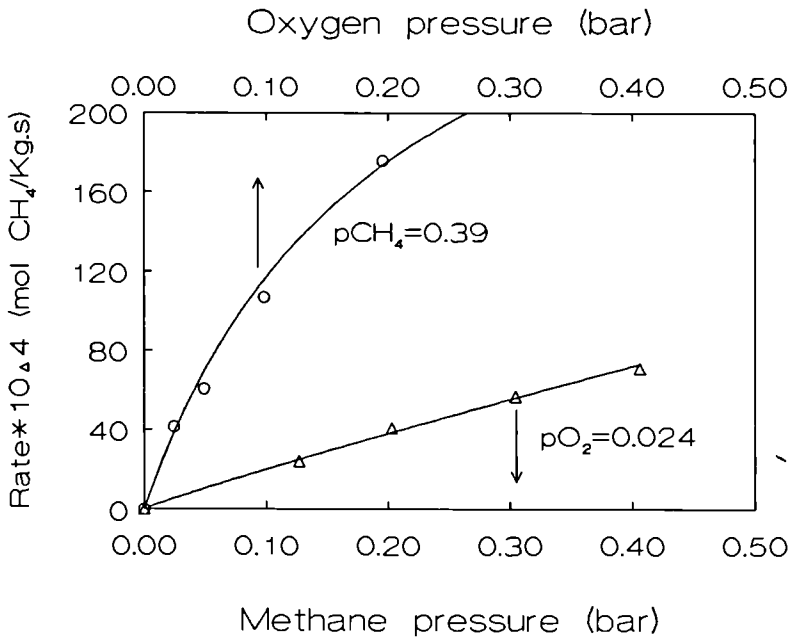

Figure 7.8.7. Reaction rate of methane as function of oxygen and methane partial pressure during methane coupling over Li/MgO. T=800°C, W/F=0.03 g.s/ml.

Table 7.9.1: The reaction parameters determined for the oxidation of ethylene.

	Homogeneous	Heterogeneous
Order in O_2	0.58	0.73
Order in C_2H_4	----	1.38
Activation energy (kJ/mole)	194	165

Table 7.9.2: Activation energies of initiation reactions of an ethylene/oxygen gas mixture containing impurities.

Initiation reaction	E_{act} (kJ/mole)
$C_2H_4 + H_2 \rightarrow C_2H_5 + H$	282
$C_2H_4 + C_2H_6 \rightarrow 2C_2H_5$	253
$C_2H_4 + C_2H_4 \rightarrow C_2H_5 + C_2H_3$	253
$C_2H_4 + O_2 \rightarrow C_2H_3 + HO_2$	253
"	123
"	241
"	203
"	257
$C_2H_4 + CO \rightarrow C_2H_3 + CHO$	379
$C_2H_4 \rightarrow C_2H_2 + H_2$	371

Table 7.9.3:
Comparison of catalytic and gas phase ethane activation.

	802°C (1.75 bar)		833°C (1.55 bar)	
	catalyst	gas phase	catalyst	gas phase
Selectivity (%)				
C_2H_4	46.0	----	45.0	58.8
CO	40.8	----	36.8	35.1
CO_2	9.6	----	16.7	1.1
Conversion (%)				
O_2	56.8	20.9	100.0	45.1
C_2H_6	51.6	33.9	79.3	82.5
Rate (10^{+2} mol/m^3 s)	1.39	0.91	1.86	1.97

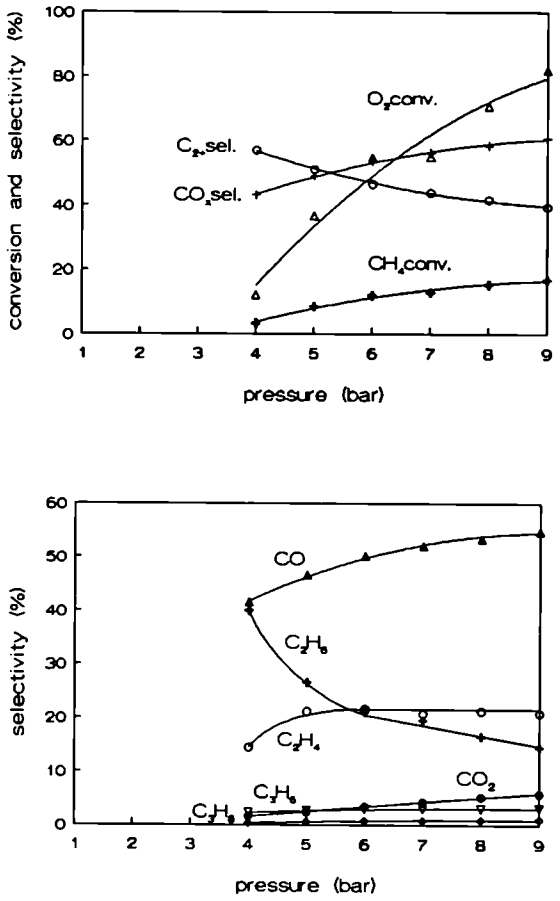

Figure 7.10.1 Pressure influence of the homogeneous gasphase reactions.
Conditions: T=800°C, τ=0.15 s, CH_4/O_2=5.

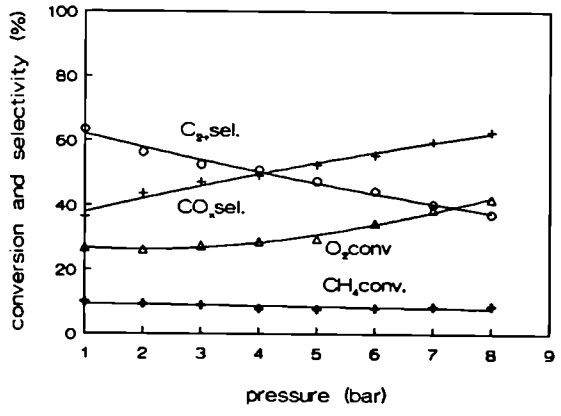

Figuur 7.10.2: Pressure influence of the oxidative coupling of methane reactions over a Li/MgO catalyst.
Conditions: T=800 °C, W/F=0.07 gs/Ncm³, CH_4/O_2=5.

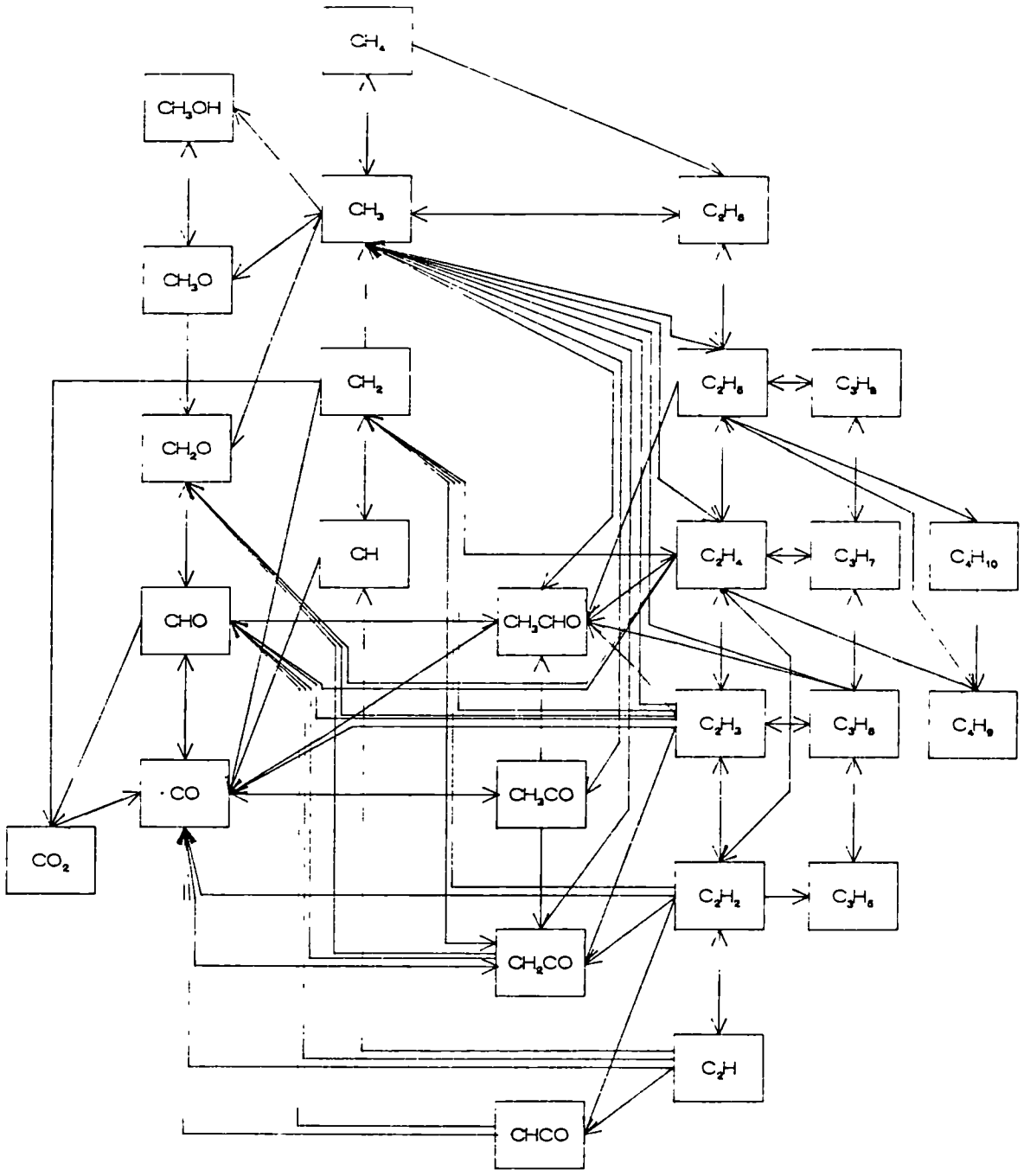

Figure 7.11.1: Reaction scheme of the carbon containing species of the homogeneous gas phase partial oxidation of methane. Downwards = H abstraction, to the right = methyl radical addition, down to the left = O addition to that specie.

Table 7.11.1:
Set of elementary radical reactions as used in the model. (Units, see text)
(Refs. 33-43)

No.	Reaction	A	b	Eact
1,	CH4 > CH3 + H	3.700E+15,	0.000E+00,	4.340E+02,
2,	CH4 + O2 > CH3 + HO2	4.000E+07,	0.000E+00,	2.380E+02,
3,	CH4 + H > CH3 + H2	2.200E-02,	3.000E+00,	3.660E+01,
4,	CH4 + O > CH3 + OH	1.200E+01,	2.100E+00,	3.190E+01,
5,	CH4 + OH > CH3 + H2O	6.000E+07,	0.000E+00,	3.850E+01,
6,	CH4 + HO2 > CH3 + H2O2	1.800E+05,	0.000E+00,	7.770E+01,
7,	CH3 + H2 > CH4 + H	6.600E-04,	3.000E+00,	3.240E+01,
8,	CH3 + H > CH4	6.000E+10,	-1.00E+00,	0.000E+00,
9,	CH3 + OH > CH4 + O	1.300E-01,	2.100E+00,	1.960E+01,
10,	CH3 + HO2 > CH4 + O2	3.600E+06,	0.000E+00,	0.000E+00,
11,	CH3 + H2O2 > CH4 + HO2	1.100E+06,	0.000E+00,	1.670E+01,
12,	CH3 + H2O > CH4 + OH	2.900E-01,	2.100E+00,	7.030E+01,
13,	CH3 + O2 > CH3O + O	2.000E+12,	-1.57E+00,	1.220E+02,
14,	CH3 + OH > CH3O + H	2.000E+10,	0.000E+00,	1.150E+02,
15,	CH3 + HO2 > CH3O + OH	7.943E+06,	0.000E+00,	0.000E+00,
16,	CH3 + CH3 > C2H6	1.500E+07,	0.000E+00,	0.000E+00,
17,	CH3 + CH4 > C2H6 + H	8.000E+07,	0.000E+00,	1.672E+02,
18,	CH3 + CH3 > C2H5 + H	8.000E+07,	0.000E+00,	1.110E+02,
19,	CH3 + CH3 > C2H4 + H2	1.000E+10,	0.000E+00,	1.340E+02,
20,	CH3 + CH2 > C2H4 + H	4.200E+07,	0.000E+00,	0.000E+00,
21,	CH3O + OH > CH3 + HO2	1.000E+07,	0.000E+00,	0.000E+00,
22,	CH3O + O > CH3 + O2	3.020E+08,	0.000E+00,	3.100E+00,
23,	CH3O > CH2O + H	1.580E+14,	0.000E+00,	1.150E+02,
24,	CH3O + O2 > CH2O + HO2	6.600E+04,	0.000E+00,	1.090E+01,
25,	CH2O + O2 > CHO + HO2	2.000E+07,	0.000E+00,	1.630E+02,
26,	CH2O + H > CHO + H2	2.500E+07,	0.000E+00,	1.670E+01,
27,	CH2O + O > CHO + OH	3.500E+07,	0.000E+00,	1.470E+01,
28,	CH2O + OH > CHO + H2O	3.000E+07,	0.000E+00,	5.000E+00,
29,	CH2O + HO2 > CHO + H2O2	1.000E+06,	0.000E+00,	3.350E+01,
30,	CH2O + CH3 > CHO + CH4	5.500E-03,	2.810E+00,	2.450E+01,
31,	CH2 + H > CH + H2	4.000E+07,	0.000E+00,	0.000E+00,
32,	CH2 + O2 > CO + H + H	1.300E+07,	0.000E+00,	6.300E+00,
33,	CH + O2 > CO + OH	2.000E+07,	0.000E+00,	0.000E+00,
34,	CH + O > CO + H	4.000E+07,	0.000E+00,	0.000E+00,
35,	CHO + H2 > CH2O + H	1.800E+00,	2.000E+00,	7.460E+01,
36,	CHO + HO2 > CH2O + O2	3.000E+08,	0.000E+00,	1.260E+01,
37,	CHO + H2O2 > CH2O + HO2	1.000E+05,	0.000E+00,	2.900E+01,
38,	CHO + CH4 > CH2O + CH3	7.300E-03,	2.850E+00,	9.420E+01,
39,	CHO + M > CO + H + M	5.000E+15,	-2.14E+00,	8.550E+01,
40,	CHO + O2 > CO + HO2	3.600E+06,	0.000E+00,	0.000E+00,
41,	CHO + CH3 > CO + CH4	1.200E+08,	0.000E+00,	0.000E+00,
42,	CO + H + M > CHO + M	6.300E+08,	-1.82E+00,	1.540E+01,
43,	CO + O2 > CO2 + O	2.500E+06,	0.000E+00,	2.000E+02,
44,	CO + O + M > CO2 + M	6.200E+02,	0.000E+00,	1.260E+01,
45,	CO + OH > CO2 + H	3.036E+05,	0.000E+00,	3.388E+00,

No.	Reaction	A	b	Eact
46,	CO + HO2 > CO2 + OH	1.500E+08,	0.000E+00,	9.890E+01,
47,	CO2 + H > CO + OH	1.500E+08,	0.000E+00,	1.110E+02,
48,	C2H6 > CH3 + CH3	3.200E+22,	-1.79E+00,	3.810E+02,
49,	C2H6 > C2H5 + H	5.000E+16,	0.000E+00,	3.720E+02,
50,	C2H6 + O2 > C2H5 + HO2	4.000E+07,	0.000E+00,	2.130E+02,
51,	C2H6 + H > C2H5 + H2	5.500E-04,	3.500E+00,	2.180E+01,
52,	C2H6 + OH > C2H5 + H2O	8.800E+03,	1.040E+00,	7.600E+00,
53,	C2H6 + HO2 > C2H5 + H2O2	2.900E+05,	0.000E+00,	6.250E+01,
54,	C2H6 + CH3 > C2H5 + CH4	5.500E-07,	4.000E+00,	3.470E+01,
55,	C2H6 + CH2 > C2H5 + CH3	2.200E+07,	0.000E+00,	3.630E+01,
56,	C2H5 + H > CH3 + CH3	3.000E+07,	0.000E+00,	0.000E+00,
57,	C2H5 + HO2 > CH3 + CH2O + OH	2.400E+07,	0.000E+00,	0.000E+00,
58,	C2H5 + H2 > C2H6 + H	3.000E-06,	3.600E+00,	3.540E+01,
59,	C2H5 + H > C2H6	3.600E+07,	0.000E+00,	0.000E+00,
60,	C2H5 + OH > C2H6 + O	3.000E+05,	0.000E+00,	2.500E+01,
61,	C2H5 + HO2 > C2H6 + O2	3.000E+05,	0.000E+00,	0.000E+00,
62,	C2H5 + H2O2 > C2H6 + HO2	8.700E+03,	0.000E+00,	4.100E+00,
63,	C2H5 + CH4 > C2H6 + CH3	8.600E-08,	4.140E+00,	5.260E+01,
64,	C2H5 + CH2O > C2H6 + CHO	5.500E-03,	2.810E+00,	2.450E+01,
65,	C2H5 + CHO > C2H6 + CO	1.200E+08,	0.000E+00,	0.000E+00,
66,	C2H5 > C2H4 + H	2.000E+13,	0.000E+00,	1.660E+02,
67,	C2H5 + O2 > C2H4 + HO2	8.400E+05,	0.000E+00,	1.620E+01,
68,	C2H4 + H > C2H5	8.400E+02,	1.490E+00,	4.100E+00,
69,	C2H4 + HO2 > C2H5 + O2	1.320E+05,	0.000E+00,	5.730E+01,
70,	C2H4 + O2 > C2H3 + HO2	3.000E+06,	0.000E+00,	1.230E+02,
71,	C2H4 + H > C2H3 + H2	1.500E+08,	0.000E+00,	4.270E+01,
72,	C2H4 + O > C2H3 + OH	1.300E+05,	6.300E-01,	5.700E+00,
73,	C2H4 + OH > C2H3 + H2O	7.000E+07,	0.000E+00,	1.260E+01,
74,	C2H4 + CH3 > C2H3 + CH4	1.500E+06,	0.000E+00,	4.970E+01,
75,	C2H4 + O > CH3 + CHO	1.320E+02,	1.550E+00,	1.800E+00,
76,	C2H4 + OH > CH3 + CH2O	1.000E+07,	0.000E+00,	0.000E+00,
77,	C2H4 + O > CH2 + CH2O	2.510E+07,	0.000E+00,	2.090E+01,
78,	C2H4 + HO2 > CH3CHO + OH	6.000E+03,	0.000E+00,	3.330E+01,
79,	C2H3 + H2 > C2H4 + H	3.000E-02,	2.630E+00,	3.570E+01,
80,	C2H3 + H2O > C2H4 + OH	4.800E-04,	2.900E+00,	6.220E+01,
81,	C2H3 + CH4 > C2H4 + CH3	1.300E+06,	0.000E+00,	3.260E+01,
82,	C2H3 + CH2O > C2H4 + CHO	5.400E-03,	2.810E+00,	2.450E+01,
83,	C2H3 + C2H6 > C2H4 + C2H5	6.000E-04,	3.300E+00,	4.390E+01,
84,	C2H3 > C2H2 + H	1.000E+15,	0.000E+00,	1.780E+02,
85,	C2H3 + HO2 > CH3 + CO + OH	3.000E+07,	0.000E+00,	0.000E+00,
86,	C2H3 + O2 > C2H2 + HO2	1.000E+06,	0.000E+00,	0.000E+00,
87,	C2H2 + H > C2H3	5.500E+06,	0.000E+00,	1.010E+01,
88,	C2H2 + O2 > CHCO + OH	2.000E+02,	1.500E+00,	1.259E+02,
89,	C2H2 + O2 > CHO + CHO	4.000E+06,	0.000E+00,	1.170E+02,
90,	C2H2 + H > C2H + H2	1.500E+08,	0.000E+00,	7.960E+01,
91,	C2H2 + OH > C2H + H2O	1.000E+07,	0.000E+00,	2.930E+01,
92,	C2H2 + OH > CH2CO + H	3.000E+06,	0.000E+00,	4.600E+00,
93,	C2H2 + CH3 > C2H + CH4	1.800E+05,	0.000E+00,	7.230E+01,
94,	C2H + H2 > C2H2 + H	3.500E+06,	0.000E+00,	8.800E+00,

No.	Reaction	A	b	Eact
95,	C2H + H2O > C2H2 + OH	4.070E+06,	0.000E+00,	5.800E+00,
96,	C2H + CH4 > C2H2 + CH3	1.000E+06,	0.000E+00,	6.000E+01,
97,	C2H + C2H6 > C2H2 + C2H5	3.600E+06,	0.000E+00,	0.000E+00,
98,	C2H2 + O > CH2 + CO	1.750E+07,	0.000E+00,	1.330E+01,
99,	C2H2 + O > CHCO + H	9.000E+06,	0.000E+00,	1.900E+01,
100,	C2H + O2 > CHO + CO	5.000E+07,	0.000E+00,	6.300E+00,
101,	C2H + O > CH + CO	1.000E+07,	0.000E+00,	0.000E+00,
102,	CH3CHO + H > CH3 + CO+ H2	4.000E+07,	0.000E+00,	1.760E+01,
103,	CH3CHO + O > CH3 + CO + OH	5.000E+06,	0.000E+00,	7.500E+00,
104,	CH3CHO + OH > CH3 + CO + H2O	1.000E+07,	0.000E+00,	0.000E+00,
105,	CH3CHO > CH3 + CHO	2.000E+15,	0.000E+00,	3.310E+02,
106,	CH3CHO + HO2 > CH3+CO + H2O2	1.700E+06,	0.000E+00,	4.480E+01,
107,	CH3CHO + O2 > CH3 + CO + HO2	2.000E+07,	5.000E-01,	1.765E+02,
108,	CH3CHO + CH3 > CH3+CO + CH4	8.000E+05,	0.000E+00,	2.510E+01,
109,	CH2CO + H > CH3 + CO	7.000E+06,	0.000E+00,	1.260E+01,
110,	CH2CO + O > CHO + CHO	2.000E+07,	0.000E+00,	9.600E+00,
111,	CH2CO + OH > CHO + CH2O	1.000E+07,	0.000E+00,	0.000E+00,
112,	CH2CO + M > CH2 + CO + M	1.000E+10,	0.000E+00,	2.480E+02,
113,	CHCO + H > CO + CH2	3.000E+06,	0.000E+00,	0.000E+00,
114,	CHCO + O > CO + CHO	1.200E+06,	0.000E+00,	0.000E+00,
115,	CHCO + OH > CHO + CO + H	1.000E+07,	0.000E+00,	0.000E+00,
116,	CHCO + O2 > CO + CO + OH	1.460E+06,	0.000E+00,	1.050E+01,
117,	C2H5 + CH3 > C3H8	1.000E+07,	0.000E+00,	0.000E+00,
118,	C2H4 + CH3 > C3H7	1.000E+05,	0.000E+00,	2.900E+01,
119,	C2H3 + CH3 > C3H6	1.000E+07,	0.000E+00,	0.000E+00,
120,	C2H2 + CH3 > C3H5	6.000E+05,	0.000E+00,	3.220E+01,
121,	C3H8 > C2H5 + CH3	7.900E+16,	0.000E+00,	3.560E+02,
122,	C3H8 + H > C3H7 + H2	1.300E+08,	0.000E+00,	4.060E+01,
123,	C3H8 + O > C3H7 + OH	3.000E+07,	0.000E+00,	2.410E+01,
124,	C3H8 + OH > C3H7 + H2O	3.700E+06,	0.000E+00,	6.900E+00,
125,	C3H8 + CH3 > C3H7 + CH4	1.550E+08,	0.000E+00,	8.900E+01,
126,	C3H7 > C2H4 + CH3	1.300E+13,	0.000E+00,	1.359E+02,
127,	C3H7 + H2 > C3H8 + H	4.000E+06,	0.000E+00,	6.980E+01,
128,	C3H7 + H > C3H8	2.000E+07,	0.000E+00,	0.000E+00,
129,	C3H7 + HO2 > C3H8 + O2	1.000E+07,	0.000E+00,	0.000E+00,
130,	C3H7 + CH4 > C3H8 + CH3	7.900E+05,	0.000E+00,	6.480E+01,
131,	C3H7 + C2H6 > C3H8 + C2H5	1.000E+05,	0.000E+00,	4.180E+01,
132,	C3H7 + C2H4 > C3H8 + C2H3	1.000E+05,	0.000E+00,	6.280E+01,
133,	C3H7 > C3H6 + H	2.000E+14,	0.000E+00,	1.630E+02,
134,	C3H7 + O2 > C3H6 + HO2	1.000E+06,	0.000E+00,	2.090E+01,
135,	C3H6 + H > C3H7	4.000E+06,	0.000E+00,	1.100E+01,
136,	C3H6 > C2H3 + CH3	7.000E+16,	0.000E+00,	3.600E+02,
137,	C3H6 + CH3 > C3H5 + CH4	2.000E+04,	0.000E+00,	1.880E+01,
138,	C3H6 + O > C2H5 + CHO	1.510E+06,	0.000E+00,	0.000E+00,
139,	C3H6 + OH > CH3CHO + CH3	1.000E+07,	0.000E+00,	0.000E+00,
140,	C3H5 + H2 > C3H6 + H	7.940E+06,	0.000E+00,	3.100E+01,
141,	O2 + H > O + OH	1.700E+11,	-9.00E-01,	7.280E+01,
142,	O2 + H + M > HO2 + M	2.000E+06,	-8.00E-01,	0.000E+00,
143,	O + OH > O2 + H	1.800E+07,	0.000E+00,	0.000E+00,

No.	Reaction	A	b	Eact
144,	O + HO2 > O2 + OH	2.000E+07,	0.000E+00,	0.000E+00,
145,	O + H2 > OH + H	1.500E+01,	2.000E+00,	3.160E+01,
146,	O + H2O > OH + OH	4.600E+03,	1.300E+00,	7.150E+01,
147,	O + H2O2 > OH + HO2	6.310E+06,	0.000E+00,	2.075E+01,
148,	OH + H > O + H2	6.700E+00,	2.000E+00,	2.330E+01,
149,	OH + OH > O + H2O	1.500E+03,	1.140E+00,	0.000E+00,
150,	OH + H2 > H2O + H	1.000E+02,	1.600E+00,	1.380E+01,
151,	OH + H + M > H2O + M	2.200E+10,	-2.00E+00,	0.000E+00,
152,	OH + HO2 > H2O + O2	2.000E+07,	0.000E+00,	0.000E+00,
153,	OH + H2O2 > H2O + HO2	1.750E+06,	0.000E+00,	1.330E+00,
154,	HO2 + M > O2 + H + M	2.100E+09,	0.000E+00,	1.910E+02,
155,	HO2 + H > O2 + H2	2.500E+07,	0.000E+00,	2.900E+00,
156,	HO2 + HO2 > O2 + OH + OH	2.000E+06,	0.000E+00,	0.000E+00,
157,	HO2 + H2 > H2O2 + H	3.000E+07,	0.000E+00,	1.090E+02,
158,	H2O2 + H > HO2 + H2	1.700E+06,	0.000E+00,	1.570E+01,
159,	OH + OH + M > H2O2 + M	3.200E+10,	-2.00E+00,	0.000E+00,
160,	HO2 + H > OH + OH	1.500E+08,	0.000E+00,	4.200E+00,
161,	H2O2 + M > OH + OH + M	3.000E+11,	0.000E+00,	1.900E+02,
162,	H2O2 + H > OH + H2O	1.000E+07,	0.000E+00,	1.660E+01,
163,	H2O + H > OH + H2	4.600E+02,	1.600E+00,	7.770E+01,
164,	H + H + M > H2 + M	1.800E+06,	-1.00E+00,	0.000E+00,

M = inert

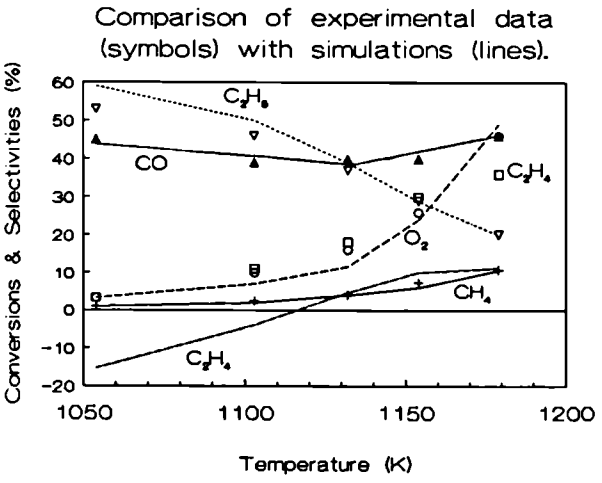

Figure 7.11.2: Comparison of experiments (symbols) with simulations (lines).
Conditions: $CH_4/O_2 = 10$, $CH_4/He = 0.8$, P = 1 bar.

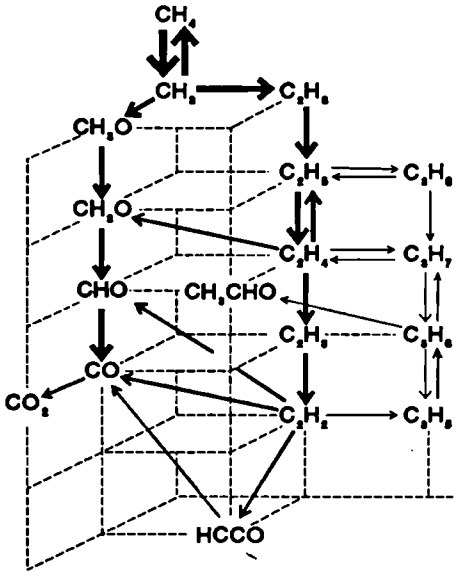

Figure 7.11.3: The simplified gas phase reaction scheme with the main reaction paths. The width of an arrow indicates the importance of that reaction path.
Conditions: T = 800°C, P = 1 bar, CH_4/O_2 = 5.

TABLE 7.11.2
Experiments and simulations of both catalytic and homogeneous gas phase reactions. Reactor made of quartz.
Conditions: T = 800°C, P = 1 bar, $CH_4/O_2 = 10$.

	Exp.	Sim.	Exp.	Sim.
Time [s]	4.6	7.9	6.0	0.5
O_2-conv [%]	28.2	28.2	92.8	92.8
CH_4-conv [%]	4.1	4.2	13.4	20.2
C_2^+sel [%]	51.1	49.7	76.2	76.9
CO_xsel [%]	48.8	50.0	23.8	22.8
CH_3 [mol/m^3]	----	5.9E-4	----	2.3E-3

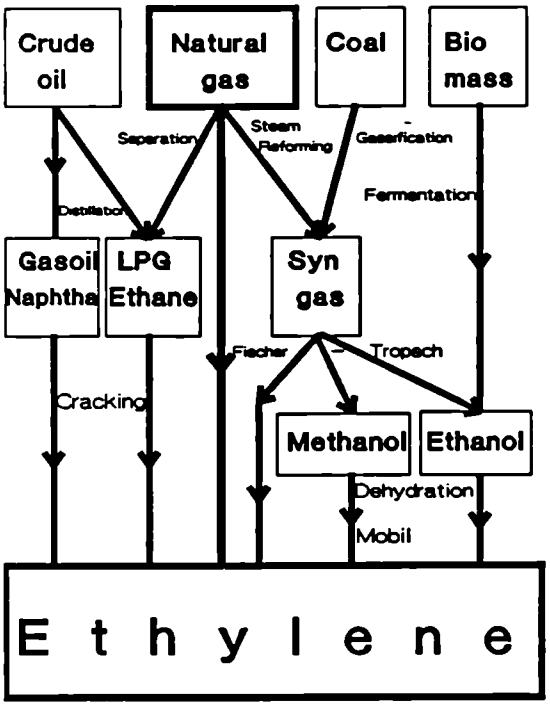

Figure 8.1.1: Ethylene production routes.

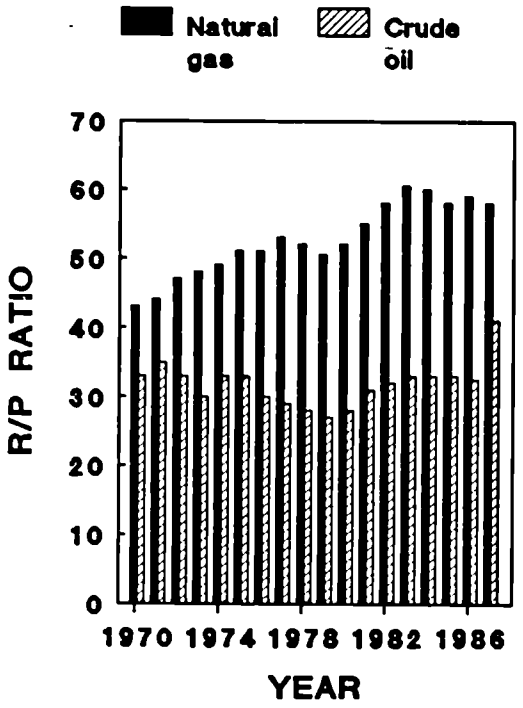

Figure 8.1.2: R/P ratios according to Britisch Petrol (Ref. 46).

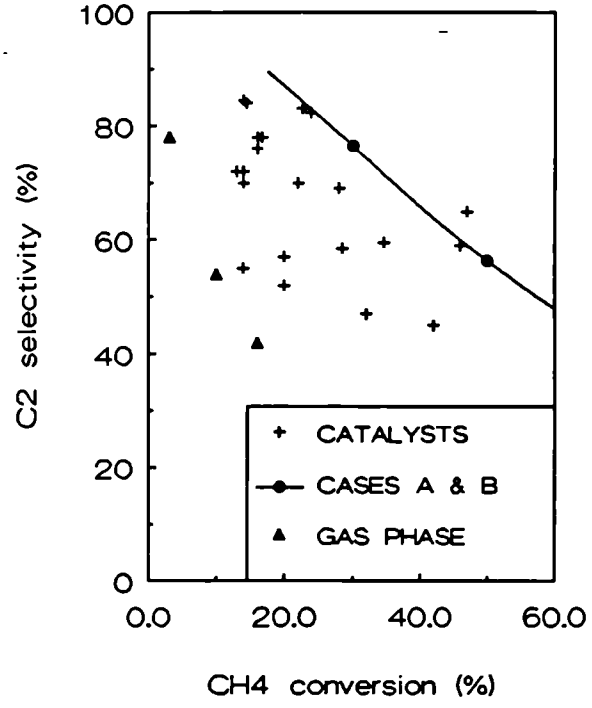

Figure 8.1.3: Survey of methane conversions and C_2 hydrocarbon selectivities.

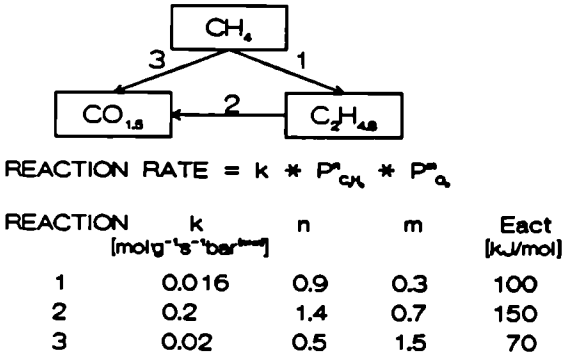

REACTION	k [mol g^{-1} s^{-1} bar$^{-(n+m)}$]	n	m	Eact [kJ/mol]
1	0.016	0.9	0.3	100
2	0.2	1.4	0.7	150
3	0.02	0.5	1.5	70

Figure 8.1.4: Simplified reaction scheme and kinetic data used for reactor design.

Table 8.1.1:
Composition of Balgzand natural gas. (in vol %)

CH_4	88.3
C_2H_6	4.3
C_3H_8	0.89
i-C_4H_8	0.11
n-C_4H_8	0.17
C_{4+}	0.108
CO_2	1.65
N_2	4.27
He	0.055
S (mg/m^3)	6-10

Table 8.1.2:
The designed multi-stage reactors for the oxidative coupling of methane process.

	Case A	Case B
Number of beds	5	11
O_2 feed in bed no.	1 & 3	1
Reactor length [m]	5.8	9.8
Reactor pressure [bar]	1	1
Inlet temperature [K]	973	973
Outlet temperature [K]	1079	1073
Maximum temperature [K]	1173	1173
CH_4 conversion [%]	30.0	50.0
C_{2+} selectivity [%]	81.0	53.3
Total heat duty [MW]	250	700

Table 8.1.3:
The designed fluidised bed reactors for cases A & B.

	Case A	Case B
Reactor:		
Number	36	43
Diameter [m]	4.6	4.6
Height [m]	2.3	2.3
Pressure [bar]	1	1
Temperature [°C]	800	800
Conversion [%]	30.6	50.3
C_{2+} selectivity [%]	89.7	59.4
Duty [MW]	5.9	13.1
Heat exchanger tubes inside the reactors:		
Number	83	147
Length [m]	2.3	2.3
Diameter [m]	0.05	0.05

Table 8.1.4:
Specifications of the process equipment for Case A.

	Duty [MW]
Compressor:	
C-1	17.5
C-2	18.0
C-3	16.7
Turbine E-1	-21.4
Heat exchangers:	
H-2	3.2
H-3	59.7
H-4	18.8
H-7	25.5
	Number of stages
Distillation towers:	
T-1	55
T-2	21
T-3	134
	Catacarb unit:
Capacity [kmol/h]	443 CO_2
	Process dryers:
Capacity [kmol/h]	79 H_2O
	Ethylene storage tank:
Number	2
Capacity [m^3]	5400

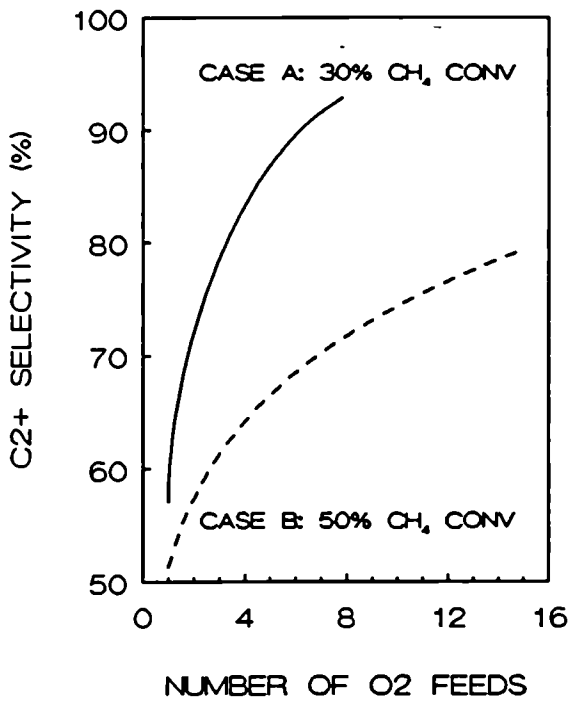

Figure 8.1.5: Selectivity as a function of the number of O_2 feeds for a multi stage reactor.

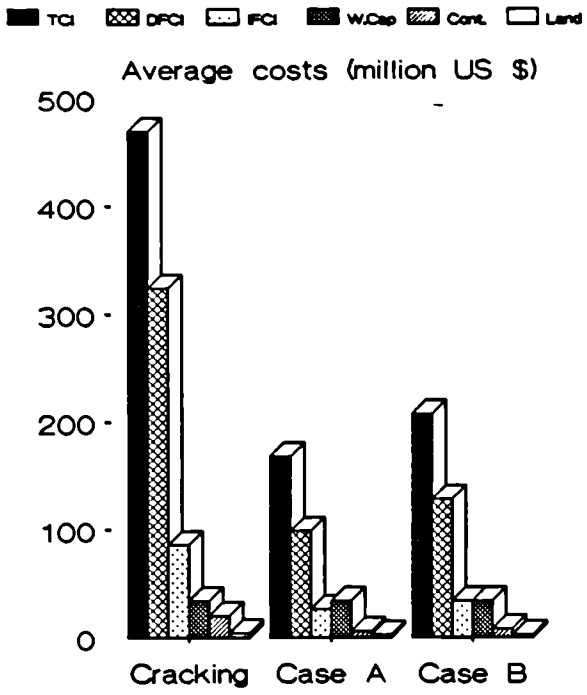

Figure 8.1.7: Break down of the investments costs for the conventional and the new process (Cases A & B).

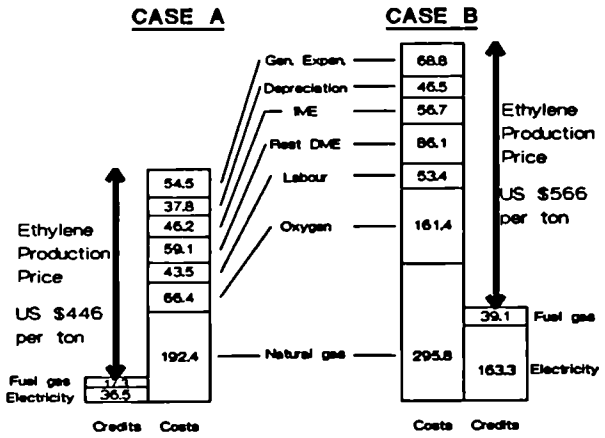

Figure 8.1.8: Price of ethylene for a direct partial oxidation process (average estimations).

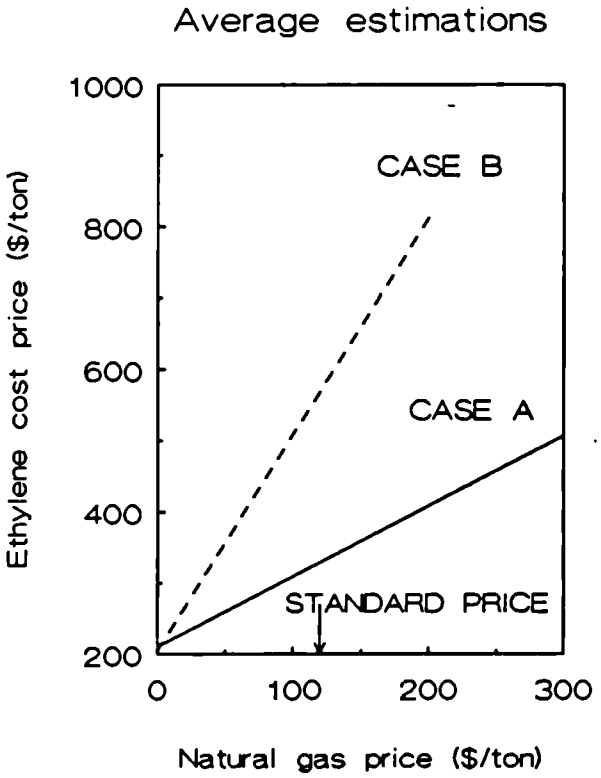

Figure 8.1.9: Influence of natural gas price on ethylene manufacturing costs.

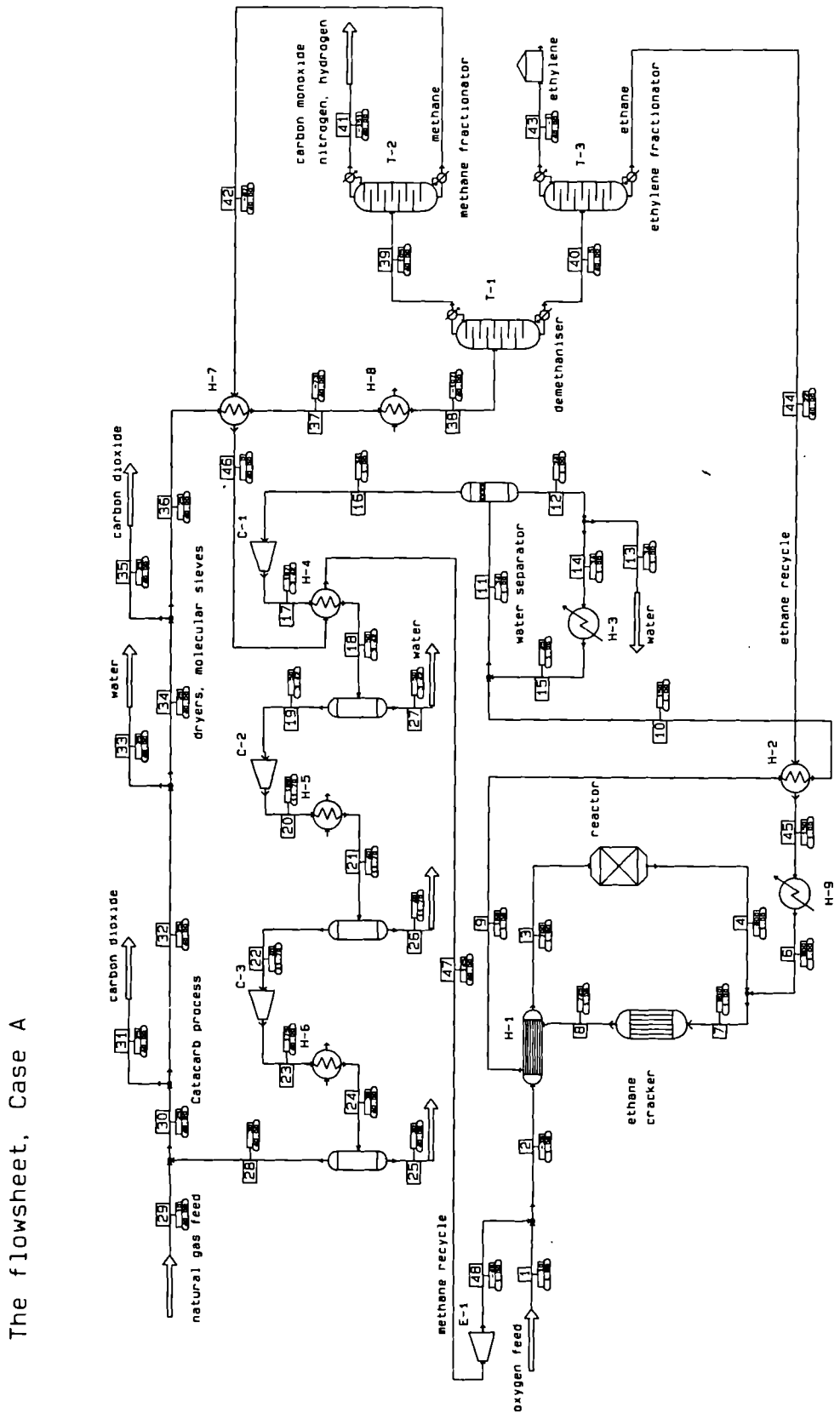

Figure 8.1.6: The designed flow sheet for the methane oxidative coupling of methane process; Case A.

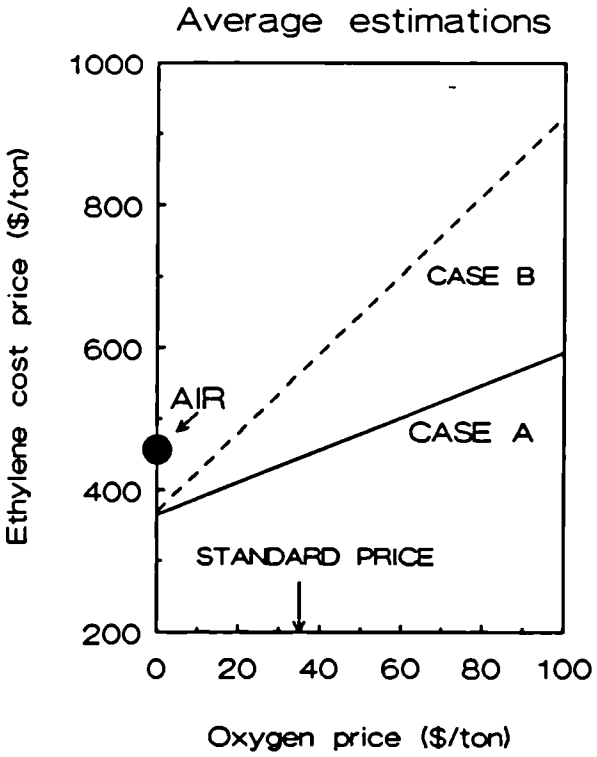

Figure 8.1.10: Influence of oxygen price on ethylene manufacturing costs.

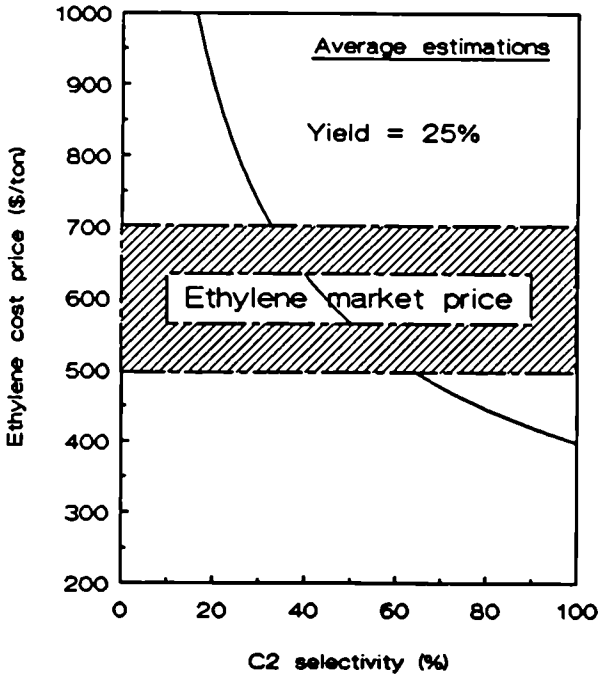

Figure 8.1.11: Influence of selectivity on ethylene manufacturing costs at a constant yield (= 25%).

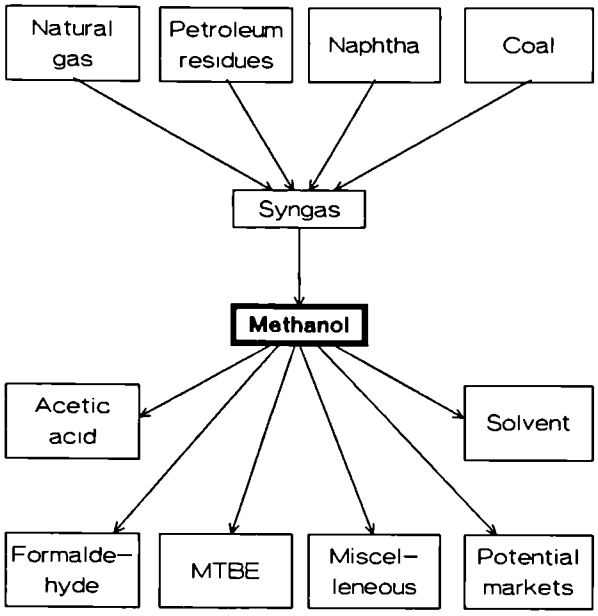

Figure 8.2.1. Methanol as an important intermediate in the chemical industry.

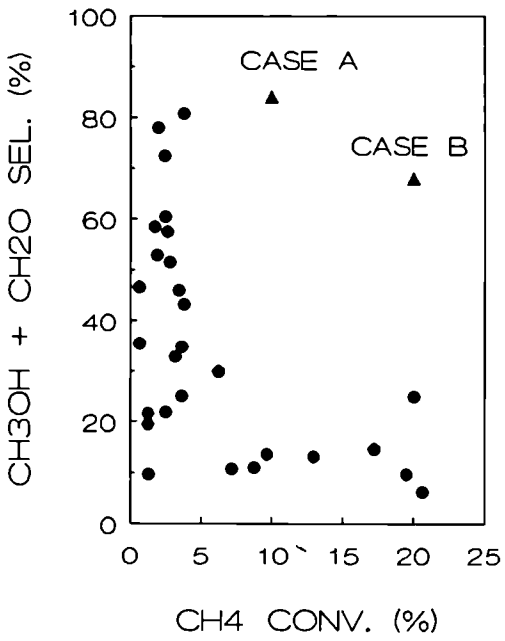

Figure 8.2.2. Selectivity with respect to methanol and formaldehyde versus methane conversion for various catalysts (Ref. 58).

TABLE 8.2.1
World methanol supply and demand (in million tons/year).

	1985	1986	1987*
supply	18.4	21.1	24.3
demand	15.9	18.1	22.0

*:Prediction

TABLE 8.2.2
Starting points of the design study. Single pass values.

	Case A	Case B
CH_4 conv.(%)	10	20
Selectivities (%):		
CH_3OH	80	60
CH_2O	4	8
CO_2	16	32

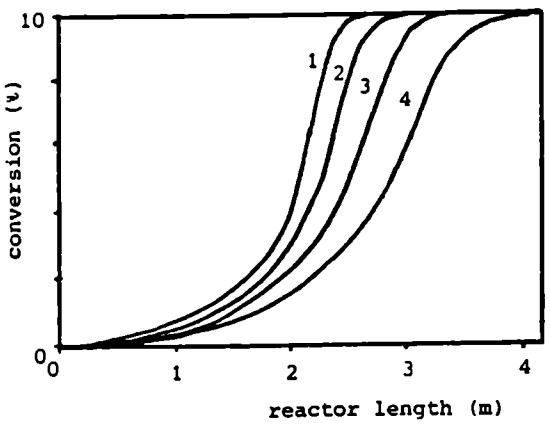

Figure 8.2.3. Case A. The methane conversion profiles as a function of the number of reactor tubes:
1 = 1900 3 = 1500
2 = 1700 4 = 1300 tubes.

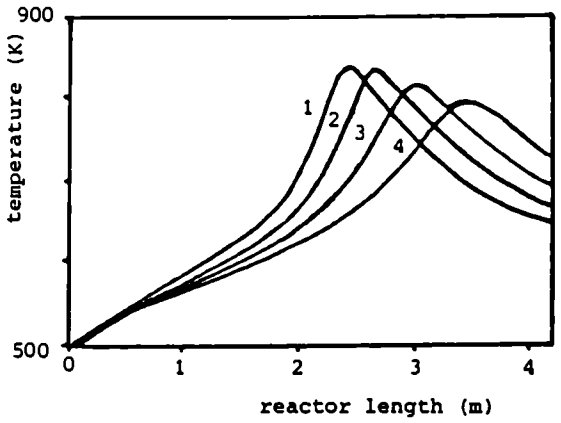

Figure 8.2.4. Case A. Axial temperature profiles as a function of the number of reactor tubes:
1 = 1900 3 = 1500
2 = 1700 4 = 1300 tubes.

TABLE 8.2.3
Relevant data for the reactor design (Catalyst; Ref. 60).

Kinetics:		
rate constant	8.8E5	m^3/skmol
activation energy	7.0E4	kJ/kmol
reaction heat (A)	2.4E5	kJ/kmol
Catalyst MoO_3·UO_2:		
spheres, diameter	2	mm
Feed (case A):		
methane	8.8	kg/s
oxygen	stoichiometric	
temperature	500	K
pressure	54	bar
Outlet O_2 conc.	0	
Methanol prod.	400,000	tons/y

TABLE 8.2.4
The designed reactor.

Number of tubes	1500	
Tube diameter	0.06	m
Tube length	3.6	m
Outlet temperature	745	K
Residence time	1.4	s
Pressure drop	0.1	bar

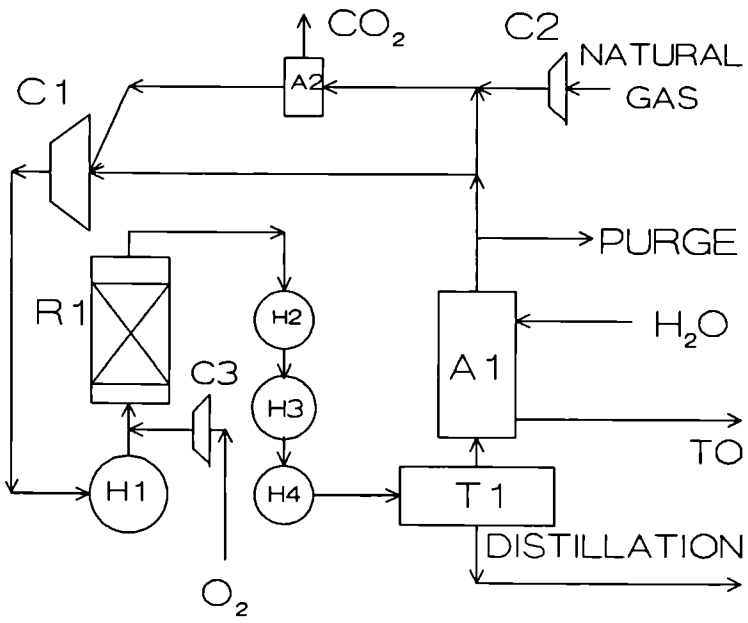

Figure 8.2.5. The flow sheet designed for the direct partial oxidation of natural gas into methanol.
R1 = Reactor C1-3 = Compressors
A1 = Wash Tower H1-4 = Heat exchangers
A2 = Benfield Unit T1 = Methanol Separator

TABLE 8.2.5
Composition of Balgzand gas in vol %.

CH_4	88.3
C_2H_6	4.3
C_3H_8	0.89
i-C_4H_8	0.11
n-C_4H_8	0.17
C_4^+	0.108
CO_2	1.65
N_2	4.27
He	0.055
S (mg/m^3)	6-10

TABLE 8.2.6
Investment estimates for the conventional process and the direct partial oxidation process (in million US $).

	Convent.	Direct ox.
Battery Limits	40	35
Utilities	41	36
Total Direct Costs	81	71
Indirect Costs	20	18
Contingencies	4	5
Fixed Capital	106	93
Land	5	5
Working Capital	15	15
Total Cap. Invest.	126	113

TABLE 8.2.7
Profitability of the conventional process and cases A and B of the direct partial oxidation process (in million US $ at Jan. 1988)

	Conv.	Case A	Case B
Total Cap. Inves	126	113	113
Direct Manu. Exp	56.3	84.9	115.8
Indir. Manu. Exp	6.0	6.0	6.0
Depreciations	11.0	9.8	9.8
General Expenses	13.8	18.6	23.9
Total Expenses	87.1	119.2	155.5
Rev. From Sales	70.2	67.5	65.6
Annual Profit	-16.9	-51.7	-89.9

European Communities — Commission

EUR 13061 — Ethylene from natural gas by direct catalytic oxidation

J.W.M.H. Geerts, J.M.N. van Kasteren, K. van der Wiele

Luxembourg: Office for Official Publications of the European Communities

1990 — V, 120 pp., num. tab., fig. — 21.0 × 29.7 cm

Energy series

ISBN 92-826-2235-5

Catalogue number: CD-NA-13061-EN-C

Price (excluding VAT) in Luxembourg: ECU 10

This report describes the research in the field of oxidative coupling of methane to ethylene carried out at Eindhoven University of Technology (The Netherlands). The aim of this work comprised the development of a process for the production of ethylene directly from natural gas by partial oxidation.

The work was focused on four major aspects: optimizing the physical parameters of the catalyst, defining the optimum reactor design and reaction conditions, collecting data for the modelling of the chemical reaction and process design and economic evaluations.

Venta y suscripciones • Salg og abonnement • Verkauf und Abonnement • Πωλήσεις και συνδρομές
Sales and subscriptions • Vente et abonnements • Vendita e abbonamenti
Verkoop en abonnementen • Venda e assinaturas

BELGIQUE / BELGIË

Moniteur belge /
Belgisch Staatsblad
Rue de Louvain 42 / Leuvenseweg 42
1000 Bruxelles / 1000 Brussel
Tél. (02) 512 00 26
Fax 511 01 84
CCP / Postrekening 000-2005502-27

Autres distributeurs /
Overige verkooppunten

Librairie européenne/
Europese Boekhandel
Avenue Albert Jonnart 50 /
Albert Jonnartlaan 50
1200 Bruxelles / 1200 Brussel
Tél. (02) 734 02 81
Fax 735 08 80

Jean De Lannoy
Avenue du Roi 202 /Koningslaan 202
1060 Bruxelles / 1060 Brussel
Tél. (02) 538 51 89
Télex 63220 UNBOOK B
Fax (02) 538 08 41

CREDOC
Rue de la Montagne 34 / Bergstraat 34
Bte 11 / Bus 11
1000 Bruxelles / 1000 Brussel

DANMARK

J. H. Schultz Information A/S
EF-Publikationer
Ottiliavej 18
2500 Valby
Tlf. 36 44 22 66
Fax 36 44 01 41
Girokonto 6 00 08 86

BR DEUTSCHLAND

Bundesanzeiger Verlag
Breite Straße
Postfach 10 80 06
5000 Köln 1
Tel. (02 21) 20 29-0
Fernschreiber:
ANZEIGER BONN 8 882 595
Fax 20 29 278

GREECE

G.C. Eleftheroudakis SA
International Bookstore
Nikis Street 4
10563 Athens
Tel. (01) 322 63 23
Telex 219410 ELEF
Fax 323 98 21

ESPAÑA

Boletín Oficial del Estado
Trafalgar, 27
28010 Madrid
Tel. (91) 44 82 135

Mundi-Prensa Libros, S.A.
Castelló, 37
28001 Madrid
Tel. (91) 431 33 99 (Libros)
431 32 22 (Suscripciones)
435 36 37 (Dirección)
Télex 49370-MPLI-E
Fax (91) 575 39 98

Sucursal:

Librería Internacional AEDOS
Consejo de Ciento, 391
08009 Barcelona
Tel. (93) 301 86 15
Fax (93) 317 01 41

Llibreria de la Generalitat
de Catalunya
Rambla dels Estudis , 118 (Palau Moja)
08002 Barcelona
Tel. (93) 302 68 35
302 64 62
Fax 302 12 99

FRANCE

Journal officiel
Service des publications
des Communautés européennes
26, rue Desaix
75727 Paris Cedex 15
Tél. (1) 40 58 75 00
Fax (1) 40 58 75 74

IRELAND

Government Publications
Sales Office
Sun Alliance House
Molesworth Street
Dublin 2
Tel. 71 03 09

or by post

Government Stationery Office
EEC Section
6th floor
Bishop Street
Dublin 8
Tel. 78 16 66
Fax 78 06 45

ITALIA

Licosa Spa
Via Benedetto Fortini, 120/10
Casella postale 552
50125 Firenze
Tel. (055) 64 54 15
Fax 64 12 57
Telex 570466 LICOSA I
CCP 343 509

Subagenti:

Libreria scientifica
Lucio de Biasio - AEIOU
Via Meravigli, 16
20123 Milano
Tel. (02) 80 76 79

Herder Editrice e Libreria
Piazza Montecitorio, 117-120
00186 Roma
Tel. (06) 679 46 28/679 53 04

Libreria giuridica
Via XII Ottobre, 172/R
16121 Genova
Tel. (010) 59 56 93

GRAND-DUCHÉ DE LUXEMBOURG

Abonnements seulement
Subscriptions only
Nur für Abonnements

Messageries Paul Kraus
11, rue Christophe Plantin
2339 Luxembourg
Tél. 499 88 88
Télex 2515
Fax 499 88 84 44
CCP 49242-63

NEDERLAND

SDU Overheidsinformatie
Externe Fondsen
Postbus 20014
2500 EA 's-Gravenhage
Tel. (070) 37 89 911
Fax (070) 34 75 778

PORTUGAL

Imprensa Nacional
Casa da Moeda, EP
Rua D. Francisco Manuel de Melo, 5
P-1092 Lisboa Codex
Tel. (01) 69 34 14

Distribuidora de Livros
Bertrand, Ld.ª
Grupo Bertrand, SA
Rua das Terras dos Vales, 4-A
Apartado 37
P-2700 Amadora Codex
Tel. (01) 49 59 050
Telex 15798 BERDIS
Fax 49 60 255

UNITED KINGDOM

HMSO Books (PC 16)
HMSO Publications Centre
51 Nine Elms Lane
London SW8 5DR
Tel. (071) 873 9090
Fax GP3 873 8463
Telex 29 71 138

Sub-agent:

Alan Armstrong Ltd
2 Arkwright Road
Reading, Berks RG2 0SQ
Tel. (0734) 75 18 55
Telex 849937 AAALTD G
Fax (0734) 75 51 64

ÖSTERREICH

Manz'sche Verlags-
und Universitätsbuchhandlung
Kohlmarkt 16
1014 Wien
Tel. (0222) 531 61-0
Telex 11 25 00 BOX A
Fax (0222) 531 61-81

SVERIGE

BTJ
Box 200
22100 Lund
Tel. (046) 18 00 00
Fax (046) 18 01 25

SCHWEIZ / SUISSE / SVIZZERA

OSEC
Stampfenbachstraße 85
8035 Zürich
Tel. (01) 365 51 51
Fax (01) 365 54 11

MAGYARORSZÁG

Agroinform
Központ:
Budapest I., Attila út 93. H-1012

Levélcím:
Budapest, Pf.: 15 H-1253
Tel. 36 (1) 56 82 11
Telex (22) 4717 AGINF H-61

POLAND

Business Foundation
ul. Wspólna 1/3
PL-00-529 Warszawa
Tel. 48 (22) 21 99 93/21 84 20
Fax 48 (22) 28 05 49

YUGOSLAVIA

Privredni Vjesnik
Bulevar Lenjina 171/XIV
11070 - Beograd
Tel. 123 23 40

TÜRKIYE

Pres Dagitim Ticaret ve sanayi A.Ş.
Narlibahçe Sokak No. 15
Cağaloğlu
Istanbul
Tel. 512 01 90
Telex 23822 DSVO-TR

AUTRES PAYS
OTHER COUNTRIES
ANDERE LÄNDER

Office des publications officielles
des Communautés européennes
2, rue Mercier
L-2985 Luxembourg
Tél. 49 92 81
Télex PUBOF LU 1324 b
Fax 48 85 73
CC bancaire BIL 8-109/6003/700

CANADA

Renouf Publishing Co. Ltd
Mail orders — Head Office:
1294 Algoma Road
Ottawa, Ontario K1B 3W8
Tel. (613) 741 43 33
Fax (613) 741 54 39
Telex 0534783

Ottawa Store:
61 Sparks Street
Tel. (613) 238 89 85

Toronto Store:
211 Yonge Street
Tel. (416) 363 31 71

UNITED STATES OF AMERICA

UNIPUB
4811-F Assembly Drive
Lanham, MD 20706-4391
Tel. Toll Free (800) 274 4888
Fax (301) 459 0056

AUSTRALIA

Hunter Publications
58A Gipps Street
Collingwood
Victoria 3066

JAPAN

Kinokuniya Company Ltd
17-7 Shinjuku 3-Chome
Shinjuku-ku
Tokyo 160-91
Tel. (03) 3439-0121

Journal Department
PO Box 55 Chitose
Tokyo 156
Tel. (03) 3439-0124

1/91

CD-NA-13061-EN-C

NOTICE TO THE READER

All scientific and technical reports published by the Commission of the European Communities are announced in the monthly periodical **'euro abstracts'**. For subscription (1 year: ECU 92) please write to the address below.

Price (excluding VAT) in Luxembourg: ECU 10

ISBN 92-826-2235-5

OFFICE FOR OFFICIAL PUBLICATIONS
OF THE EUROPEAN COMMUNITIES

L-2985 Luxembourg